
ESCAPING LOCAL MINIMA PROVABLY IN NON-CONVEX MATRIX SENSING: A DETERMINISTIC FRAMEWORK VIA SIMULATED LIFTING *

Tianqi Shen, Jinji Yang, Junze He[†], Kunhan Gao[†], Ziye Ma[‡]

Department of Computer Science
City University of Hong Kong (CityUHK)
Hong Kong SAR, China
tianqshen5-c@my.cityu.edu.hk, ziyma@cityu.edu.hk

ABSTRACT

Low-rank matrix sensing is a fundamental yet challenging nonconvex problem whose optimization landscape typically contains numerous spurious local minima, making it difficult for gradient-based optimizers to converge to the global optimum. Recent work has shown that over-parameterization via tensor lifting can convert such local minima into strict saddle points, an insight that also partially explains why massive scaling can improve generalization and performance in modern machine learning. Motivated by this observation, we propose a **Simulated Oracle Direction** (SOD) escape mechanism that *simulates* the landscape and escape direction of the over-parametrized space, without resorting to actually lifting the problem, since that would be computationally intractable. In essence, we designed a mathematical framework to project over-parametrized escape directions onto the original parameter space to guarantee a strict decrease of objective value from existing local minima. To the best of our knowledge, this represents the first deterministic framework that could escape spurious local minima with guarantee, especially without using random perturbations or heuristic estimates. Numerical experiments demonstrate that our framework reliably escapes local minima and facilitates convergence to global optima, while incurring minimal computational cost when compared to explicit tensor over-parameterization. We believe this framework has non-trivial implications for nonconvex optimization beyond matrix sensing, by showcasing how simulated over-parameterization can be leveraged to tame challenging optimization landscapes. The project website is publicly accessible at <https://sodescape.github.io/>.

Keywords Non-convex optimization · Low-rank matrix sensing · Tensor over-parametrization · Spurious local minima

1 Introduction

Non-convex optimization plays a crucial role in numerous fields such as signal processing, machine learning, and control theory [1]. However, these problems are often NP-hard and characterized by a loss landscape abundant in spurious local minima, saddle points, and extended flat regions [2]. Such geometric irregularities make it challenging for algorithms originally developed for convex settings to identify global minimizers efficiently. Formally, given an objective function $f : \text{dom } f \rightarrow \mathbb{R}$ with *effective domain* $\text{dom } f$, a point x^* is called a *global minimizer* and a point \hat{x} is called a *local minimizer* if

$$\begin{aligned} f(x^*) &\leq f(x), \quad \forall x \in \text{dom } f, & (\text{global minimizer}) \\ f(\hat{x}) &\leq f(x), \quad \forall x \in \mathbb{B}(\hat{x}, \varepsilon), \quad \exists \varepsilon > 0, & (\text{local minimizer}) \end{aligned}$$

where $\mathbb{B}(\hat{x}, \varepsilon)$ represents the Euclidean ball of radius ε centered at \hat{x} . A non-global local minimizer is typically referred to as a *spurious solution*. From a dynamical systems perspective [3], the iterative optimization process can be viewed as

*Under Review. [†]These authors contributed equally to this work. [‡]Corresponding author.

a discretization of a continuous-time *gradient flow* characterized by $\dot{x}(t) = -\nabla f(x(t))$. Under this viewpoint, every *critical point* of f corresponds to an *equilibrium* of the flow [4]. In particular, spurious solutions behave as stable equilibria, meaning that once the trajectory of gradient flow enters their *attraction basin*, it is theoretically incapable of escaping when the step size is reasonably small. Consequently, such stable yet non-global equilibria \hat{x} can severely hinder convergence to the global solution x^* , thereby degrading both performance and generalization capability.

A natural remedy is convex relaxation: replace a non-convex problem with a convex formulation that removes spurious local minima and permits off-the-shelf convex optimization [5, 6]. Yet relaxations can be lossy [7], and more importantly such relaxations are both theoretically intractable and computationally infeasible for modern machine learning models. This calls for improving the non-convex dynamics itself, instead of designing good convex surrogates. Thus, we directly tackle one of the major challenges in non-convex optimization in this work, the escaping from local minima \hat{x} [1]. Table 1 shows that existing escape strategies largely fall into two categories: *random perturbations* and *heuristics* (see Section 2.1 for details). Random methods add stochastic perturbations to change descent directions, enabling traversal of sharp attraction basins [8]; although somewhat effective in expectation over repeated runs, they often exhibit a low success rate in a single run [9] and could only obtain theoretical guarantees for saddles instead of local minima. Heuristic methods reshape the local descent trajectory through hand-crafted or adaptive rules, bypassing small basins even without explicit noise [10]; however, they are typically not rooted in theory and may cause unintended side effects [11]. Recent theoretical and empirical studies [12, 13, 14, 15, 16, 17] increasingly support the view that over-parameterization can significantly improve the optimization landscape during training, effectively eliminating many spurious local minima and fundamentally mitigating the challenge of escaping from them. However, over-parametrization is currently implemented at substantial computational and memory cost in large-scale settings [18] (see Section 2.2 for details), which calls for better strategies to utilize its power without incurring prohibitive costs.

Table 1: Some techniques for handling spurious solutions in non-convex optimization.

Method	Mechanism for Avoiding \hat{x}	Limitation
Random Methods	Escape by chance	Low success rate
Heuristics	Highly subjective rules	Lacking theoretical guarantees
Our Approach	Based on theoretical derivation	Limited by numerical precision

To address this challenge and to fill this important gap, this work designs a theoretically grounded deterministic escape mechanism that leverages oracle direction informed by simulated over-parameterization, without relying on randomness or heuristic strategies. Specifically, the interpolation capability of over-parameterized models can reveal escape directions that exist in the high-dimensional space but remain invisible in the original, low-dimensional domain [19, 20, 21]. We utilize these hidden directions as oracles to construct a deterministic escape mechanism termed *Simulated Oracle Direction* (SOD) Escape that operates entirely within the original domain. A central challenge arises: oracle directions do not typically correspond to single axes in the low-dimensional space; rather, they form superpositions of multiple states in the over-parameterized space [22]. The primary theoretical task of this paper is therefore to characterize the conditions under which such superpositions can be meaningfully projected back to the original domain, thereby providing actionable guidance for escaping non-global spurious solutions. To concretize the above intuition, we investigate the mathematically structured *matrix sensing* (MS) problem [23], which aims to recover a low-rank positive semidefinite (PSD) matrix $M^* \in \mathbb{R}^{n \times n}$ with rank $r := \text{rank}(M^*) < n$ from a set of linear measurements \mathcal{A} . This problem arises in numerous applications, including phase retrieval [24], quantum tomography [25], collaborative filtering [26], and power system state estimation [27]. It is worth noting that the insights developed in this work have the potential to extend beyond MS and offer general guidance for designing deterministic escape strategies in broader classes of non-convex optimization problems [28].

The remainder of the paper is organized as follows. Section 1 finalizes the MS setup and preliminaries; Section 2 reviews non-convex optimization background and prior MS results; Section 3 states our main theorems and interpretations. We develop a deterministic escape mechanism and guarantees in two stages: Section 4 covers restricted regimes where a one-step escape in the overparameterized space followed by projection yields a closed-form escape point \tilde{X} ; Section 5 treats general regimes where direct projection may fail, proposing truncated projected gradient descent (TPGD) to enable provably valid projection and showing that the resulting escape point \tilde{X} still has a closed-form representation, effectively simulating the TPGD process without explicit lifting. Finally, Section 6 presents two case studies and a success rate comparison study, and Section 7 concludes this paper.

1.1 Problem Setup and Short Preliminaries

Problem Setup. This paper considers the *Burer-Monteiro* (BM) factorized formulation, which replaces the rank constraint (NP-hard [29]) with the product of two smaller matrices. Specifically, one optimizes over $X \in \mathbb{R}^{n \times r_{\text{search}}}$ such that $XX^\top \approx M^* = ZZ^\top$. The BM-factorized MS problem is formulated as the following optimization problem

in this study:

$$\min_{X \in \mathbb{R}^{n \times r_{\text{search}}}} h(X) := f(X X^\top) = \frac{1}{2} \|\mathcal{A}(X X^\top) - b\|_2^2, \quad (\text{P1})$$

where $b = \mathcal{A}(Z Z^\top)$, and $\mathcal{A} : \mathbb{R}^{n \times n} \rightarrow \mathbb{R}^m$ is a known sensing operator defined as $\mathcal{A}(M) = [\langle A_1, M \rangle, \langle A_2, M \rangle, \dots, \langle A_m, M \rangle]^\top$, with symmetric sensing matrices $A_i \in \mathbb{R}^{n \times n}$. The notation $\langle A_i, M \rangle = \text{Tr}(A_i^\top M)$ denotes the Frobenius inner product. Throughout this paper, $\|\cdot\|_F$ and $\|\cdot\|_2$ represent the Frobenius norm and the spectral norm, respectively.

This formulation induces a non-convex landscape. It can represent general polynomial optimization problems [30] and is equivalent to training two-layer quadratic neural networks [31]. A basic example of a rank-1 MS problem from [32], which illustrates the structure of the objective, is given below:

Basic Example. Recover $M^* = z z^\top$ under the following setting:

$$z = \begin{bmatrix} 1 \\ 0 \end{bmatrix}, A_1 = \begin{bmatrix} 1 & 0 \\ 0 & 1/2 \end{bmatrix}, A_2 = \begin{bmatrix} 0 & \sqrt{3}/2 \\ \sqrt{3}/2 & 0 \end{bmatrix}, A_3 = \begin{bmatrix} 0 & 0 \\ 0 & \sqrt{3}/2 \end{bmatrix}. \quad (1)$$

One can verify that this non-convex landscape has a local minimum at $\hat{x} = (0, \pm 1/\sqrt{2})$, and the number of spurious solutions increases as loss landscape becomes more expressive. Consequently, BM-factorized MS problems provide a rich and analyzable *testbed* for evaluating our proposed escape mechanism. Figure 1 illustrates the example in Equation (1). The figure demonstrates how the optimization trajectories of SGD and our proposed escape method will traverse the landscape. Starting from random initializations, traditional SGD algorithm can become trapped inside attraction basins of spurious local minima, whereas our SOD step enables a direct jump out of these basins, landing near the ground truth M^* . This highlights the effectiveness of deterministic escape.

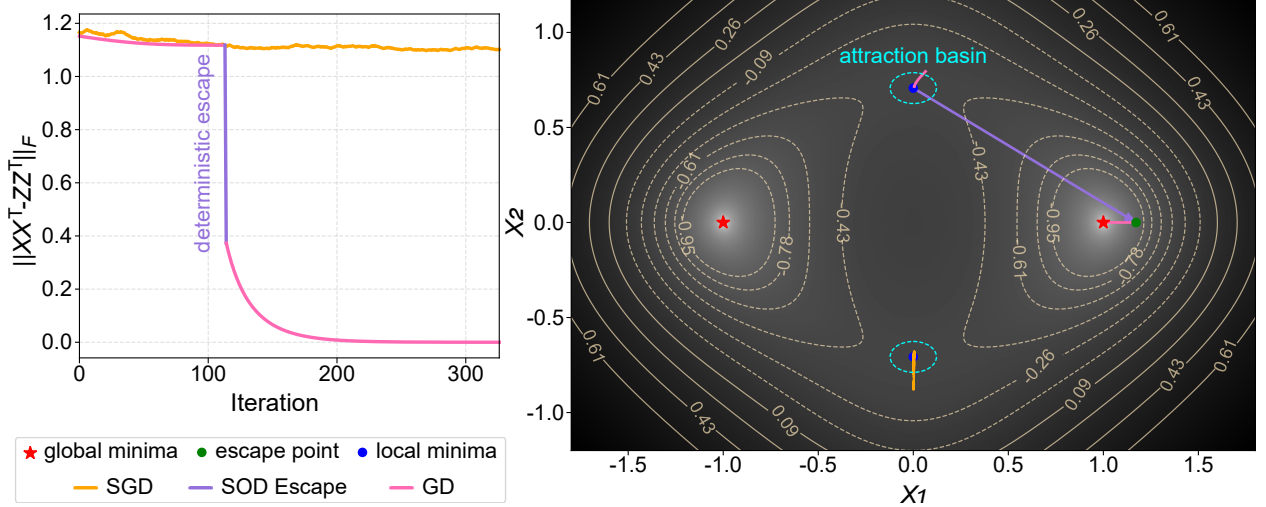


Figure 1: Escape behavior of the proposed SOD method from a spurious solution \hat{x} . Left: distance to the M^* versus iterations. Right: loss landscape (log-scaled contour map) and trajectories. SOD jumps from \hat{x} to \check{x} (green) and subsequent GD converges to M^* , whereas GD alone is trapped (blue) and SGD does not escape the basin within the iteration budget.

Short Preliminaries. Before we introduce the formal results of this work, we would like to first introduce some preliminary concepts and notations related to MS to facilitate understanding. In particular, the gradient of h w.r.t. $X \in \mathbb{R}^{n \times r_{\text{search}}}$ is given by

$$\nabla h(X) = 2\mathcal{A}^* \mathcal{A}(X X^\top - M^*) X = 2 \sum_{i=1}^m \langle A_i, X X^\top - M^* \rangle A_i X, \quad (2)$$

where $\mathcal{A}^* : \mathbb{R}^m \rightarrow \mathbb{R}^{n \times n}$ is the adjoint operator defined as $\mathcal{A}^*(y) = \sum_{i=1}^m y_i A_i$. Moreover, if $\nabla f(M) = \mathcal{A}^*(\mathcal{A}(M) - b)$ denotes the gradient of the matrix objective f , then the chain rule yields $\nabla h(X) = 2\nabla f(X X^\top) X$.

To analyze problem P1, a standard assumption in the MS literature is the Restricted Isometry Property (RIP) [33, 34].

Definition 1.1 (Restricted Isometry Property (RIP)). *A linear operator \mathcal{A} satisfies the δ_p -RIP for some $\delta_p \in [0, 1]$ if, for all symmetric matrices M with $\text{rank}(M) \leq p$, the following inequality holds:*

$$(1 - \delta_p) \|M\|_F^2 \leq \|\mathcal{A}(M)\|_2^2 \leq (1 + \delta_p) \|M\|_F^2. \quad (\text{RIP})$$

RIP implies that the linear measurement approximately preserves the Frobenius norm of all low-rank matrices. This assumption is satisfied by a wide range of random measurement operators [35]. A smaller RIP constant δ_p leads to a more benign optimization landscape for problem (P1), while larger values of δ_p (closer to 1) correspond to increasingly complicated loss surfaces often containing numerous spurious solutions [36]. Hence, deterministic (non-randomized, e.g. vanilla GD) algorithms may struggle to converge to the global optimum (as shown in Figure 1), namely the *ground-truth* matrix M^* .

1.2 Notation

Throughout the paper, we adopt the following notation. Lowercase Roman letters (e.g., a) denote scalars or vectors, depending on the context. Uppercase Roman letters (e.g., A) represent matrices. Bold lowercase and uppercase letters (e.g., \mathbf{a} , \mathbf{A}) indicate tensors. Calligraphic letters (e.g., \mathcal{A}) denote linear operators. Let $\hat{X} \in \mathbb{R}^{n \times r}$ be a local minimum of h , meaning that $\nabla h(\hat{X}) = 0$. Let the eigendecomposition of $\nabla f(\hat{X} \hat{X}^\top)$ be $\sum_{\varphi=1}^n \lambda_\varphi u_\varphi u_\varphi^\top$ where the eigenvalues are ordered as $\lambda_1 \geq \dots \geq \lambda_n$. Suppose \hat{X} has a thin singular value decomposition $\hat{X} = \sum_{\phi=1}^r \sigma_\phi v_\phi q_\phi^\top$ with singular values ordered $\sigma_1 \geq \dots \geq \sigma_r$. The first-order optimality condition implies that $u_n \perp v_\phi$ for all ϕ . We use the shorthand $\circ l$ for the l -fold Cartesian product, and write $[l] := \{1, \dots, l\}$. The symbol \otimes denotes the tensor (outer) product. For $Y \in \mathbb{R}^{n \times r}$, we let $\text{vec}(Y) \in \mathbb{R}^{nr}$ be its vectorization, and define the l -fold symmetric tensor power $\text{vec}(Y)^{\otimes l} \in \mathbb{R}^{nr \circ l}$. Conversely, for a tensor $\mathbf{v} \in \mathbb{R}^{(nr) \circ l}$, we denote by $\text{stack}(\mathbf{v}) \in \mathbb{R}^{nr l}$ its stacked vector form. The operators unvec and unstack are defined as the inverses of vec and stack , respectively.

2 Background and Related Work

2.1 Non-Convex Optimization and Escaping Spurious Solutions

Convex optimization admits a benign landscape in which every local minimum is global, enabling gradient-based methods to converge reliably under mild conditions [37, 38]. In contrast, non-convex optimization arises when the *objective function or feasible region* lacks convexity [1], typically inducing complex landscapes populated by multiple critical points (e.g. local minima and saddle points) [39]. Of particular concern are *spurious local minima*, namely second-order critical points that satisfy local optimality conditions but are suboptimal globally. Such spurious solutions are prevalent in structured problems such as matrix factorization [40], tensor decomposition [41], and neural network training [2], and pose a fundamental obstacle to reliable optimization.

Existing strategies for escaping spurious local minima fall into two main categories: probabilistic perturbation (Randomized) and rule-based adaptation (Heuristic). While both have achieved some success, their underlying mechanisms largely rely on repeated random trials or subjective estimates, motivating the development of more effective and fine-grained solutions.

Probabilistic perturbation injects randomness into optimization dynamics to destabilize stationary points. Beyond stochastic gradient descent (SGD), where minibatch sampling induces implicit gradient noise [42], several explicit variants have been proposed. SGLD [43] adds Gaussian noise to gradient updates to enable approximate posterior sampling, while Simulated Annealing [44] employs temperature-controlled noise with diminishing variance, theoretically guaranteeing infinite-time global convergence. Notably, Perturbed Gradient Descent [45] and its variants [46] inject isotropic noise near critical points to provably escape saddles in polynomial time. However, such noise injection provably degrades success rates due to disrupting deterministic gradient flow, often causing *oscillations* near local minima and poor global convergence [8].

Rule-based adaptation avoids explicit noise by heuristically modifying descent trajectories. Besides momentum-based optimizers such as Adam [47] and its decoupled weight decay variant [48], more sophisticated strategies have been proposed. The Barzilai-Borwein step size [49] adapts learning rates using historical gradient differences, while Nesterov's accelerated gradient [50] employs a lookahead mechanism to anticipate gradient changes. ALTO [51], extending L-BFGS with curvature thresholding [52], leverages approximate curvature information to efficiently traverse flatter regions. Despite strong empirical performance in specific regimes (e.g., accelerated progress through certain

landscape regions), these heuristic methods often lack theoretical guarantees and may introduce unintended side effects due to sensitivity to hyperparameters.

2.2 Typical Over-parameterization Methods in MS

Over-parameterization has recently emerged as a key paradigm in non-convex optimization [14]. By enlarging the parameter space beyond the problem's intrinsic degrees of freedom, it can reshape the loss landscape [53], often turning local minima into global minima or saddle points [19]. This effect resembles interpolation [54], smoothing the surface and improving the attainability of optimal solutions. Rank over-parameterization (i.e. $r_{\text{search}} > r$) under suitable RIP-type conditions can remove spurious solutions. For instance, [55] show that if $n > r_{\text{search}} > r[(1 + \delta_p)/(1 - \delta_p) - 1]^2/4$, then every solution X^* to (P1) satisfies $X^* X^{*\top} = M^*$. Analogous RIP-based guarantees for the ℓ_1 loss are given in [56]. Beyond increasing search rank, convex relaxation offers another form of over-parameterization by lifting the factorized variable ($O(nr)$ parameters) to a full matrix ($O(n^2)$ parameters) [34]. As shown in [7], when M^* has sufficiently high rank, the RIP threshold for exact recovery via semidefinite programming can approach 1, underscoring the strength of such lifted formulations. However, [57] reports that over-parameterization may make GD exponentially slower than in the exactly parameterized case, suggesting that these guarantees can be practically limited.

2.3 Tensor Over-Parameterization: Introduction and Foundational Results

[21, 22] introduce a tensor-based over-parameterization framework that lifts the original decision variable from a matrix to a higher-order tensor by embedding the matrix variable $X \in \mathbb{R}^{n \times r}$ into a higher-dimensional tensor space. Specifically, they define the lifted tensor as $\mathbf{w} = \text{vec}(X)^{\otimes l} \in \mathbb{R}^{n \times r \times \dots \times r}$, where l is the lifting order. To preserve the structure of the original matrix during lifting and recovery, a permutation tensor $\mathbf{P} \in \mathbb{R}^{n \times r \times \dots \times r}$ is introduced, satisfying the following identity for any $X \in \mathbb{R}^{n \times r}$:

$$\langle \mathbf{P}, \text{vec}(X) \rangle_3 = X \Rightarrow \mathbf{P}(\mathbf{w}) = \langle \mathbf{P}^{\otimes l}, \text{vec}(X)^{\otimes l} \rangle_{3*[[l]]} = X^{\otimes l} \in \mathbb{R}^{[n \times r]^{\otimes l}}, \quad (3)$$

where $\langle \cdot, \cdot \rangle_3$ denotes contraction along the third mode of \mathbf{P} , and $\langle \cdot, \cdot \rangle_{3*[[l]]}$ generalizes mode-wise contraction for order- l tensors. This mapping ensures that any X can be faithfully reconstructed from the tensor space using \mathbf{P} . The sensing operator \mathcal{A} is subsequently extended to the tensor domain to align with the lifted representation. Specifically, the original linear operator \mathcal{A} is first encoded as a third-order tensor $\mathbf{A} \in \mathbb{R}^{m \times n \times n}$, where $\mathbf{A}_{ijk} = (A_i)_{jk}$ for $i \in [m]$ and $(j, k) \in [n] \times [n]$. This tensorized form is then consistently lifted to $\mathbf{A}^{\otimes l}$, enabling it to operate on higher-order tensor variables in the lifted space.

By defining the reconstruction error as $f^l(\mathbf{M}) := \|\langle \mathbf{A}^{\otimes l}, \mathbf{M} \rangle - b^{\otimes l}\|_F^2$, where $\mathbf{M} \in \mathbb{R}^{[n \times n]^{\otimes l}}$ denotes a candidate tensor in the lifted space, the optimization problem is reformulated in the high-dimensional domain as:

$$\min_{\mathbf{w} \in \mathbb{R}^{n \times r \times \dots \times r}} h^l(\mathbf{w}) := f^l(\langle \mathbf{P}(\mathbf{w}), \mathbf{P}(\mathbf{w}) \rangle_{2*[[l]]}), \quad (\text{P2})$$

where $\langle \mathbf{P}(\mathbf{w}), \mathbf{P}(\mathbf{w}) \rangle_{2*[[l]]}$ performs contraction along modes $\{2, 4, \dots, 2l\}$, preserving the bilinear structure of the original matrix formulation. This reformulation enables the problem to be addressed within a higher-order tensor space, while maintaining a consistent mapping to the matrix domain (but only limited to the rank-1 tensor). The key theoretical results characterizing this lifted optimization problem are summarized as follows.

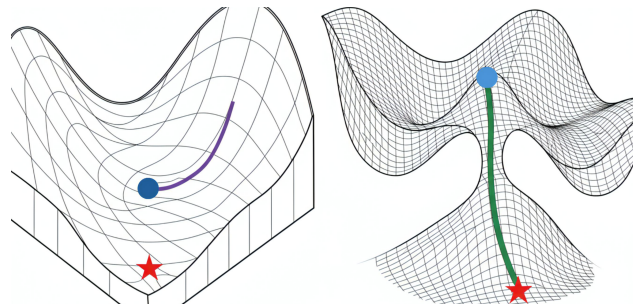


Figure 2: Comparison of optimization landscapes in matrix and tensor spaces. Left: in matrix space, GD (purple) becomes trapped at a local minimum (dark blue), away from the global minimum (red pentagram). Right: in tensor space, the corresponding point becomes a saddle (light blue), and GD (green) traverses it and converges to the global minimum. This schematic is illustrative; real landscapes are far more complex.

First, [21, Thm. 5.4] shows that tensor lifting with odd l reshapes the landscape: spurious local minima in the matrix space become strict saddle points in the tensor domain, and these saddles admit explicit rank-1 escape directions of the form $\text{vec}(u_n q_r^\top)^{\otimes l}$. Ideally, one would preserve a rank-1 structure to enable a clean, interpretable projection back to the matrix space; however, due to the superposition effect discussed in Section 1, even an infinitesimal step along a rank-1 direction typically produces a rank-2 tensor. This difficulty is alleviated by [22, Thm. 1], which reveals an implicit-regularization phenomenon for GD in the tensor space: along the trajectory, iterates tend to be approximately rank-1. Motivated by this, we can extract the dominant rank-1 component and operate projection to obtain an escape matrix \check{X} . Figure 2 visualizes this geometric transformation and the benefits of tensor lifting.

3 Main Results

Tensor over-parameterization lifts a matrix-space local minimum \hat{X} to the tensor $\hat{\mathbf{w}} := \text{vec}(\hat{X})^{\otimes l}$, incurring an exponential increase in dimension and making gradient-based optimization in the lifted space computationally prohibitive. To circumvent this cost, our main theorem constructs an escape point \check{X} directly in the original matrix space by moving along the oracle escape direction $\text{vec}(u_n q_r^\top)^{\otimes l}$ and emulating the tensor-space gradient dynamics without explicitly optimizing in the tensor domain. For notational convenience, define $E := \mathcal{A}^* \mathcal{A}(u_n v_r^\top + v_r u_n^\top) \in \mathbb{R}^{n \times n}$, and introduce the post-escape tensor

$$\mathbf{w}_{\text{escape}} := \hat{\mathbf{w}} + \rho \text{vec}(u_n q_r^\top)^{\otimes l}, \quad \text{escape step size } \rho > 0, \quad (4)$$

where $\lambda_n < 0$, u_n are the smallest eigenvalue and eigenvector of $\nabla f(\hat{X} \hat{X}^\top)$, and σ_r, v_r, q_r are the smallest nonzero singular value and corresponding singular vectors of \hat{X} (see Section 1.2, notation introduction). The matrix E implicitly encodes the "invisible" escape information available in the matrix space. The rank-2 tensor $\mathbf{w}_{\text{escape}}$ corresponds to a one-step simulation of the lifted escape in Section 4, and it also serves as the initialization $\tilde{\mathbf{w}}^{(0)}$ for the multi-step simulation in Section 5.

3.1 Single-step SOD Escape Mechanism

This SOD escape mechanism directly collapses the tensor-space point $\mathbf{w}_{\text{escape}}$ back into the matrix space. This involves the following three components: 1) identifying a rank-1 tensor that closely approximates $\mathbf{w}_{\text{escape}}$ under a suitable norm, i.e., ensuring $\|\text{vec}(\check{X})^{\otimes l} - \mathbf{w}_{\text{escape}}\|$ approaches zero; 2) determining the conditions under which the \check{X} can successfully escape the attraction basin of \hat{X} ; 3) establishing when such conditions are satisfied. These lead to the following Thm. 3.1.

We study the condition $\text{EFS} > 1$ for single-step SOD escape under a symmetric Gaussian sensing ensemble (see Equation (11)). As illustrated in Figure 3, the parameter space is partitioned by two radii r_1 and r_2 into three regimes: outside r_2 , escape is guaranteed; inside r_1 , escape is impossible; and between them, escape occurs with a probability that depends on both the sensing realization and the distance $\|\hat{X} \hat{X}^\top - ZZ^\top\|_F$. Overall, when aggregating the latter two regimes, we show in Section 4.3 that $\mathbb{P}(\text{EFS} > 1) < 1/3$, implying that single-step SOD escape is unlikely in many MS instances. This limitation fundamentally arises from the irreducible mismatch between the rank-2 escape tensor $\mathbf{w}_{\text{escape}}$ and its rank-1 approximation $\text{vec}(\check{X})^{\otimes l}$ under the tensor spectral norm, which incurs a non-negligible approximation error.

Theorem 3.1 (Single-step SOD Escape, informal). *Consider the problem of escaping from a local minimum \hat{X} of the objective function (P1). Define the EFS as follows:*

$$\text{EFS} = \frac{-\lambda_n}{\sigma_r^2(1 + \delta_p)} + \frac{\langle E, u_n u_n^\top \rangle^2}{2(1 + \delta_p)^2}, \quad E := \mathcal{A}^* \mathcal{A}(u_n v_r^\top + v_r u_n^\top) \in \mathbb{R}^{n \times n},$$

where $(\lambda_n < 0, u_n), (\sigma_r, v_r, q_r)$ are the eigenpair and singular value-vector triples of $\nabla f(\hat{X} \hat{X}^\top)$ and \hat{X} , respectively.

If $\text{EFS} > 1$, then the matrix $\check{X} = \hat{X} + \hat{\rho} u_n q_r^\top$ serves as a valid escape point, i.e., $h(\check{X}) < h(\hat{X})$. The point \check{X} is capable of escaping the attraction basin of \hat{X} , provided that $\hat{\rho}$ lies in the interval $\hat{\rho}_1 < \hat{\rho} < \hat{\rho}_2$, where

$$\hat{\rho}_1, \hat{\rho}_2 := \frac{-\sigma_r \langle E, u_n u_n^\top \rangle}{(1 + \delta_p)} \mp \sigma_r \sqrt{2(\text{EFS} - 1)}.$$

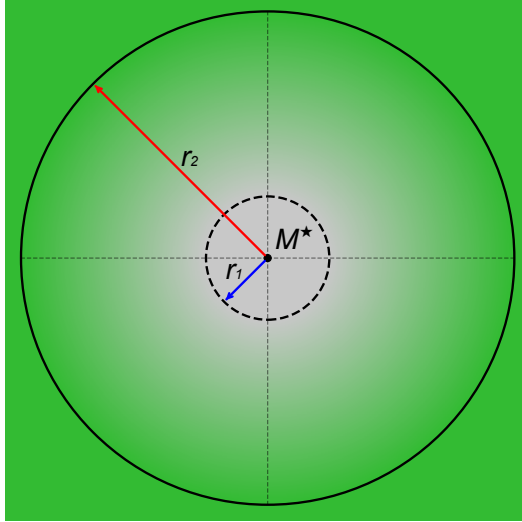


Figure 3: Visualization of escape regions (concentric circles) with EFS zones. The radius of the inner circle is r_1 , defined in Equation (14), and the radius of the outer circle is r_2 , defined in Equation (13). The greener the region, the higher the probability $\mathbb{P}(\text{EFS} > 1)$.

3.2 Multi-step SOD Escape Mechanism

The goal of SOD escape is to identify a tensor along the lifted trajectory that admits a well-structured matrix correspondence. As discussed above, when $\text{EFS} > 1$, a single step from the saddle point $\tilde{\mathbf{w}}$ can be directly projected back into the matrix space. However, this behavior does not occur universally across all MS instances, necessitating more robust projection strategies. To address this, we simulate multiple steps within the tensor space while maintaining control over the trajectory to ensure that it remains easily projectable. This simulated algorithm is referred to as TPGD (see Section 5). Due to the implicit regularization in [22, Thm. 1], this iterative process gradually promotes an approximately rank-1 structure. Ultimately, this leads to a well-defined matrix escape point \hat{X} in the original space. We summarize the key results above.

Theorem 3.2 (Multi-step SOD Escape, informal). *Consider the goal of escaping from a local minima \hat{X} of (P1). Given constants $1 > \rho, \eta > 0$ and a sufficiently large odd integer $l \geq 3$ (representing order of simulated lifting), there exist two disjoint sets $U_\beta, U_\gamma \subset \mathbb{R}$ with $\sup U_\beta < \inf U_\gamma$ corresponding to two deterministic points of escape from \hat{X} :*

$$\begin{aligned} \check{X} &= \left\{ \rho^{1/l} (1 - \eta \lambda_n^l)^{t/l} \right\} \cdot u_n q_r^\top \quad \text{with } t \in U_\beta & (\beta\text{-type}) \\ \check{X} &= \left\{ -\frac{1}{2} (2\eta\rho)^{1/l} \left[\sum_{\tau=0}^{t-1} (1 - \eta \lambda_n^l)^\tau \right]^{1/l} \sigma_r \right\} E \hat{X} \quad \text{with } t \in U_\gamma & (\gamma\text{-type}) \end{aligned}$$

such that both escape points are guaranteed to yield lower objective values, i.e., $h(\check{X}) < h(\hat{X})$, where $E := \mathcal{A}^* \mathcal{A} (u_n v_r^\top + v_r u_n^\top) \in \mathbb{R}^{n \times n}$ and $(\lambda_n < 0, u_n), (\sigma_r, v_r, q_r)$ are the eigenpair and singular value-vector triples of $\nabla f(\hat{X} \hat{X}^\top)$ and \hat{X} , respectively. While both \check{X} are easy to compute, the β -type escape point has a simpler form but higher requirement on numerical precision when l is large, whereas the γ -type escape point has a complicated form but is more numerically stable.

One of the main issues in choosing between the β -type and γ -type escape points is that the choice depends on the values of both t and l ; this dependence is best understood by examining the trajectory of the simulated TPGD algorithm. Although the detailed description of TPGD is deferred to Algorithm 1, we provide a high-level overview here. At each iteration t , the iterate $\tilde{\mathbf{w}}^{(t)}$ admits a closed-form decomposition into three structured components, $\tilde{\mathbf{w}}^{(t)} = \tilde{\alpha}^{(t)} \mathbf{a} + \tilde{\beta}^{(t)} \mathbf{b} + \tilde{\gamma}^{(t)} \mathbf{c}$, as characterized in Equation (16) and Equation (23). The two multi-step escape mechanisms correspond to distinct dominant components in this decomposition. Specifically, the β -type escape arises

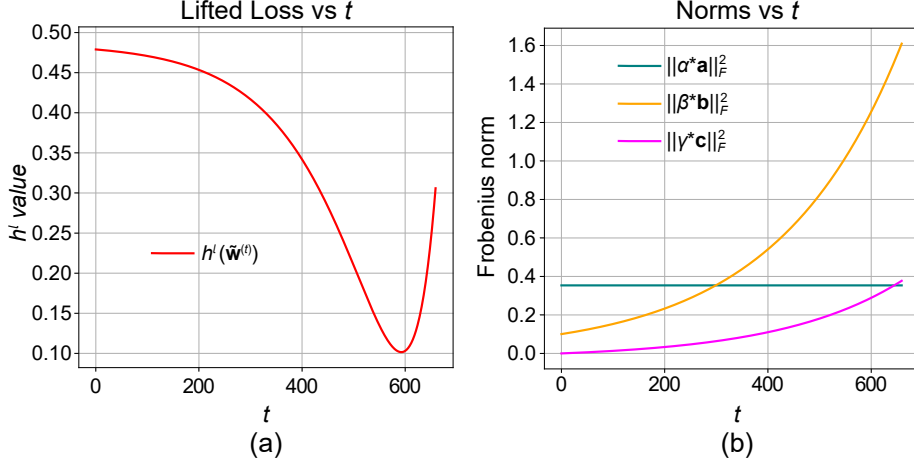


Figure 4: Simulation of the TPGD trajectory in a basic example. (a) Evolution of the lifted objective value $h^l(\tilde{\mathbf{w}}^{(t)})$ as a function of the iteration count t . The objective decreases in the early stage, while for sufficiently large t , truncation errors accumulate and eventually lead to an increase in the objective value. (b) Norms of the three components in the decomposition of $\tilde{\mathbf{w}}^{(t)}$. As t increases, the \mathbf{b} -term exhibits clear norm separation from the \mathbf{a} - and \mathbf{c} -terms, indicating the emergence of a β -type escape direction.

when the \mathbf{b} -term becomes dominant, i.e., when $\|\tilde{\beta}^{(t)}\mathbf{b}\|$ separates from the other two terms. Projecting this dominant direction back to the matrix space yields \check{X} with $t \in U_\beta$. Analogously, the γ -type escape corresponds to dominance of the \mathbf{c} -term, whose projection induces \check{X} with $t \in U_\gamma$. The complementary dependence of these two regimes on l and t is illustrated in Figure 7.

From an algorithmic perspective, a practical criterion for identifying a valid escape point is as follows. During the simulated TPGD trajectory, if (1) either the \mathbf{b} -term or the \mathbf{c} -term exhibits clear norm separation from the remaining components, and (2) the corresponding projected point \check{X} satisfies $h^l(\text{vec}(\check{X})^{\otimes l}) \approx h^l(\tilde{\mathbf{w}}^{(t)}) < h^l(\hat{\mathbf{w}})$, then \check{X} can be regarded as a valid multi-step SOD escape candidate after safely projection. This behavior is empirically demonstrated in Figure 4 by adopting basic example in Equation 1.

4 Single-step SOD Escape (Special Case)

We first examine the single-step version, which clearly demonstrates the fundamental ideas and introduces the essential quantities. The proofs of Thm. 3.1 can be summarized in the following sketch:

- We first show that the rank-2 tensor $\mathbf{w}_{\text{escape}}$ defined in Equation (4) admits a rank-1 approximation under the tensor spectral norm, i.e.
$$\|\text{vec}(\check{X})^{\otimes l} - \mathbf{w}_{\text{escape}}\|_{S \otimes R} \rightarrow 0, \quad \text{where } \check{X} = \hat{X} + \hat{\rho}u_nq_r^\top, \quad \exists \hat{\rho} > 0.$$
- By analyzing the descent condition $h(\check{X}) < h(\hat{X})$, we derive a constraint on the admissible range of $\hat{\rho}$, motivating the definition of the *Escape Feasibility Score* (EFS). $\text{EFS} > 1$ certifies the existence of a valid escape direction.
- Assuming that the linear measurement operator \mathcal{A} is drawn from a Gaussian ensemble, we then conduct a probabilistic analysis of the event $\mathbb{P}(\text{EFS} > 1)$ to quantify the likelihood of successful escape.

4.1 Rank-1 Approximation for Single-step Escape

Proposition 4.1 (Closed-form Structure of Single-step SOD Point \check{X}). *The strict rank-1 tensor $\text{vec}(\check{X})^{\otimes l}$, which serves as a spectral-norm approximation of the tensor-space escape point $\mathbf{w}_{\text{escape}}$ within the subspace*

$$R := \text{span} \{ \text{vec}(u_nq_r^\top)^{\otimes l}, \text{vec}(v_rq_r^\top)^{\otimes l} \}, \quad (5)$$

has the closed-form representation

$$\check{X} = \sum_{\phi=1}^{r-1} \sigma_\phi v_\phi q_\phi^\top + \sigma_r(\beta u_n + \alpha v_r)q_r^\top. \quad (6)$$

The approximation error measured by the tensor spectral norm satisfies

$$\|\text{vec}(\check{X})^{\otimes l} - \mathbf{w}_{\text{escape}}\|_{S \bowtie R} \rightarrow 0, \quad \text{if } \sigma_r^l \beta^l \rightarrow \rho \text{ and } \alpha^l \rightarrow 1, \quad (7)$$

where $\|\cdot\|_{S \bowtie R}$ denotes the tensor spectral norm with projection onto R .

The proof proceeds as follows. We first show that $\check{\mathbf{w}}$ approximates $\mathbf{w}_{\text{escape}}$ along the projection directions $\text{vec}(u_n q_r^\top)^{\otimes l}$ and $\text{vec}(v_r q_r^\top)^{\otimes l}$, respectively. We then demonstrate that these components lie approximately within the tensor subspace R spanned by these two orthonormal directions. Consequently, the approximation is valid under the tensor spectral norm within R .

Proof. We begin by examining two key projection directions that characterize the approximation structure.

Orthogonality Between Tensor Projection Directions. Using first-order optimality condition, we have $u_n \perp v_\phi$ for all $\phi = 1, \dots, r$ and this yields:

$$\text{vec}(u_n q_r^\top)^{\otimes l} \perp \text{vec}(v_r q_r^\top)^{\otimes l}.$$

Such two tensors thus form orthogonal basis vectors in the spectral subspace R , providing the foundation for subsequent analysis of the rank-1 approximation.

Approximation in the Projection Direction of $\text{vec}(u_n q_r^\top)^{\otimes l}$. To establish this result, we evaluate the approximation condition:

$$\langle \text{vec}(\check{X})^{\otimes l}, \text{vec}(u_n q_r^\top)^{\otimes l} \rangle \rightarrow \langle \hat{\mathbf{w}} + \rho \text{vec}(u_n q_r^\top)^{\otimes l}, \text{vec}(u_n q_r^\top)^{\otimes l} \rangle.$$

This is equivalent to approximating $\langle \check{X}^{\otimes l}, (u_n q_r^\top)^{\otimes l} \rangle$ by $\langle \hat{X}^{\otimes l} + \rho(u_n q_r^\top)^{\otimes l}, (u_n q_r^\top)^{\otimes l} \rangle$. By substituting the expression of \check{X} and using Lem. A.5, we obtain:

$$\langle \check{X}^{\otimes l}, (u_n q_r^\top)^{\otimes l} \rangle = \text{Tr} \left\{ \left[\sum_{\phi=1}^{r-1} \sigma_\phi v_\phi q_\phi^\top + \sigma_r (\alpha v_r + \beta u_n) q_r^\top \right] q_r u_n^\top \right\}^l = \text{Tr} \{ \sigma_r (\alpha v_r + \beta u_n) u_n^\top \}^l = \sigma_r^l \beta^l.$$

Similarly, we compute:

$$\langle \hat{X}^{\otimes l} + \rho(u_n q_r^\top)^{\otimes l}, (u_n q_r^\top)^{\otimes l} \rangle = \text{Tr}(\hat{X} q_r u_n^\top)^l + \rho \text{Tr}(u_n q_r^\top q_r u_n^\top)^l = \rho.$$

Therefore, to satisfy the approximation condition, it must hold that $\sigma_r^l \beta^l \rightarrow \rho$.

Approximation in the Projection Direction of $\text{vec}(v_r q_r^\top)^{\otimes l}$. The condition for this approximation can be derived through a similar argument, which leads to $\alpha^l \rightarrow 1$. Since l is odd (see [21, Thm. 5.4]), it follows that $\alpha \rightarrow 1$.

Approximation Guarantee in Terms of Tensor Spectral Norm. We now present the formal proof of Prop. 4.1. Define the residual tensor \mathbf{d}_p as:

$$\mathbf{d}_p := \text{vec}(\check{X})^{\otimes l} - [\hat{\mathbf{w}} + \rho \text{vec}(u_n q_r^\top)^{\otimes l}].$$

By the definitions of the tensor spectral norm and nuclear norm (see Defin. A.6), and since u_n, v_r , and q_r are unit vectors, we have:

$$\|\text{vec}(u_n q_r^\top)^{\otimes l}\|_* = \|\text{vec}(v_r q_r^\top)^{\otimes l}\|_* = 1.$$

Let $\mathbf{d}_s \in R$ be the dual tensor defined in Lem. A.7 which satisfies the conditions given in [22, Lem. 10], and:

$$\|\mathbf{d}_p\|_{S \bowtie R} = |\langle \mathbf{d}_p, \mathbf{d}_s \rangle|, \quad \|\mathbf{d}_s\|_* \leq 1, \quad \mathbf{d}_s \in \mathbb{R}^{n \times r \times l}.$$

Since $\text{vec}(u_n q_r^\top)^{\otimes l}$ and $\text{vec}(v_r q_r^\top)^{\otimes l}$ form an orthogonal basis of R , \mathbf{d}_s must belong to their span. Therefore, there exist scalars λ_{u_n} and λ_{v_r} such that:

$$\mathbf{d}_s = \lambda_{u_n} \text{vec}(u_n q_r^\top)^{\otimes l} + \lambda_{v_r} \text{vec}(v_r q_r^\top)^{\otimes l}, \quad \text{with } |\lambda_{u_n}| + |\lambda_{v_r}| \leq 1.$$

Using the approximation results along the projection directions $\text{vec}(u_n q_r^\top)^{\otimes l}$ and $\text{vec}(v_r q_r^\top)^{\otimes l}$, we compute:

$$\begin{aligned} \langle \mathbf{d}_p, \mathbf{d}_s \rangle &= \langle \text{vec}(\check{X})^{\otimes l} - [\hat{\mathbf{w}} + \rho \text{vec}(u_n q_r^\top)^{\otimes l}], \lambda_{u_n} \text{vec}(u_n q_r^\top)^{\otimes l} + \lambda_{v_r} \text{vec}(v_r q_r^\top)^{\otimes l} \rangle \\ &= \lambda_{u_n} \langle \text{vec}(\check{X})^{\otimes l} - [\hat{\mathbf{w}} + \rho \text{vec}(u_n q_r^\top)^{\otimes l}], \text{vec}(u_n q_r^\top)^{\otimes l} \rangle + \lambda_{v_r} \langle \text{vec}(\check{X})^{\otimes l} - [\hat{\mathbf{w}} + \rho \text{vec}(u_n q_r^\top)^{\otimes l}], \text{vec}(v_r q_r^\top)^{\otimes l} \rangle \\ &= \lambda_{u_n} (\sigma_r^l \beta^l - \rho) + \lambda_{v_r} \sigma_r^l (\alpha^l - 1). \end{aligned}$$

Thus, the spectral norm of \mathbf{d}_p is bounded by:

$$\|\mathbf{d}_p\|_{S \bowtie R} = |\langle \mathbf{d}_p, \mathbf{d}_s \rangle| \leq |\lambda_{u_n}| \cdot |\sigma_r^l \beta^l - \rho| + |\lambda_{v_r}| \cdot \sigma_r^l \cdot |\alpha^l - 1|.$$

As $\text{vec}(\check{X})^{\otimes l}$ becomes aligned with $\text{vec}(u_n q_r^\top)^{\otimes l}$ and $\text{vec}(v_r q_r^\top)^{\otimes l}$, we have $\sigma_r^l \beta^l \rightarrow \rho$ and $\alpha^l \rightarrow 1$, yielding $\|\mathbf{d}_p\|_{S \bowtie R} \rightarrow 0$. This concludes the proof. \square

Remark 4.2. Prop. 4.1 indicates that the appropriate rank-1 approximation to be further explored takes the form $\text{vec}(\check{X})^{\otimes l}$, where

$$\check{X} = \sum_{\phi=1}^{r-1} \sigma_{\phi} v_{\phi} q_{\phi}^{\top} + \sigma_r \left(\frac{\rho^{1/l}}{\sigma_r} u_n + v_r \right) q_r^{\top} = \hat{X} + \rho^{1/l} u_n q_r^{\top} := \hat{X} + \hat{\rho} u_n q_r^{\top}.$$

4.2 Escape Inequality and Escape Feasibility Score

Proposition 4.3. Let the single-step SOD escape point be defined as

$$\check{X} := \hat{X} + \hat{\rho} u_n q_r^{\top}, \quad \text{where } \hat{\rho} > 0 \text{ is the escape step amplitude.}$$

Then, a necessary condition for achieving descent, i.e., $h(\check{X}) < h(\hat{X})$, is that $\hat{\rho}$ satisfies the following quadratic escape inequality:

$$(1 + \delta_p) \hat{\rho}^2 + 2\sigma_r \langle E, u_n u_n^{\top} \rangle \hat{\rho} + 2\sigma_r^2 (1 + \delta_p) + 2\lambda_n < 0. \quad (8)$$

Proof. Our goal is to establish that $\|\mathcal{A}(\hat{X} \hat{X}^{\top} - M^{\star})\|_2^2 > \|\mathcal{A}(\check{X} \check{X}^{\top} - M^{\star})\|_2^2$, which can be rewritten as

$$\langle \mathcal{A}^* \mathcal{A}(\hat{X} \hat{X}^{\top} - M^{\star}), \hat{X} \hat{X}^{\top} - M^{\star} \rangle > \langle \mathcal{A}^* \mathcal{A}(\check{X} \check{X}^{\top} - M^{\star}), \check{X} \check{X}^{\top} - M^{\star} \rangle.$$

Since the gradient vanishes at \hat{X} , we have $\mathcal{A}^* \mathcal{A}(\hat{X} \hat{X}^{\top} - M^{\star}) \hat{X} = 0$. Thus,

$$\underbrace{\langle \mathcal{A}^* \mathcal{A}(\check{X} \check{X}^{\top} - \hat{X} \hat{X}^{\top}), M^{\star} \rangle}_{:=S} > \underbrace{\langle \mathcal{A}^* \mathcal{A}(\check{X} \check{X}^{\top} - M^{\star}), \check{X} \check{X}^{\top} \rangle}_{:=T}. \quad (9)$$

From the definition $\check{X} = \hat{X} + \hat{\rho} u_n q_r^{\top}$, it follows that

$$\begin{aligned} \check{X} \check{X}^{\top} &= [\hat{X} + \hat{\rho}(u_n q_r^{\top})][\hat{X} + \hat{\rho}(u_n q_r^{\top})]^{\top} = [\hat{X} + \hat{\rho}(u_n q_r^{\top})][\hat{X}^{\top} + \hat{\rho}(q_r u_n^{\top})] \\ &= \hat{X} \hat{X}^{\top} + \hat{\rho} \hat{X} q_r u_n^{\top} + \hat{\rho} u_n q_r^{\top} \hat{X}^{\top} + \hat{\rho}^2 u_n q_r^{\top} q_r u_n^{\top} \\ &= \hat{X} \hat{X}^{\top} + \hat{\rho} \sigma_r (v_r u_n^{\top} + u_n v_r^{\top}) + \hat{\rho}^2 u_n u_n^{\top}, \end{aligned}$$

where we have used $\hat{X} q_r = \sigma_r v_r$ and $q_r^{\top} \hat{X}^{\top} = \sigma_r v_r^{\top}$. Substituting this decomposition into Equation (9), we proceed with term-by-term expansion.

Expansion of S Term. The S term decomposes as

$$\begin{aligned} S &= \langle \mathcal{A}^* \mathcal{A}(\hat{X} \hat{X}^{\top} + \hat{\rho} \sigma_r (v_r u_n^{\top} + u_n v_r^{\top}) + \hat{\rho}^2 u_n u_n^{\top} - \hat{X} \hat{X}^{\top}), M^{\star} \rangle \\ &= \underbrace{\hat{\rho} \sigma_r \langle E, M^{\star} \rangle}_{:=S_1} + \underbrace{\hat{\rho}^2 \langle \mathcal{A}^* \mathcal{A}(u_n u_n^{\top}), M^{\star} \rangle}_{:=S_2}. \end{aligned}$$

Expansion of T Term. The T term decomposes as a sum of nine interactions:

$$\begin{aligned} T &= \underbrace{\langle \mathcal{A}^* \mathcal{A}(\hat{X} \hat{X}^{\top} - M^{\star}), \hat{X} \hat{X}^{\top} \rangle}_{:=T_1} + \underbrace{\langle \mathcal{A}^* \mathcal{A}(\hat{X} \hat{X}^{\top} - M^{\star}), \hat{\rho} \sigma_r (v_r u_n^{\top} + u_n v_r^{\top}) \rangle}_{:=T_2} \\ &\quad + \underbrace{\langle \mathcal{A}^* \mathcal{A}(\hat{\rho} \sigma_r (v_r u_n^{\top} + u_n v_r^{\top})), \hat{\rho} \sigma_r (v_r u_n^{\top} + u_n v_r^{\top}) \rangle}_{:=T_5} + \underbrace{\langle \mathcal{A}^* \mathcal{A}(\hat{\rho}^2 u_n u_n^{\top}), \hat{\rho}^2 u_n u_n^{\top} \rangle}_{:=T_9} \\ &\quad + \underbrace{\langle \mathcal{A}^* \mathcal{A}(\hat{\rho} \sigma_r (v_r u_n^{\top} + u_n v_r^{\top})), \hat{\rho}^2 u_n u_n^{\top} \rangle}_{:=T_6} + \underbrace{\langle \mathcal{A}^* \mathcal{A}(\hat{\rho}^2 u_n u_n^{\top}), \hat{\rho} \sigma_r (v_r u_n^{\top} + u_n v_r^{\top}) \rangle}_{:=T_8} \\ &\quad + \underbrace{\langle \hat{\rho} \sigma_r E, \hat{X} \hat{X}^{\top} \rangle}_{:=T_4} + \underbrace{\langle \mathcal{A}^* \mathcal{A}(\hat{\rho}^2 u_n u_n^{\top}), \hat{X} \hat{X}^{\top} \rangle}_{:=T_7} + \underbrace{\langle \mathcal{A}^* \mathcal{A}(\hat{X} \hat{X}^{\top} - M^{\star}), \hat{\rho}^2 u_n u_n^{\top} \rangle}_{:=T_3}. \end{aligned}$$

Subcomponent Analysis. Using first-order optimality and orthogonality properties, we summarize the simplifications in Table 2.

Table 2: Simplified expressions of all subterms.

Term	Simplified Expression
T_1	$\nabla f(\hat{X}\hat{X}^\top)\hat{X}\hat{X}^\top = 0$
T_2	$2\hat{\rho}\sigma_r\lambda_nv_r^\top u_n = 0$
T_5	$\hat{\rho}^2\sigma_r^2\ \mathcal{A}(v_ru_n^\top + u_nv_r^\top)\ _2^2$
T_9	$\hat{\rho}^4\ \mathcal{A}(u_nu_n^\top)\ _2^2$
$T_6 + T_8$	$2\hat{\rho}^3\sigma_r\langle E, u_nu_n^\top \rangle$
$S_1 - T_4$	$-\hat{\rho}\sigma_r\langle \nabla f(\hat{X}\hat{X}^\top), v_ru_n^\top + u_nv_r^\top \rangle = 0$
$S_2 - T_7$	$-\hat{\rho}^2\langle \nabla f(\hat{X}\hat{X}^\top), u_nu_n^\top \rangle = -\hat{\rho}^2\lambda_n$
$-T_3$	$-\hat{\rho}^2\langle \nabla f(\hat{X}\hat{X}^\top), u_nu_n^\top \rangle = -\hat{\rho}^2\lambda_n$

Derivation of the Escape Inequality. Combining all corresponding terms yields

$$(S_1 - T_4) + (S_2 - T_7) + (-T_3) > T_1 + T_2 + T_5 + (T_6 + T_8) + T_9 \\ \Rightarrow -2\lambda_n > \sigma_r^2 \|\mathcal{A}(v_r u_n^\top + u_n v_r^\top)\|_2^2 + 2\hat{\rho}\sigma_r \langle E, u_n u_n^\top \rangle + \hat{\rho}^2 \|\mathcal{A}(u_n u_n^\top)\|_2^2.$$

Applying the RIP condition gives the strengthened inequality:

$$-2\lambda_n > 2\sigma_r^2(1 + \delta_p) + 2\hat{\rho}\sigma_r\langle E, u_n u_n^\top \rangle + (1 + \delta_p)\hat{\rho}^2,$$

where $\|u_n v_r^\top + v_r u_n^\top\|_F^2 = 2$ and $\|u_n u_n^\top\|_F^2 = 1$ are used. This directly corresponds to the quadratic form in $\hat{\rho}$ stated in Prop. 4.3, concluding the proof. \square

Note that the escape inequality takes the form of a quadratic equation in $\hat{\rho}$. Since $1 + \delta_p > 0$, the corresponding parabola opens upward. The constant term $2\sigma_r^2(1 + \delta_p) + 2\lambda_n > 0$ holds according to [58, Lem. 2]. Therefore, a valid real-valued solution for $\hat{\rho}$ exists if the discriminant of Equation (8) is positive:

$$0 < \Delta := 4\sigma_r^2 \langle E, u_n u_n^\top \rangle^2 - 4(1 + \delta_p)[2\sigma_r^2(1 + \delta_p) - 2(-\lambda_n)].$$

Rearranging the inequality yields that an escape is feasible when the *Escape Feasibility Score* (EFS) exceeds one. The EFS is defined as follows.

Definition 4.4 (Escape Feasibility Score (EFS)).

$$\underbrace{\frac{-\lambda_n}{\sigma_r^2(1+\delta_p)}}_{:=\text{NCM}} + \underbrace{\frac{1}{2(1+\delta_p)^2} \langle E, u_n u_n^\top \rangle^2}_{:=\text{AIC}} \quad (\text{EFS})$$

As shown in Defin. 4.4, the EFS consists of two components: the Negative Curvature Margin (NCM) and the Alignment-Induced Curvature (AIC). NCM quantifies the ratio between the smallest eigenvalue λ_n ($\lambda_n < 0$) of $\nabla f(\hat{X}\hat{X}^\top)$ and the smallest non-zero eigenvalue σ_r^2 of $\hat{X}\hat{X}^\top$. AIC characterizes the alignment between the hidden escape direction matrix E and the rank-1 projection matrix $u_n u_n^\top$ formed from λ_n 's eigenvector u_n . Next, we verify Thm. 3.1.

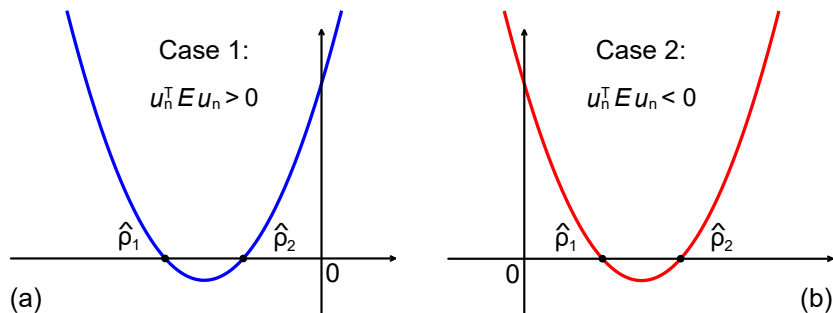


Figure 5: Visualization of quadratic inequality (8).

Proof. We now proceed to prove the deterministic part of Thm. 4.6 (as well as Thm. 3.1). When the computed EFS value exceeds one, the discriminant satisfies $\Delta > 0$, which guarantees that a real-valued $\hat{\rho}$ exists, leading to deterministic escape from the local minimum.

We define the two roots of the quadratic equation (8) as

$$\hat{\rho}_1 := \frac{-2\sigma_r \langle E, u_n u_n^\top \rangle - \sqrt{\Delta}}{2(1 + \delta_p)}, \quad \hat{\rho}_2 := \frac{-2\sigma_r \langle E, u_n u_n^\top \rangle + \sqrt{\Delta}}{2(1 + \delta_p)}. \quad (10)$$

As depicted in Figure 5, two distinct cases emerge based on the sign of the inner product $u_n^\top E u_n$:

- **Case 1:** If $\langle E, u_n u_n^\top \rangle > 0$, then any $\hat{\rho}$ satisfying $\hat{\rho}_1 < \hat{\rho} < \hat{\rho}_2 < 0$ leads to successful escape from $-\hat{X}$ via the update $\check{X} = -\hat{X} + \hat{\rho} u_n q_r^\top$.
- **Case 2:** If $\langle E, u_n u_n^\top \rangle < 0$, then any $\hat{\rho}$ satisfying $0 < \hat{\rho}_1 < \hat{\rho} < \hat{\rho}_2$ enables successful escape from \hat{X} via the update $\check{X} = \hat{X} + \hat{\rho} u_n q_r^\top$.

This completes the proof. \square

4.3 Probabilistic Escape Analysis

4.3.1 Gaussian Ensemble Modeling

Consider independent symmetric measurement matrices $\{A_i\}_{i=1}^m$ drawn from a Gaussian ensemble, which is frequently applied in RIP-related proofs [35]:

$$(A_i)_{jk} \sim \begin{cases} \mathcal{N}(0, m^{-1}), & j = k, \\ \mathcal{N}(0, (2m)^{-1}), & j < k, \end{cases} \quad \text{and} \quad (A_i)_{jk} = (A_i)_{kj} \quad \forall j \neq k \quad (11)$$

This choice ensures that, for arbitrary $M \in \mathbb{R}^{n \times n}$ we have $\mathbb{E}[\|\mathcal{A}(M)\|_2^2] = \|M\|_F^2$. Let $P = u_n v_r^\top + v_r u_n^\top$, $Q = u_n u_n^\top$, $\psi_i = \langle A_i, P \rangle$ and $\omega_i = \langle A_i, Q \rangle$. The AIC term in the EFS is determined by the squared correlation sum:

$$\text{AIC} = \frac{1}{2(1 + \delta_p)^2} S_{\mathcal{A}}^2(P, Q), \quad \text{where } S_{\mathcal{A}}(P, Q) := \sum_{i=1}^m \psi_i \omega_i.$$

The Gaussian ensemble is zero-mean, i.e. $\mathbb{E}[\psi_i] = \mathbb{E}[\omega_i] = 0$. By linearity of expectation and the orthogonality of P and Q , we obtain

$$\mathbb{E}[S_{\mathcal{A}}(P, Q)] = m \cdot \mathbb{E}[\langle A, P \rangle \langle A, Q \rangle] = m \cdot m^{-1} \langle P, Q \rangle = \langle P, Q \rangle = 0.$$

Using the independence of $\{A_i\}_{i=1}^m$ and Isserlis' theorem [59] for Gaussian random variables, the second moment $\mathbb{E}[S_{\mathcal{A}}^2(P, Q)]$ can be computed as:

$$m \cdot \mathbb{E}[\langle A, P \rangle^2 \langle A, Q \rangle^2] = m \cdot \left(\mathbb{E}[\langle A, P \rangle^2] \mathbb{E}[\langle A, Q \rangle^2] + 2 \mathbb{E}[\langle A, P \rangle \langle A, Q \rangle]^2 \right).$$

Under the isotropy assumption, it follows that $\mathbb{E}[\langle A, P \rangle^2] = \|P\|_F^2/m = 2/m$ and $\mathbb{E}[\langle A, Q \rangle^2] = \|Q\|_F^2/m = 1/m$. Moreover, since $\langle P, Q \rangle = 0$, the cross term vanishes. Therefore, we obtain

$$\mathbb{E}[S_{\mathcal{A}}^2(P, Q)] = m \cdot (m^{-1} \cdot 2)(m^{-1} \cdot 1) = 2m^{-1}.$$

To evaluate the concentration properties of $S_{\mathcal{A}}(P, Q)$, we compute its fourth moment. Since $\langle A, P \rangle$ and $\langle A, Q \rangle$ are independent, we have $\psi_i \sim \mathcal{N}(0, 2m^{-1})$ and $\omega_i \sim \mathcal{N}(0, m^{-1})$. Therefore,

$$\begin{aligned} \mathbb{E}[\psi_i^2 \omega_i^2] &= \mathbb{E}[\psi_i^2] \mathbb{E}[\omega_i^2] = (2m^{-1})(m^{-1}) = 2m^{-2}, \\ \mathbb{E}[\psi_i^4 \omega_i^4] &= \mathbb{E}[\psi_i^4] \mathbb{E}[\omega_i^4] = [3 \cdot (2m^{-1})^2][3 \cdot (m^{-1})^2] = 36m^{-4}. \end{aligned}$$

Using mutual independence across the indices, the fourth moment becomes

$$\begin{aligned} \mathbb{E}[S_{\mathcal{A}}^4(P, Q)] &= \sum_{i=1}^m \mathbb{E}[\psi_i^4 \omega_i^4] + 3 \sum_{i \neq j} \mathbb{E}[\psi_i^2 \omega_i^2] \mathbb{E}[\psi_j^2 \omega_j^2] \\ &= m \cdot 36m^{-4} + 3m(m-1) \cdot (2m^{-2})^2 = \frac{12(m+2)}{m^3}. \end{aligned}$$

4.3.2 Statistical Lower Bound Analysis for EFS

To obtain a probabilistic guarantee for escaping local minima \hat{X} , we make use of the Paley–Zygmund inequality [60]. For any random variable $V \geq 0$ with finite second moment and any $0 < \theta < 1$, the inequality states:

$$\mathbb{P}(V \geq \theta \mathbb{E}[V]) \geq (1 - \theta)^2 \frac{\mathbb{E}[V]^2}{\mathbb{E}[V^2]}. \quad (12)$$

The first and second moments of the AIC term can be written as

$$\begin{aligned} \mathbb{E}[\text{AIC}] &= \frac{1}{2(1 + \delta_p)^2} \mathbb{E}[S_{\mathcal{A}}^2(P, Q)] = \frac{1}{(1 + \delta_p)^2 m}, \\ \mathbb{E}[(\text{AIC})^2] &= \frac{1}{4(1 + \delta_p)^4} \mathbb{E}[S_{\mathcal{A}}^4(P, Q)] = \frac{3(m + 2)}{(1 + \delta_p)^4 m^3}. \end{aligned}$$

Applying the inequality (12) to $V = \text{AIC}$, we compute the moment ratio as

$$\frac{\mathbb{E}[\text{AIC}]^2}{\mathbb{E}[\text{AIC}^2]} = \frac{(1 + \delta_p)^{-4} m^{-2}}{3(m + 2) / ((1 + \delta_p)^4 m^3)} = \frac{m}{3(m + 2)}.$$

Hence, for any $0 < \theta < 1$, the Paley–Zygmund bound yields

$$\mathbb{P}\left(\text{AIC} \geq \theta \cdot \frac{1}{(1 + \delta_p)^2 m}\right) \geq (1 - \theta)^2 \cdot \frac{m}{3(m + 2)}.$$

As $m \rightarrow \infty$ and $\theta \rightarrow 0$, this lower bound approaches $1/3$. However, the bound is smaller for finite m , reflecting finite-sample effects in the ensemble behavior. To guarantee escape from attraction basin of \hat{X} , the EFS must exceed 1 , giving us $\text{AIC} > 1 - \text{NCM}$. According to [21, Thm. 5.4], the NCM satisfies

$$1 - \text{NCM} \leq 1 - \frac{1 - \delta_p}{1 + \delta_p} \cdot \frac{\|\hat{X}\hat{X}^\top - M^*\|_F^2}{2\sigma_r^2 \text{Tr}(M^*)}.$$

To establish the lower bound on the probability of escape, we define the interval

$$U_\theta := \left(0, \frac{1}{(1 + \delta_p)^2 m}\right),$$

which represents the range of values that $1 - \text{NCM}$ can assume in comparison with the typical scale of the AIC term. Next, we verify Thm. 4.6.

Proof. We now proceed to prove the probabilistic part of Thm. 4.6 (as well as discussion after Thm. 3.1). As shown in Figure 3, we examine three distinct regimes according to the relationship between $1 - \text{NCM}$ and U_θ :

- **Case 1:** $1 - \text{NCM} \leq 0$. In this case,

$$\|\hat{X}\hat{X}^\top - M^*\|_F^2 \geq 2 \frac{1 + \delta_p}{1 - \delta_p} \sigma_r^2 \text{Tr}(M^*) =: r_2. \quad (13)$$

Since $\text{AIC} \geq 0$ almost surely, $\text{AIC} > 1 - \text{NCM}$ always holds, leading to $\mathbb{P}(\text{EFS} > 1) = 1$. This corresponds to iterations that are significantly away from M^* , where escape is guaranteed regardless of random perturbations.

- **Case 2:** $1 - \text{NCM} > (1 + \delta_p)^{-2} m^{-1}$. Here,

$$\|\hat{X}\hat{X}^\top - M^*\|_F^2 < 2 \left[1 - \frac{1}{(1 + \delta_p)^2 m}\right] \frac{1 + \delta_p}{1 - \delta_p} \sigma_r^2 \text{Tr}(M^*) =: r_1. \quad (14)$$

In this situation, \hat{X} lies very close to Z . The threshold required for AIC to trigger SOD escape becomes larger than its mean value, implying that no meaningful lower bound for the escape probability can be asserted.

- **Case 3:** $1 - \text{NCM} \in U_\theta$. Here we parameterize the gap as

$$1 - \text{NCM} = \frac{\theta}{(1 + \delta_p)^2 m}, \quad \theta \in (0, 1).$$

Hence, the deviation is confined within $r_1 \leq \|\hat{X}\hat{X}^\top - M^*\|_F^2 \leq r_2$ because

$$\|\hat{X}\hat{X}^\top - M^*\|_F^2 = 2 \left[1 - \frac{\theta}{(1 + \delta_p)^2 m} \right] \frac{1 + \delta_p}{1 - \delta_p} \sigma_r^2 \text{Tr}(M^*).$$

Within this bounded region, the escape probability is given by

$$\mathbb{P}(\text{AIC} > 1 - \text{NCM}) = \mathbb{P} \left(\text{AIC} > \frac{\theta}{(1 + \delta_p)^2 m} \right) \geq (1 - \theta)^2 \cdot \frac{m}{3(m + 2)}.$$

This completes the proof. \square

Remark 4.5. When $r > r_2$, our characterization aligns with [36, Thm. 1]. Despite different derivations, both results show that $u_n q_r^\top$ is a valid descent direction in the matrix landscape, implying that \hat{X} in this case is a saddle rather than a local minimum. By contrast, the bound on the inner radius r_1 is not tight. In particular, [22, Thm. 4] shows that under full tensor lifting, where all components are lifted rather than simulating over-parameterization, r_1 can approach $r_2/2$. This gap indicates that our single-step SOD Escape captures only a subset of the geometric structure revealed by complete tensor lifting.

4.4 Formal Theorem and Limitations of the Single-Step SOD Escape

Building on Sections 4.1, 4.2, and 4.3, we can reformulate the informal version of Thm. 3.1 into its formal counterpart, Thm. 4.6. The single-step SOD escape strategy can be concluded as

$$\hat{X} \xrightarrow{\text{Single-step SOD}} \hat{X} + \hat{\rho} u_n q_r^\top, \quad (15)$$

While conceptually simple, this approach has several limitations. It provides only an inexact approximation under the tensor spectral norm, which is restricted to the subspace R . Thus, the method strongly relies on the EFS exceeding 1. These motivate us to develop a multi-step SOD escape mechanism.

Theorem 4.6 (Single-step SOD Escape, formal). *Consider the problem of escaping from a local minimum \hat{X} of the objective function (P1). If the EFS defined in Definition 4.4 exceeds 1, then there exist two constants*

$$\hat{\rho}_1 := \frac{-2\sigma_r \langle E, u_n u_n^\top \rangle - \sqrt{\Delta}}{2(1 + \delta_p)}, \quad \hat{\rho}_2 := \frac{-2\sigma_r \langle E, u_n u_n^\top \rangle + \sqrt{\Delta}}{2(1 + \delta_p)},$$

such that for any $\hat{\rho}$ satisfying $\hat{\rho}_1 < \hat{\rho} < \hat{\rho}_2$, $\hat{X} + \hat{\rho} u_n q_r^\top$ is a valid escape point under spectral norm (Equation 7), ensuring that $h(\hat{X}) < h(\hat{X})$. This indicates that the \hat{X} leaves the attraction basin of \hat{X} . Furthermore, suppose $\{A_i\}_{i=1}^m$ are drawn from a symmetric Gaussian ensemble as defined in Equation 11. Then, the escape behavior can be categorized into three cases, characterized by two concentric spheres with radii r_1 and r_2 defined as

$$r_1 = 2 \left[1 - \frac{1}{(1 + \delta_p)^2 m} \right] \frac{1 + \delta_p}{1 - \delta_p} \sigma_r^2 \text{Tr}(M^*), \quad r_2 = 2 \frac{1 + \delta_p}{1 - \delta_p} \sigma_r^2 \text{Tr}(M^*).$$

- *Case 1: If $\|\hat{X}\hat{X}^\top - M^*\|_F^2 \geq r_2$, then $\mathbb{P}(\text{EFS} > 1) = 1$.*
- *Case 2: If $\|\hat{X}\hat{X}^\top - M^*\|_F^2 < r_1$, then $\mathbb{P}(\text{EFS} > 1) = 0$.*
- *Case 3: If $\|\hat{X}\hat{X}^\top - M^*\|_F^2 = \theta r_1 + (1 - \theta)r_2$ for some $\theta \in (0, 1]$, then the probability of escape satisfies $\mathbb{P}(\text{EFS} > 1) \geq (1 - \theta)^2 \cdot \frac{m}{3(m + 2)}$.*

Proof. The proof follows directly from Prop. 4.1, Prop. 4.3, and the analysis (and proof) presented in Section 4.3. \square

5 Multi-step SOD Escape (General Case)

As explained previously, single-step SOD will only be successful when $\mathbf{w}_{\text{escape}}$ has a low-dimensional counterpart, as guaranteed by a EFS score larger than 1. However, this is usually not the case, and we need to choose a $\mathbf{w}_{\text{escape}}$ that corresponds to an iterate further along the optimization trajectory in the lifted tensor space. Nevertheless, without constraining the trajectory in the tensor space, the tensor rank can grow rapidly, making projection back to the matrix

space nearly intractable. To address this issue, we carefully design a low-dimensional subspace in which the trajectory evolves, ensuring that it both decreases the lifted loss (enabling successful escape) and remains accessible to analytical projection. The subspace S is formally introduced below:

$$S = \text{span} \left\{ \underbrace{\text{vec}(\hat{X})^{\otimes l}}_{:=\mathbf{a} \in \mathbb{R}^{nrl}}, \underbrace{\text{vec}(u_n q_r^\top)^{\otimes l}}_{:=\mathbf{b} \in \mathbb{R}^{nrl}}, \underbrace{\text{vec}(E \hat{X})^{\otimes l}}_{:=\mathbf{c} \in \mathbb{R}^{nrl}} \right\}, \quad l \geq 3 \text{ is odd} \quad (16)$$

where $\mathbf{a}, \mathbf{b}, \mathbf{c}$ are order- l hypercubic tensors, and $E := \mathcal{A}^* \mathcal{A}(u_n v_r^\top + v_r u_n^\top)$. The multi-step SOD escape simulates the Truncated Projected Gradient Descent (TPGD) procedure in the tensor space, originating from the matrix space. This procedure is described in Algorithm 1.

Algorithm 1 Truncated Projected Gradient Descent (TPGD)

Require: Select $1 > \eta, \rho > 0$ sufficiently small. Set $\tilde{\mathbf{w}}^{(0)} \leftarrow \mathbf{w}_{\text{escape}}$

- 1: **for** $t = 0, 1, 2, \dots$ **do**
- 2: Vanilla Gradient Descent Step: $\mathbf{v}^{(t)} \leftarrow \tilde{\mathbf{w}}^{(t)} - \eta \nabla h^l(\tilde{\mathbf{w}}^{(t)})$
- 3: Projection Step: $\mathbf{w}^{(t+1)} \leftarrow \Pi_S(\mathbf{v}^{(t)})$
- 4: Truncation Step:

$$\tilde{\mathbf{w}}^{(t+1)} \leftarrow \mathbf{w}^{(t+1)} - \begin{cases} \tilde{O}_\alpha(\rho^2)\mathbf{a} + \tilde{O}_\beta(\rho^2)\mathbf{b} + \tilde{O}_\gamma(\rho^2)\mathbf{c}, & t = 0, \\ \tilde{O}_\alpha((\rho + \eta)\rho\eta)\mathbf{a} + \tilde{O}_\beta((\rho + \eta)\rho\eta)\mathbf{b} + \tilde{O}_\gamma((\rho + \eta)\rho\eta)\mathbf{c}, & t \geq 1. \end{cases}$$

- 5: **end for**

As illustrated in Figure 6, TPGD adapts to the descent condition. Specifically, after a sufficiently large number of iterations t , we can guarantee that $h^l(\tilde{\mathbf{w}}^{(t)}) < h^l(\hat{\mathbf{w}})$. More importantly, TPGD yields a closed-form expression for $\tilde{\mathbf{w}}^{(t)}$, given by $\tilde{\mathbf{w}}^{(t)} = \tilde{\alpha}^{(t)}\mathbf{a} + \tilde{\beta}^{(t)}\mathbf{b} + \tilde{\gamma}^{(t)}\mathbf{c}$, where $\tilde{\alpha}^{(t)} = 1$, and $\tilde{\beta}^{(t)}, \tilde{\gamma}^{(t)}$ are t -dependent coefficients. This structure enables us to deterministically amplify either (with its coefficient):

- the escape component \mathbf{b} identified in [21, Thm. 5.4], or
- the principal superposition term \mathbf{c} derived from the single-step analysis,

while simultaneously discarding other superposition components. Unlike the single-step warm-up which depends on EFS, our multi-step framework leverages the algebraic structure of S and the closed-form coefficient dynamics to ensure successful escape. The entire section constitutes the proof of Thm. 3.2.

Subsection 5.1 introduces preliminary concepts for PGD. Subsection 5.2 derives the coefficients of $\mathbf{a}, \mathbf{b}, \mathbf{c}$ after the first TPGD step. In Subsection 5.3, assuming these coefficients are known at the t -th TPGD step, we derive their values at the $(t+1)$ -th step using a mathematical induction framework, which leads to closed-form expressions for the coefficient dynamics. The final two subsections, 5.4 and 5.5, analyze conditions that guarantee successful escape via the multi-step SOD escape mechanism. In Subsection 5.4, we establish a sufficient condition under which the objective function (P2) decreases, even in the presence of truncation errors. Subsection 5.5 identifies conditions under which either $\tilde{\beta}^{(t)}\mathbf{b}$ or $\tilde{\gamma}^{(t)}\mathbf{c}$ dominates among the components $\{\tilde{\alpha}^{(t)}\mathbf{a}, \tilde{\beta}^{(t)}\mathbf{b}, \tilde{\gamma}^{(t)}\mathbf{c}\}$.

5.1 Projection After Escape and PGD Preparation

According to the definition of the subspace S in Equation (16), the corresponding projection matrix onto S is defined as:

$$P_S := C(C^\top C)^{-1}C^\top \in \mathbb{R}^{nrl \times nrl}, \quad (17)$$

where $C = [\text{stack}(\mathbf{a}), \text{stack}(\mathbf{b}), \text{stack}(\mathbf{c})] \in \mathbb{R}^{nrl \times 3}$. Given any tensor $\mathbf{v} \in \mathbb{R}^{nrl}$, its projection onto subspace S is

$$\Pi_S(\mathbf{v}) = \text{unstack}(P_S \text{stack}(\mathbf{v})), \quad (18)$$

where $\text{unstack} : \mathbb{R}^{nrl} \rightarrow \mathbb{R}^{nrl}$ denotes the inverse of the stacking operation.

At each iteration t , the update rule of tensor space PGD is $\mathbf{w}^{(t+1)} \leftarrow \Pi_S(\mathbf{v}^{(t)})$, where $\mathbf{v}^{(t)}$ is the result of a vanilla GD on the smooth component h^l with step size $\eta > 0$: $\mathbf{v}^{(t)} \leftarrow \mathbf{w}^{(t)} - \eta \nabla h^l(\mathbf{w}^{(t)})$. The TPGD procedure is initialized from the post-escape tensor defined in Equation 4:

$$\tilde{\mathbf{w}}^{(0)} \leftarrow \mathbf{w}_{\text{escape}} = \hat{\mathbf{w}} + \rho \text{vec}(u_n q_r^\top)^{\otimes l} = \text{vec}(\hat{X})^{\otimes l} + \rho \text{vec}(u_n q_r^\top)^{\otimes l},$$

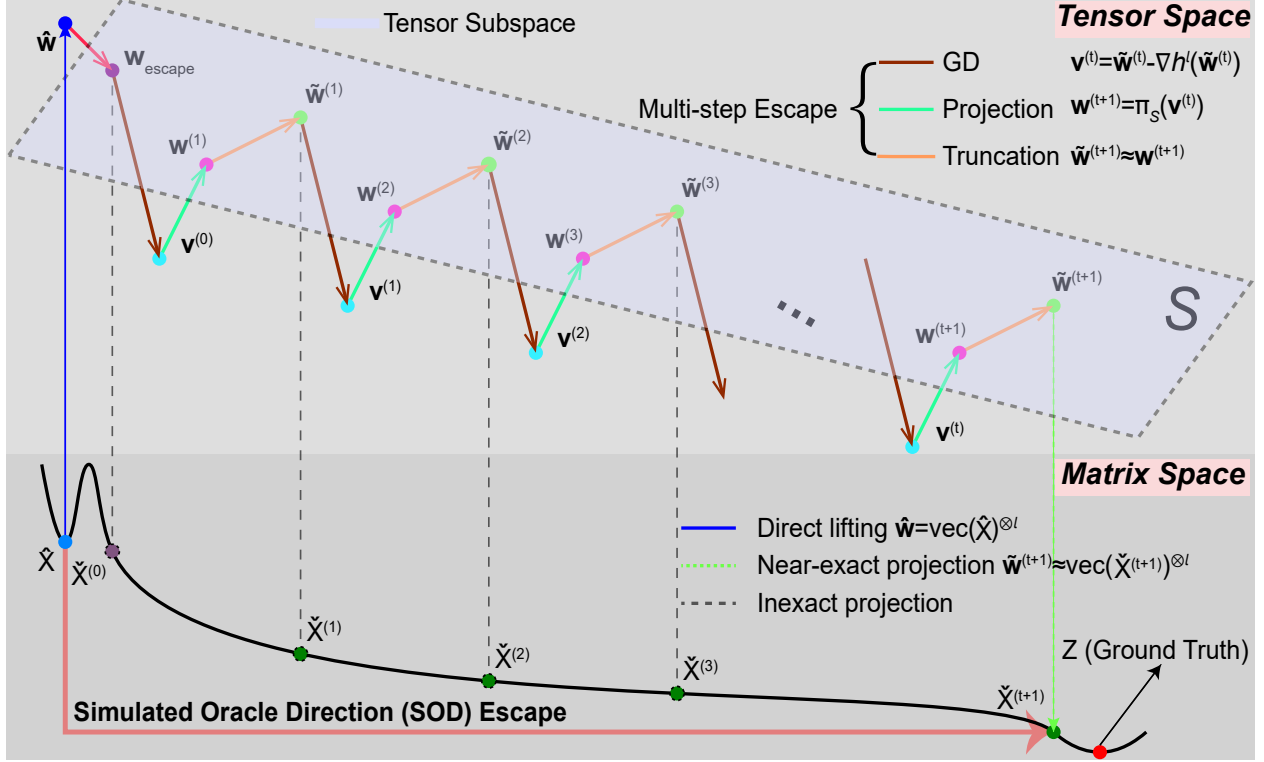


Figure 6: Simulating multi-step tensor-space PGD with truncation after each step, yielding a closed-form iterate $\check{X}^{(t)}$ that escapes the basin of \hat{X} along the SOD direction (red transparent arrow).

where $\rho > 0$ is the escape step size. If no TPGD iterations are performed (i.e., zero steps), this reduces to the single-step SOD escape case.

To simplify the notation involved in tensor gradient derivations, we introduce the following auxiliary function:

$$\mathcal{M}(\mathbf{s}, \mathbf{t}) = \langle \mathbf{P}(\mathbf{s}), \mathbf{P}(\mathbf{t}) \rangle_{2* [l]} = \langle \langle \mathbf{P}^{\otimes l}, \mathbf{s} \rangle_{3* [l]}, \langle \mathbf{P}^{\otimes l}, \mathbf{t} \rangle_{3* [l]} \rangle_{2* [l]}, \quad (19)$$

and define its self-pairing form as $\tilde{\mathcal{M}}(\mathbf{s}) := \mathcal{M}(\mathbf{s}, \mathbf{s})$. Here, the permutation tensor \mathbf{P} and the reshaping operator $\mathbf{P}(\cdot)$ are specified in Equation (3).

For analytical clarity and algebraic convenience, we further define the Gram matrix $G = C^\top C$ associated with the tensor basis in subspace S as

$$G := \begin{bmatrix} \bar{a} & 0 & \bar{s} \\ 0 & \bar{b} & \bar{t} \\ \bar{s} & \bar{t} & \bar{c} \end{bmatrix}, \quad \text{where } \begin{cases} \bar{a} := \langle \mathbf{a}, \mathbf{a} \rangle, & \bar{b} := \langle \mathbf{b}, \mathbf{b} \rangle, & \bar{c} := \langle \mathbf{c}, \mathbf{c} \rangle, \\ \bar{s} := \langle \mathbf{a}, \mathbf{c} \rangle, & \bar{t} := \langle \mathbf{b}, \mathbf{c} \rangle, & 0 = \langle \mathbf{a}, \mathbf{b} \rangle. \end{cases}$$

Notably, the cross-term $\langle \mathbf{a}, \mathbf{b} \rangle = 0$ arises from $u_n \perp v_\phi$ for all $\phi = 1, \dots, r$.

The matrix E , which implicitly encodes the "invisible" escape information available in the matrix space, is defined as

$$E := \mathcal{A}^* \mathcal{A}(v_r u_n^\top + u_n v_r^\top) = \mathcal{A}^* \mathcal{A}(v_r u_n^\top) + \mathcal{A}^* \mathcal{A}(u_n v_r^\top) := E_1 + E_2.$$

It follows that E is symmetric and satisfies $E_1 = E_2$.

5.2 The First Truncated Projected Gradient Descent Step

Proposition 5.1 (The First TPGD Point). *If ρ is sufficiently small, then the first TPGD point $\tilde{\mathbf{w}}^{(1)}$ has the following form:*

$$\tilde{\mathbf{w}}^{(1)} = \mathbf{a} + \rho(1 - \eta \lambda_n^l) \mathbf{b} - \eta \rho \sigma_r^l \frac{1}{2^{l-1}} \mathbf{c}.$$

5.2.1 Tensor Gradient at the First PGD Step

By substituting the initialization point $\tilde{\mathbf{w}}^{(0)}$ into $\tilde{\mathcal{M}}(\cdot)$, we obtain:

$$\begin{aligned}\tilde{\mathcal{M}}(\mathbf{w}^{(0)}) &= \langle \langle \mathbf{P}^{\otimes l}, \hat{\mathbf{w}} + \rho \operatorname{vec}(u_n q_r^\top)^{\otimes l} \rangle_{3* [l]}, \langle \mathbf{P}^{\otimes l}, \hat{\mathbf{w}} + \rho \operatorname{vec}(u_n q_r^\top)^{\otimes l} \rangle_{2* [l]} \rangle_{2* [l]} \\ &= (\hat{X} \hat{X}^\top)^{\otimes l} + \rho \sigma_r^l (v_r u_n^\top)^{\otimes l} + \rho \sigma_r^l (u_n v_r^\top)^{\otimes l} + \rho^2 (u_n u_n^\top)^{\otimes l}.\end{aligned}$$

We now proceed to compute the tensor gradient based on Lem. A.8:

$$\begin{aligned}\nabla h^l(\tilde{\mathbf{w}}^{(0)}) &= \langle \langle \mathbf{A}_r^{\otimes l}, \tilde{\mathbf{w}}^{(0)} \rangle_{[3l-1]}, \langle \mathbf{A}^{\otimes l}, \tilde{\mathcal{M}}(\tilde{\mathbf{w}}^{(0)}) - \tilde{\mathcal{M}}(\operatorname{vec}(Z)^{\otimes l}) \rangle_{[3l-1, 3l]} \rangle_{[2l-1]} \\ &= \left\langle \langle \mathbf{A}_r^{\otimes l}, \hat{\mathbf{w}} + \rho \operatorname{vec}(u_n q_r^\top)^{\otimes l} \rangle_{[3l-1]}, \langle \mathbf{A}^{\otimes l}, \tilde{\mathcal{M}}(\hat{\mathbf{w}}) - \tilde{\mathcal{M}}(\operatorname{vec}(Z)^{\otimes l}) \rangle_{[3l-1, 3l]} \right. \\ &\quad \left. + \langle \mathbf{A}^{\otimes l}, \rho \sigma_r^l (v_r u_n^\top)^{\otimes l} + \rho \sigma_r^l (u_n v_r^\top)^{\otimes l} + \rho^2 (u_n u_n^\top)^{\otimes l} \rangle_{[3l-1, 3l]} \right\rangle_{[2l-1]}.\end{aligned}$$

This gradient can be naturally decomposed into several sub-components.

The First Sub-Term H_1 .

$$H_1 = \left\langle \langle \mathbf{A}_r^{\otimes l}, \hat{\mathbf{w}} \rangle_{[3l-1]}, \langle \mathbf{A}^{\otimes l}, \tilde{\mathcal{M}}(\hat{\mathbf{w}}) - \tilde{\mathcal{M}}(\operatorname{vec}(Z)^{\otimes l}) \rangle_{[3l-1, 3l]} \right\rangle_{[2l-1]} = 0,$$

because $H_1 = \nabla h^l(\hat{\mathbf{w}})$ where $\mathbf{a} = \hat{\mathbf{w}} = \operatorname{vec}(\hat{X})^{\otimes l}$ is a saddle point.

The Second Sub-Term H_2 .

$$H_2 := \left\langle \langle \mathbf{A}_r^{\otimes l}, \hat{\mathbf{w}} \rangle_{[3l-1]}, \langle \mathbf{A}^{\otimes l}, \rho \sigma_r^l (v_r u_n^\top)^{\otimes l} + \rho \sigma_r^l (u_n v_r^\top)^{\otimes l} + \rho^2 (u_n u_n^\top)^{\otimes l} \rangle_{[3l-1, 3l]} \right\rangle_{[2l-1]},$$

which we decompose as $H_2 := H_2^1 + H_2^2 + H_2^3$. For the first term, we compute:

$$\begin{aligned}H_2^1 &= \left\langle \sum_{j_1=1, \dots, j_l=1}^{n, \dots, n} \mathbf{A}_{i_1 j_1 k_1} \cdots \mathbf{A}_{i_l j_l k_l} \hat{X}_{j_1 p_1} \cdots \hat{X}_{j_l p_l}, \right. \\ &\quad \left. \sum_{j'_1=1, \dots, j'_l=1}^{n, \dots, n} \sum_{k'_1=1, \dots, k'_l=1}^{n, \dots, n} \mathbf{A}_{i_1 j'_1 k'_1} \cdots \mathbf{A}_{i_l j'_l k'_l} \left[\rho (\sigma_r v_r u_n^\top)_{j'_1 k'_1} \cdots (\sigma_r v_r u_n^\top)_{j'_l k'_l} \right] \right\rangle_{[2l-1]} \\ &= \rho \sigma_r^l \left\langle \begin{bmatrix} A_1 \hat{X} \\ \vdots \\ A_m \hat{X} \end{bmatrix}^{\otimes l}, \begin{bmatrix} \langle A_1, v_r u_n^\top \rangle \\ \vdots \\ \langle A_m, v_r u_n^\top \rangle \end{bmatrix}^{\otimes l} \right\rangle_{[2l-1]} = \rho \sigma_r^l \operatorname{vec}(E_1 \hat{X})^{\otimes l}.\end{aligned}$$

Analogously,

$$H_2^2 = \rho \sigma_r^l \operatorname{vec}(E_2 \hat{X})^{\otimes l}, \quad H_2^3 = \rho^2 \operatorname{vec} \left(\sum_{i=1}^m \langle A_i, u_n u_n^\top \rangle A_i \hat{X} \right)^{\otimes l}.$$

Since the sensing matrices A_i are symmetric, we have $\langle A_i, u_n v_r^\top \rangle = \langle A_i, v_r u_n^\top \rangle$, implying $H_2^1 = H_2^2$. Therefore, the second sub-term simplifies to:

$$H_2 = \rho \sigma_r^l \frac{1}{2^{l-1}} \operatorname{vec}(E \hat{X})^{\otimes l} + \rho^2 \operatorname{vec} \left(\sum_{i=1}^m \langle A_i, u_n u_n^\top \rangle A_i \hat{X} \right)^{\otimes l}.$$

The Third Sub-Term H_3 . Through direct expansion, we have:

$$\begin{aligned}H_3 &:= \left\langle \langle \mathbf{A}_r^{\otimes l}, \rho \operatorname{vec}(u_n q_r^\top)^{\otimes l} \rangle_{[3l-1]}, \langle \mathbf{A}^{\otimes l}, \tilde{\mathcal{M}}(\hat{\mathbf{w}}) - \tilde{\mathcal{M}}(\operatorname{vec}(Z)^{\otimes l}) \rangle_{[3l-1, 3l]} \right\rangle_{[2l-1]} \\ &= \rho \left\langle \begin{bmatrix} A_1 u_n q_r^\top \\ \vdots \\ A_m u_n q_r^\top \end{bmatrix}^{\otimes l}, \begin{bmatrix} \langle A_1, \hat{X} \hat{X}^\top - Z Z^\top \rangle \\ \vdots \\ \langle A_m, \hat{X} \hat{X}^\top - Z Z^\top \rangle \end{bmatrix}^{\otimes l} \right\rangle_{1, 3, \dots, 2l-1} \\ &= \rho \operatorname{vec}(\nabla f(\hat{X} \hat{X}^\top) u_n q_r^\top)^{\otimes l} = \rho \lambda_n^l \operatorname{vec}(u_n q_r^\top)^{\otimes l}.\end{aligned}$$

The Fourth Sub-Term H_4 . Applying analogous logic to the preceding derivations, we can immediately express:

$$\begin{aligned} H_4 &:= \langle \langle \mathbf{A}_r^{\otimes l}, \rho \operatorname{vec}(u_n q_r^\top)^{\otimes l} \rangle \rangle_{[3l-1]}, \langle \mathbf{A}^{\otimes l}, \rho \sigma_r^l (v_r u_n^\top)^{\otimes l} + \rho \sigma_r^l (u_n v_r^\top)^{\otimes l} + \rho^2 (u_n u_n^\top)^{\otimes l} \rangle \rangle_{[3l-1, 3l]} \\ &= \rho^2 \sigma_r^l \frac{1}{2^{l-1}} \operatorname{vec}(E u_n q_r^\top)^{\otimes l} + \rho^3 \operatorname{vec} \left(\sum_{i=1}^m \langle A_i, u_n u_n^\top \rangle A_i u_n q_r^\top \right)^{\otimes l}. \end{aligned}$$

5.2.2 First PGD Point and Its Truncated Approximation

The intermediate point $\mathbf{v}^{(0)}$, obtained after one step of GD, is given by:

$$\begin{aligned} \mathbf{v}^{(0)} &= \tilde{\mathbf{w}}^{(0)} - \eta \nabla h^l(\tilde{\mathbf{w}}^{(0)}) = \operatorname{vec}(\hat{X})^{\otimes l} + \rho \operatorname{vec}(u_n q_r^\top)^{\otimes l} - \eta [H_2 + H_3 + H_4] \\ &= \operatorname{vec}(\hat{X})^{\otimes l} + \rho(1 - \eta \lambda_n^l) \operatorname{vec}(u_n q_r^\top)^{\otimes l} - \eta \rho \sigma_r^l \frac{1}{2^{l-1}} \operatorname{vec}(E \hat{X})^{\otimes l} \\ &\quad - \eta \rho^2 \operatorname{vec} \left(\sum_{i=1}^m \langle A_i, u_n u_n^\top \rangle A_i \hat{X} \right)^{\otimes l} - \eta \rho^2 \sigma_r^l \frac{1}{2^{l-1}} \operatorname{vec}(E u_n q_r^\top)^{\otimes l} - \eta \rho^3 \operatorname{vec} \left(\sum_{i=1}^m \langle A_i, u_n u_n^\top \rangle A_i u_n q_r^\top \right)^{\otimes l} \\ &= \mathbf{a} + \rho(1 - \eta \lambda_n^l) \mathbf{b} - \eta \rho \sigma_r^l \frac{1}{2^{l-1}} \mathbf{c} + O(\rho^2). \end{aligned}$$

Since the projection operator Π_S maps any point onto the subspace $S = \operatorname{span}\{\mathbf{a}, \mathbf{b}, \mathbf{c}\}$, and the vectors $\operatorname{vec}(\mathbf{a}), \operatorname{vec}(\mathbf{b}), \operatorname{vec}(\mathbf{c}) \in \mathbb{R}^{nrl}$ are linearly independent by construction, the projected point $\mathbf{w}^{(1)} \in S$ can be uniquely expressed as:

$$\mathbf{w}^{(1)} = \Pi_S(\mathbf{v}^{(0)}) = P_S \left[\mathbf{a} + \rho(1 - \eta \lambda_n^l) \mathbf{b} - \eta \rho \sigma_r^l \frac{1}{2^{l-1}} \mathbf{c} + O(\rho^2) \right] := \alpha^{(1)} \mathbf{a} + \beta^{(1)} \mathbf{b} + \gamma^{(1)} \mathbf{c}.$$

The coefficients $\alpha^{(1)}, \beta^{(1)}$, and $\gamma^{(1)}$ satisfy the following linear relation:

$$G \begin{bmatrix} \alpha^{(1)} \\ \beta^{(1)} \\ \gamma^{(1)} \end{bmatrix} = C^\top \operatorname{vec}(\mathbf{v}^{(0)}) = C^\top \left[\operatorname{vec} \left(\mathbf{a} + \rho(1 - \eta \lambda_n^l) \mathbf{b} - \eta \rho \sigma_r^l \frac{1}{2^{l-1}} \mathbf{c} \right) + O(\rho^2) \right].$$

Consequently, these coefficients must solve the associated least-squares system:

$$\begin{aligned} \bar{a} \alpha^{(1)} + \bar{s} \gamma^{(1)} &= \langle \mathbf{a}, \mathbf{v}^{(0)} \rangle = \bar{a} - \eta \rho \sigma_r^l \frac{1}{2^{l-1}} \bar{s} + \langle \mathbf{a}, O(\rho^2) \rangle, \\ \bar{b} \beta^{(1)} + \bar{t} \gamma^{(1)} &= \langle \mathbf{b}, \mathbf{v}^{(0)} \rangle = \rho(1 - \eta \lambda_n^l) \bar{b} - \eta \rho \sigma_r^l \frac{1}{2^{l-1}} \bar{t} + \langle \mathbf{b}, O(\rho^2) \rangle, \\ \bar{c} \alpha^{(1)} + \bar{t} \beta^{(1)} + \bar{c} \gamma^{(1)} &= \langle \mathbf{c}, \mathbf{v}^{(0)} \rangle = \bar{c} + \rho(1 - \eta \lambda_n^l) \bar{t} - \eta \rho \sigma_r^l \frac{1}{2^{l-1}} \bar{c} + \langle \mathbf{c}, O(\rho^2) \rangle. \end{aligned}$$

By performing a Schur complement elimination on $\alpha^{(1)}$ and $\beta^{(1)}$, we isolate $\gamma^{(1)}$ as:

$$\gamma^{(1)} = -\eta \rho \sigma_r^l \frac{1}{2^{l-1}} + \underbrace{\frac{\langle \mathbf{c} - (\bar{s}/\bar{a}) \mathbf{a} - (\bar{t}/\bar{b}) \mathbf{b}, O(\rho^2) \rangle}{\langle \mathbf{c} - (\bar{s}/\bar{a}) \mathbf{a} - (\bar{t}/\bar{b}) \mathbf{b}, \mathbf{c} \rangle}}_{:= \tilde{O}_\gamma(\rho^2)}.$$

Ignoring higher-order $O(\rho^2)$ corrections, we approximate $\gamma^{(1)}$ by its leading-order component $\tilde{\gamma}^{(1)} := -\eta \rho \sigma_r^l \frac{1}{2^{l-1}}$. In a similar manner, the approximations for $\alpha^{(1)}$ and $\beta^{(1)}$ are:

$$\begin{aligned} \alpha^{(1)} &= 1 + \tilde{O}_\alpha(\rho^2) \approx \tilde{\alpha}^{(1)} := 1, \\ \beta^{(1)} &= \rho(1 - \eta \lambda_n^l) + \tilde{O}_\beta(\rho^2) \approx \tilde{\beta}^{(1)} := \rho(1 - \eta \lambda_n^l). \end{aligned}$$

These findings reveal that, up to first order in ρ , the coefficients $\alpha^{(1)}, \beta^{(1)}$, and $\gamma^{(1)}$ correspond exactly to the directional components of $\mathbf{v}^{(0)}$ along \mathbf{a}, \mathbf{b} , and \mathbf{c} respectively. Thus,

$$\begin{aligned} \mathbf{w}^{(1)} &= \left(\tilde{\alpha}^{(1)} + \tilde{O}_\alpha(\rho^2) \right) \mathbf{a} + \left(\tilde{\beta}^{(1)} + \tilde{O}_\beta(\rho^2) \right) \mathbf{b} + \left(\tilde{\gamma}^{(1)} + \tilde{O}_\gamma(\rho^2) \right) \mathbf{c} \\ &= \left(\tilde{\alpha}^{(1)} \mathbf{a} + \tilde{\beta}^{(1)} \mathbf{b} + \tilde{\gamma}^{(1)} \mathbf{c} \right) + \left[\tilde{O}_\alpha(\rho^2) \cdot \mathbf{a} + \tilde{O}_\beta(\rho^2) \cdot \mathbf{b} + \tilde{O}_\gamma(\rho^2) \cdot \mathbf{c} \right] \\ &:= \tilde{\mathbf{w}}^{(1)} + \left[\tilde{O}_\alpha(\rho^2) \cdot \mathbf{a} + \tilde{O}_\beta(\rho^2) \cdot \mathbf{b} + \tilde{O}_\gamma(\rho^2) \cdot \mathbf{c} \right]. \end{aligned} \tag{20}$$

We define $\tilde{\mathbf{w}}^{(1)}$ as the *first TPGD point*, obtained by discarding the high-order $\tilde{O}(\rho^2)$ contributions from $\mathbf{w}^{(1)}$. This completes the proof of Prop. 5.1.

5.3 The $(t+1)$ -th Truncated Projected Gradient Descent Step

Proposition 5.2 (The $(t+1)$ -th TPGD Point). *Suppose that ρ and η are sufficiently small. Assume that for an arbitrary $t \in \{1, 2, 3, \dots\}$, the following coefficients hold:*

$$\tilde{\alpha}^{(t)} = 1, \quad \tilde{\beta}^{(t)} = \rho(1 - \eta\lambda_n^l)^t, \quad \tilde{\gamma}^{(t)} = -\frac{\rho\eta}{2^{l-1}} \left[\sum_{\tau=0}^{t-1} (1 - \eta\lambda_n^l)^\tau \right] \sigma_r^l.$$

This implies that $\tilde{\mathbf{w}}^{(t)} = \tilde{\alpha}^{(t)}\mathbf{a} + \tilde{\beta}^{(t)}\mathbf{b} + \tilde{\gamma}^{(t)}\mathbf{c}$. Then the recurrence relations for the next TPGD step are given by:

$$\tilde{\alpha}^{(t+1)} = 1, \quad \tilde{\beta}^{(t+1)} = \rho(1 - \eta\lambda_n^l)^{t+1}, \quad \tilde{\gamma}^{(t+1)} = -\frac{\rho\eta}{2^{l-1}} \left[\sum_{\tau=0}^t (1 - \eta\lambda_n^l)^\tau \right] \sigma_r^l.$$

In other words, the $(t+1)$ -th TPGD point $\tilde{\mathbf{w}}^{(t+1)}$ has the following form:

$$\tilde{\mathbf{w}}^{(t+1)} = \tilde{\alpha}^{(t+1)}\mathbf{a} + \tilde{\beta}^{(t+1)}\mathbf{b} + \tilde{\gamma}^{(t+1)}\mathbf{c}.$$

5.3.1 Tensor Gradient at the $(t+1)$ -th PGD Step

By substituting the expression of $\tilde{\mathbf{w}}^{(t)}$ into the function $\tilde{\mathcal{M}}(\cdot)$, we obtain:

$$\begin{aligned} & \langle \langle \mathbf{P}^{\otimes l}, \tilde{\alpha}^{(t)}\mathbf{a} + \tilde{\beta}^{(t)}\mathbf{b} + \tilde{\gamma}^{(t)}\mathbf{c} \rangle_{3*}[l], \langle \mathbf{P}^{\otimes l}, \tilde{\alpha}^{(t)}\mathbf{a} + \tilde{\beta}^{(t)}\mathbf{b} + \tilde{\gamma}^{(t)}\mathbf{c} \rangle_{2*}[l] \rangle_{2*}[l] \\ &= (\hat{X}\hat{X}^\top)^{\otimes l} + \tilde{\beta}^{(t)}\sigma_r^l(v_r u_n^\top)^{\otimes l} + \tilde{\beta}^{(t)}\sigma_r^l(u_n v_r^\top)^{\otimes l} + (\tilde{\beta}^{(t)})^2(u_n u_n^\top)^{\otimes l} \\ &+ \tilde{\gamma}^{(t)}(\hat{X}\hat{X}^\top E)^{\otimes l} + \tilde{\gamma}^{(t)}(E\hat{X}\hat{X}^\top)^{\otimes l} + (\tilde{\beta}^{(t)}\tilde{\gamma}^{(t)})\sigma_r^l(u_n v_r^\top E)^{\otimes l} + (\tilde{\gamma}^{(t)}\tilde{\beta}^{(t)})\sigma_r^l(E v_r u_n^\top)^{\otimes l} + (\tilde{\gamma}^{(t)})^2(E\hat{X}\hat{X}^\top E)^{\otimes l}, \end{aligned}$$

where we directly use the induction assumption that $\tilde{\alpha}^{(t)} = 1$.

Next, we compute the gradient $\nabla h^l(\tilde{\mathbf{w}}^{(t)})$ by using Lem. A.8 again:

$$\begin{aligned} & \left\langle \langle \mathbf{A}_r^{\otimes l}, \mathbf{a} + \tilde{\beta}^{(t)}\mathbf{b} + \tilde{\gamma}^{(t)}\mathbf{c} \rangle_{[3l-1]}, \langle \mathbf{A}^{\otimes l}, \tilde{\mathcal{M}}(\hat{\mathbf{w}}) - \tilde{\mathcal{M}}(\text{vec}(Z)^{\otimes l}) \rangle_{[3l-1, 3l]} \right. \\ &+ \langle \mathbf{A}^{\otimes l}, \tilde{\beta}^{(t)}\sigma_r^l(v_r u_n^\top)^{\otimes l} + \tilde{\beta}^{(t)}\sigma_r^l(u_n v_r^\top)^{\otimes l} + (\tilde{\beta}^{(t)})^2(u_n u_n^\top)^{\otimes l} \rangle_{[3l-1, 3l]} \\ &+ \langle \mathbf{A}^{\otimes l}, \tilde{\gamma}^{(t)}(\hat{X}\hat{X}^\top Y)^{\otimes l} + \tilde{\gamma}^{(t)}(Y\hat{X}\hat{X}^\top)^{\otimes l} + (\tilde{\gamma}^{(t)})^2(Y\hat{X}\hat{X}^\top Y)^{\otimes l} \rangle_{[3l-1, 3l]} \\ &+ \left. \langle \mathbf{A}^{\otimes l}, (\tilde{\beta}^{(t)}\tilde{\gamma}^{(t)})\sigma_r^l(u_n v_r^\top Y)^{\otimes l} + (\tilde{\gamma}^{(t)}\tilde{\beta}^{(t)})\sigma_r^l(Y v_r u_n^\top)^{\otimes l} \rangle_{[3l-1, 3l]} \right\rangle_{[2l-1]}. \end{aligned}$$

This gradient naturally decomposes into 18 sub-components, which are summarized in Table 3. We focus on the most significant contributions, H_1^1 and H_2^1 , which are computed as follows:

$$\begin{aligned} H_1^1 &= \langle \langle \mathbf{A}_r^{\otimes l}, \tilde{\beta}^{(t)}\mathbf{b} \rangle_{[3l-1]}, \langle \mathbf{A}^{\otimes l}, \tilde{\mathcal{M}}(\hat{\mathbf{w}}) - \tilde{\mathcal{M}}(\text{vec}(Z)^{\otimes l}) \rangle_{[3l-1, 3l]} \rangle_{[2l-1]} \\ &= \tilde{\beta}^{(t)} \text{vec}(\nabla f(\hat{X}\hat{X}^\top)u_n q_r^\top)^{\otimes l} = \tilde{\beta}^{(t)}\lambda_n^l \text{vec}(u_n q_r^\top)^{\otimes l}, \\ H_2^1 &= \langle \langle \mathbf{A}_r^{\otimes l}, \mathbf{a} \rangle_{[3l-1]}, \langle \mathbf{A}^{\otimes l}, \tilde{\beta}^{(t)}\sigma_r^l(v_r u_n^\top)^{\otimes l} + \tilde{\beta}^{(t)}\sigma_r^l(u_n v_r^\top)^{\otimes l} \rangle_{[3l-1, 3l]} \rangle_{[2l-1]} \\ &= \tilde{\beta}^{(t)}\sigma_r^l \text{vec}(E_1 \hat{X})^{\otimes l} + \tilde{\beta}^{(t)}\sigma_r^l \text{vec}(E_2 \hat{X})^{\otimes l} = \tilde{\beta}^{(t)}\sigma_r^l \frac{1}{2^{l-1}} \text{vec}(E\hat{X})^{\otimes l}. \end{aligned}$$

5.3.2 $(t+1)$ -th PGD Point and Its Truncated Approximation

The intermediate point $\mathbf{v}^{(t)}$, obtained after one step of GD, is given by:

$$\begin{aligned} \mathbf{v}^{(t)} &= \tilde{\mathbf{w}}^{(t)} - \eta \nabla h^l(\tilde{\mathbf{w}}^{(t)}) \\ &= \text{vec}(\hat{X})^{\otimes l} + \tilde{\beta}^{(t)} \text{vec}(u_n q_r^\top)^{\otimes l} + \tilde{\gamma}^{(t)} \text{vec}(E\hat{X})^{\otimes l} \\ &- \eta[H_1^1 + H_2^1 + H_2^1 + H_2^2 + H_2^3 + H_2^4 + H_2^5 + H_2^6 + H_3^1 + H_3^2 + H_3^3 + H_3^4 + H_3^5 + H_3^6 + H_4^1 + H_4^2 + H_4^3] \\ &= \text{vec}(\hat{X})^{\otimes l} + [\tilde{\beta}^{(t)} \text{vec}(u_n q_r^\top)^{\otimes l} - \eta H_1^1] + [\tilde{\gamma}^{(t)} \text{vec}(E\hat{X})^{\otimes l} - \eta H_2^1] + \text{remaining terms}, \end{aligned} \tag{21}$$

where $\tilde{\alpha}^{(t+1)}$ remains equal to 1. Furthermore, the following identities hold:

$$\begin{aligned} \tilde{\beta}^{(t)} \text{vec}(u_n q_r^\top)^{\otimes l} - \eta H_1^1 &= \rho(1 - \eta\lambda_n^l)^{t+1} \mathbf{b} = \tilde{\beta}^{(t+1)} \mathbf{b}, \\ \tilde{\gamma}^{(t)} \text{vec}(E\hat{X})^{\otimes l} - \eta H_2^1 &= -\frac{\rho\eta}{2^{l-1}} \left[\sum_{\tau=0}^t (1 - \eta\lambda_n^l)^\tau \right] \sigma_r^l \mathbf{c} = \tilde{\gamma}^{(t+1)} \mathbf{c}. \end{aligned}$$

Table 4 enumerates the remainder components from Equation (21). By aggregating all 15 residual terms, we find:

$$\mathbf{v}^{(t)} = \tilde{\alpha}^{(t+1)} \mathbf{a} + \tilde{\beta}^{(t+1)} \mathbf{b} + \tilde{\gamma}^{(t+1)} \mathbf{c} + O((\rho + \eta) \rho \eta).$$

Analogous to the initial TPGD iteration, the $(t + 1)$ -th point is derived as:

$$\mathbf{w}^{(t+1)} = \Pi_S(\mathbf{v}^{(t)}) = P_S \left[\tilde{\alpha}^{(t+1)} \mathbf{a} + \tilde{\beta}^{(t+1)} \mathbf{b} + \tilde{\gamma}^{(t+1)} \mathbf{c} + O((\rho + \eta) \rho \eta) \right] := \alpha^{(t+1)} \mathbf{a} + \beta^{(t+1)} \mathbf{b} + \gamma^{(t+1)} \mathbf{c}.$$

The coefficients $\alpha^{(t+1)}$, $\beta^{(t+1)}$, and $\gamma^{(t+1)}$ are obtained by solving the following least-squares projection:

$$G \begin{bmatrix} \alpha^{(t+1)} \\ \beta^{(t+1)} \\ \gamma^{(t+1)} \end{bmatrix} = C^\top \left[\text{vec} \left(\tilde{\alpha}^{(t+1)} \mathbf{a} + \tilde{\beta}^{(t+1)} \mathbf{b} + \tilde{\gamma}^{(t+1)} \mathbf{c} \right) + O((\rho + \eta) \rho \eta) \right].$$

To exemplify the computation, consider $\gamma^{(t+1)}$. Eliminating $\alpha^{(t+1)}$ and $\beta^{(t+1)}$, the Schur complement leads to:

$$\gamma^{(t+1)} = -\frac{\eta \rho}{2^{t-1}} \left[\sum_{\tau=0}^t (1 - \eta \lambda_n^l)^\tau \right] \sigma_r^l + \underbrace{\frac{\langle \mathbf{c} - (\bar{s}/\bar{a}) \mathbf{a} - (\bar{t}/\bar{b}) \mathbf{b}, O((\rho + \eta) \rho \eta) \rangle}{\langle \mathbf{c} - (\bar{s}/\bar{a}) \mathbf{a} - (\bar{t}/\bar{b}) \mathbf{b}, \mathbf{c} \rangle}}_{:= \tilde{O}_\gamma((\rho + \eta) \rho \eta)}.$$

Similarly, the other two coefficients are given by:

$$\begin{aligned} \alpha^{(t+1)} &= 1 + \tilde{O}_\alpha((\rho + \eta) \rho \eta) \approx \tilde{\alpha}^{(t+1)} := 1 \\ \beta^{(t+1)} &= \rho(1 - \eta \lambda_n^l)^{t+1} + \tilde{O}_\beta((\rho + \eta) \rho \eta) \approx \tilde{\beta}^{(t+1)} := \rho(1 - \eta \lambda_n^l)^{t+1} \end{aligned}$$

This result indicates that, up to an error of order $\tilde{O}((\rho + \eta) \rho \eta)$, the coefficients $\alpha^{(t+1)}$, $\beta^{(t+1)}$ and $\gamma^{(t+1)}$ coincide with the coefficients of \mathbf{a} , \mathbf{b} and \mathbf{c} in the intermediate tensor $\mathbf{v}^{(t)}$, respectively. Hence, $\mathbf{w}^{(t+1)}$ can be reformulated as:

$$\tilde{\mathbf{w}}^{(t+1)} + \left[\tilde{O}_\alpha((\rho + \eta) \rho \eta) \cdot \mathbf{a} + \tilde{O}_\beta((\rho + \eta) \rho \eta) \cdot \mathbf{b} + \tilde{O}_\gamma((\rho + \eta) \rho \eta) \cdot \mathbf{c} \right]. \quad (22)$$

The tensor $\tilde{\mathbf{w}}^{(t+1)}$ is referred to as the $(t + 1)$ -th TPGD point, as it neglects higher-order error contributions.

Therefore, the induction provides the closed-form expression for $\tilde{\mathbf{w}}^{(t)}$ and completes the proof of Prop. 5.2.

$$\tilde{\mathbf{w}}^{(t)} = \underbrace{\text{vec}(\hat{X})^{\otimes l}}_{(\mathbf{a}-\text{term is } \tilde{\alpha}^{(t)} \mathbf{a})} + \underbrace{\rho(1 - \eta \lambda_n^l)^t \text{vec}(u_n q_r^\top)^{\otimes l}}_{(\mathbf{b}-\text{term is } \tilde{\beta}^{(t)} \mathbf{b})} - \underbrace{\frac{\eta \rho}{2^{t-1}} \left[\sum_{\tau=0}^{t-1} (1 - \eta \lambda_n^l)^\tau \right] \sigma_r^l \text{vec}(E \hat{X})^{\otimes l}}_{(\mathbf{c}-\text{term is } \tilde{\gamma}^{(t)} \mathbf{c})}. \quad (23)$$

5.4 Sufficient Conditions for Objective Decrease under Truncation Error

Proposition 5.3 (Sufficient Descent of TPGD). *Let $\rho, \eta > 0$, and suppose the tensor objective function h^l , defined in Equation P2, is L -smooth. Then there exist upper bounds on both ρ and η such that*

$$h^l(\tilde{\mathbf{w}}^{(t+1)}) < h^l(\tilde{\mathbf{w}}^{(t)}),$$

which implies that each step of the TPGD algorithm guarantees a decrease in the tensor objective value.

Proof. By building upon the results from Appendix B.2, we now analyze the sufficient decrease condition for the TPGD. Let $\tilde{\mathbf{w}}^{(t+1)}$ denote the truncated point after projection and post-processing. Leveraging the L -smoothness of $h^l(\cdot)$, we apply the standard upper bound again:

$$\begin{aligned} h^l(\tilde{\mathbf{w}}^{(t+1)}) - h^l(\mathbf{w}^{(t+1)}) &\leq \langle \nabla h^l(\mathbf{w}^{(t+1)}), \tilde{\mathbf{w}}^{(t+1)} - \mathbf{w}^{(t+1)} \rangle + \frac{L}{2} \|\tilde{\mathbf{w}}^{(t+1)} - \mathbf{w}^{(t+1)}\|_F^2 \\ &\leq \|\nabla h^l(\mathbf{w}^{(t+1)})\|_F \|\tilde{\mathbf{w}}^{(t+1)} - \mathbf{w}^{(t+1)}\|_F + \frac{L}{2} \|\tilde{\mathbf{w}}^{(t+1)} - \mathbf{w}^{(t+1)}\|_F^2. \end{aligned}$$

Based on the truncation structure, the deviation between $\tilde{\mathbf{w}}^{(t+1)}$ and $\mathbf{w}^{(t+1)}$ admits the following bound as shown in Equation (20) and Equation (22):

$$\mathbf{w}^{(t+1)} - \tilde{\mathbf{w}}^{(t+1)} = \begin{cases} \tilde{O}_\alpha(\rho^2) \cdot \mathbf{a} + \tilde{O}_\beta(\rho^2) \cdot \mathbf{b} + \tilde{O}_\gamma(\rho^2) \cdot \mathbf{c}, & t = 0, \\ \tilde{O}_\alpha((\rho + \eta) \rho \eta) \cdot \mathbf{a} + \tilde{O}_\beta((\rho + \eta) \rho \eta) \cdot \mathbf{b} + \tilde{O}_\gamma((\rho + \eta) \rho \eta) \cdot \mathbf{c}, & t \geq 1. \end{cases}$$

Consequently, we obtain the following norm bound:

$$\|\tilde{\mathbf{w}}^{(t+1)} - \mathbf{w}^{(t+1)}\|_F \leq \begin{cases} C\rho^2, & t = 0, \\ C(\rho + \eta)\rho\eta, & t \geq 1. \end{cases}$$

where $C = \tilde{O}(1) \cdot (\|\mathbf{a}\|_F + \|\mathbf{b}\|_F + \|\mathbf{c}\|_F)$ is a constant. Substituting into the previous inequality, we further obtain:

$$h^l(\tilde{\mathbf{w}}^{(t+1)}) - h^l(\mathbf{w}^{(t+1)}) \leq \begin{cases} G^{(t+1)}C\rho^2 + \frac{L}{2}C^2\rho^4, & t = 0, \\ G^{(t+1)}C(\rho + \eta)\rho\eta + \frac{L}{2}C^2(\rho + \eta)^2\rho^2\eta^2, & t \geq 1. \end{cases} \quad (24)$$

where we define $G^{(t+1)} := \|\nabla h^l(\mathbf{w}^{(t+1)})\|_F$. Adding the two inequalities (52) and (24), we arrive at (where $\Delta^{(t+1)}$ is defined in (52)):

$$h^l(\tilde{\mathbf{w}}^{(t+1)}) - h^l(\tilde{\mathbf{w}}^{(t)}) \leq -\Delta^{(t+1)} + \begin{cases} G^{(t+1)}C\rho^2 + \frac{L}{2}C^2\rho^4, & t = 0, \\ G^{(t+1)}C(\rho + \eta)\rho\eta + \frac{L}{2}C^2(\rho + \eta)^2\rho^2\eta^2, & t \geq 1. \end{cases}$$

To ensure sufficient decrease, we require:

$$\max \left\{ G^{(t+1)}C\rho^2 + \frac{L}{2}C^2\rho^4, G^{(t+1)}C(\rho + \eta)\rho\eta + \frac{L}{2}C^2(\rho + \eta)^2\rho^2\eta^2 \right\} < \Delta^{(t+1)}.$$

Assuming that both ρ and η are sufficiently small, we neglect higher-order terms $O(\rho^3)$ and $O(\eta^3)$, obtaining an approximate condition:

$$\max\{G^{(t+1)}C\rho^2, G^{(t+1)}C(\rho + \eta)\rho\eta\} < \Delta^{(t+1)}.$$

From the first inequality, we derive a bound on ρ :

$$G^{(t+1)}C\rho^2 < \Delta^{(t+1)} \Rightarrow \rho < \sqrt{\frac{\Delta^{(t+1)}}{C \cdot G^{(t+1)}}}.$$

Substituting this into the second term:

$$G^{(t+1)}C(\rho + \eta)\rho\eta = G^{(t+1)}C\rho^2\eta + G^{(t+1)}C\rho\eta^2 < \Delta^{(t+1)}\eta + \sqrt{C \cdot G^{(t+1)}\Delta^{(t+1)}}\eta^2.$$

To satisfy the sufficient decrease condition, we require:

$$\Delta^{(t+1)}\eta + \sqrt{C \cdot G^{(t+1)}\Delta^{(t+1)}}\eta^2 < \Delta^{(t+1)}.$$

Solving this quadratic inequality with respect to η , we obtain:

$$\eta < \frac{-\Delta^{(t+1)} + \sqrt{\Delta^{(t+1)}^2 + 4\sqrt{C \cdot G^{(t+1)}\Delta^{(t+1)}}\Delta^{(t+1)}}}{2\sqrt{C \cdot G^{(t+1)}\Delta^{(t+1)}}} := \hat{\eta}.$$

In conclusion, to ensure the objective function consistently decreases at each truncated PGD (TPGD) step t , i.e.,

$$h^l(\tilde{\mathbf{w}}^{(t+1)}) < h^l(\tilde{\mathbf{w}}^{(t)}),$$

it suffices to choose PGD step size η and escape step size ρ satisfying:

$$0 < \rho < \sqrt{\frac{\Delta^{(t+1)}}{C \cdot G^{(t+1)}}}, \quad 0 < \eta < \min \left\{ \hat{\eta}, \frac{2}{L} \right\}. \quad (25)$$

This completes the proof. \square

5.5 Dominance Criteria for the Coefficient Dynamics

In this subsection, we investigate the conditions under which one of the three terms (a-term, b-term, or c-term) in Equation (23) becomes the leading term. Since the a-term always corresponds to a strict saddle point in the tensor space that is lifted from a local minimum in the matrix space, it cannot serve as an escape direction. Consequently, we can rule out the possibility of the a-term dominating the other two. We therefore focus on the scenarios in which either the b-term or the c-term becomes dominant. For each case, we derive the corresponding range of the number of simulated TPGD steps t required for dominance to occur, as well as the necessary order l of tensor over-parameterization. Throughout this analysis, we assume that the constants ρ and η satisfy the sufficient descent condition for TPGD, as given in Equation (25).

Proposition 5.4 (Dominance Criteria). *There exist two disjoint intervals $U_\beta, U_\gamma \subset \mathbb{R}$ such that $\sup U_\beta < \inf U_\gamma$. When the order l is small, there exists $t \in U_\gamma$ for which the term $\tilde{\gamma}^{(t)}\mathbf{c}$ dominates. In contrast, for $\tilde{\beta}^{(t)}\mathbf{b}$ to dominate, the order l must be sufficiently large so that there exists $t \in U_\beta$.*

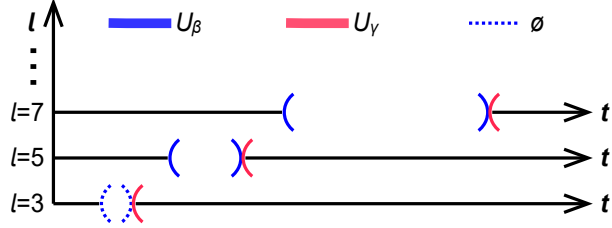


Figure 7: Illustration of the requirements on l and t for different leading terms with two distinct admissible regions U_β and U_γ . When l is small, U_β may be empty if the condition in Equation (28) is not satisfied, while U_γ always exists. As l increases, U_β gradually emerges based on Equation (29), allowing smaller values of t for $\tilde{\beta}^{(t)}\mathbf{b}$ to dominate. In contrast, $\tilde{\gamma}^{(t)}\mathbf{c}$ requires larger t to become dominant.

5.5.1 Dominance of $\tilde{\beta}^{(t)}\mathbf{b}$

We begin by examining the condition:

$$\|\tilde{\beta}^{(t)}\mathbf{b}\|_F > \max\{\|\tilde{\alpha}^{(t)}\mathbf{a}\|_F, \|\tilde{\gamma}^{(t)}\mathbf{c}\|_F\},$$

which implies that the component $\tilde{\beta}^{(t)}\mathbf{b}$ dominates the other two in magnitude.

Condition for $\tilde{\beta}^{(t)}\mathbf{b}$ to dominate $\tilde{\alpha}^{(t)}\mathbf{a}$. Consider the ratio:

$$\frac{\|\tilde{\beta}^{(t)}\mathbf{b}\|_F}{\|\tilde{\alpha}^{(t)}\mathbf{a}\|_F} = \frac{|\tilde{\beta}^{(t)}|}{|\tilde{\alpha}^{(t)}|} \cdot \frac{\|\mathbf{b}\|_F}{\|\mathbf{a}\|_F} = \frac{|\tilde{\beta}^{(t)}|}{|\tilde{\alpha}^{(t)}|} \cdot \frac{\|\text{vec}(u_n q_r^\top)\|_F^l}{\|\text{vec}(\hat{X})\|_F^l} = \frac{|\tilde{\beta}^{(t)}|}{|\tilde{\alpha}^{(t)}|} \cdot \frac{\|u_n q_r^\top\|_F^l}{\|\hat{X}\|_F^l}.$$

Substituting the expressions for $\tilde{\beta}^{(t)}$ and $\tilde{\alpha}^{(t)}$, and using the fact that both u_n and q_r are unit vectors, the ratio simplifies to:

$$\frac{\|\tilde{\beta}^{(t)}\mathbf{b}\|_F}{\|\tilde{\alpha}^{(t)}\mathbf{a}\|_F} = \frac{\rho(1 - \eta\lambda_n^l)^t}{\|\hat{X}\|_F^l} > 1 \quad \Rightarrow \quad t > \frac{\log \|\hat{X}\|_F^l - \log \rho}{\log(1 - \eta\lambda_n^l)}. \quad (26)$$

Condition for $\tilde{\beta}^{(t)}\mathbf{b}$ to dominate $\tilde{\gamma}^{(t)}\mathbf{c}$. Now consider:

$$\frac{\|\tilde{\beta}^{(t)}\mathbf{b}\|_F}{\|\tilde{\gamma}^{(t)}\mathbf{c}\|_F} = \frac{|\tilde{\beta}^{(t)}|}{|\tilde{\gamma}^{(t)}|} \cdot \frac{\|\mathbf{b}\|_F}{\|\mathbf{c}\|_F} = \frac{|\tilde{\beta}^{(t)}|}{|\tilde{\gamma}^{(t)}|} \cdot \frac{\|u_n q_r^\top\|_F^l}{\|E\hat{X}\|_F^l}.$$

Substituting the expressions for $\tilde{\beta}^{(t)}$ and $\tilde{\gamma}^{(t)}$, and using the fact that both u_n and q_r are unit vectors, we obtain:

$$\begin{aligned} \frac{\|\tilde{\beta}^{(t)}\mathbf{b}\|_F}{\|\tilde{\gamma}^{(t)}\mathbf{c}\|_F} &= \frac{\rho(1 - \eta\lambda_n^l)^t}{\frac{\eta\rho}{2^{l-1}} [\sum_{\tau=0}^{t-1} (1 - \eta\lambda_n^l)^\tau] \sigma_r^l \|\hat{X}\|_F^l} \frac{1}{\|E\hat{X}\|_F^l} > 1 \\ \Rightarrow t &< \frac{-1}{\log(1 - \eta\lambda_n^l)} \log \left[1 - 2^{l-1} \frac{(-\lambda_n)^l}{\sigma_r^l} \frac{1}{\|E\hat{X}\|_F^l} \right], \end{aligned} \quad (27)$$

where the inequality holds under the assumptions $\rho, \eta > 0$, $\lambda_n < 0$, and odd l .

Combining both requirements, we define the interval U_β in which $\tilde{\beta}^{(t)}\mathbf{b}$ dominates both $\tilde{\alpha}^{(t)}\mathbf{a}$ and $\tilde{\gamma}^{(t)}\mathbf{c}$, i.e. $t \in U_\beta \cap (0, +\infty)$

$$U_\beta := \frac{1}{\log(1 - \eta\lambda_n^l)} \left(\log \frac{\|\hat{X}\|_F^l}{\rho}, -\log \left[1 - 2^{l-1} \frac{(-\lambda_n)^l}{\sigma_r^l} \frac{1}{\|E\hat{X}\|_F^l} \right] \right). \quad (U_\beta)$$

Validation of the Range U_β . A valid interval U_β must satisfy the condition that its left endpoint is less than its right endpoint. This implies:

$$1 > \rho > \|\hat{X}\|_F^l - 2^{l-1} \frac{(-\lambda_n)^l}{\sigma_r^l} \frac{\|\hat{X}\|_F^l}{\|E\hat{X}\|_F^l} =: \rho_{\min}. \quad (28)$$

We provide an upper bound for the denominator using operator norms from Lemma A.9 where $\Xi^2 := \max\{\|A_1\|_2^2, \dots, \|A_m\|_2^2\}$. Specifically,

$$\|E\hat{X}\|_F^l \leq \|E\|_2^l \|\hat{X}\|_F^l \leq [m(1 + \delta_p)]^{\frac{l}{2}} \Xi^l \|(v_r u_n^\top + u_n v_r^\top)\|_F^l \|\hat{X}\|_F^l = [2m(1 + \delta_p)]^{\frac{l}{2}} \Xi^l \|\hat{X}\|_F^l.$$

Substituting this into the inequality, we require:

$$\begin{aligned} 1 &> \|\hat{X}\|_F^l - 2^{l-1} \frac{(-\lambda_n)^l}{\sigma_r^l} \frac{\|\hat{X}\|_F^l}{[2m(1 + \delta_p)]^{\frac{l}{2}} \Xi^l \|\hat{X}\|_F^l} = \|\hat{X}\|_F^l - \frac{2^{\frac{l}{2}} (-\lambda_n)^l}{2[m(1 + \delta_p)]^{\frac{l}{2}} \Xi^l \sigma_r^l} \\ &= (\sigma_1^2 + \dots + \sigma_r^2)^{\frac{l}{2}} - \frac{2^{\frac{l}{2}} (-\lambda_n)^l}{2[m(1 + \delta_p)]^{\frac{l}{2}} \Xi^l \sigma_r^l} \end{aligned}$$

in order for the condition $\rho < 1$ to hold, where $\sigma_1 \geq \dots \geq \sigma_r > 0$.

Typically, if $-\lambda_n > \sqrt{m(1 + \delta_p)/2} \Xi \sigma_r$, then for sufficiently large l , it follows that $-\lambda_n > 2^{\frac{l}{2} - \frac{1}{2}} \sqrt{m(1 + \delta_p)} \Xi \sigma_r$. Consequently, we have:

$$\begin{aligned} \frac{2^{\frac{l}{2}} (-\lambda_n)^l}{2[m(1 + \delta_p)]^{\frac{l}{2}} \Xi^l \sigma_r^l} &\approx 1 + \frac{2^{\frac{l}{2}} (-\lambda_n)^l}{2[m(1 + \delta_p)]^{\frac{l}{2}} \Xi^l \sigma_r^l} > (\sigma_1^2 + \dots + \sigma_r^2)^{\frac{l}{2}} \\ &\Rightarrow 2^{\frac{l}{2}} < \frac{\sqrt{2} (-\lambda_n)}{\sqrt{m(1 + \delta_p)} (\sigma_1^2 + \dots + \sigma_r^2) \Xi \sigma_r} =: \bar{\Xi}. \end{aligned}$$

Therefore, the range U_β is valid provided that (sufficient condition):

$$l > \{\log_2 \bar{\Xi}\}^{-1}. \quad (29)$$

Remark 5.5. We observe that when l is sufficiently large, U_β is valid, and it is possible to find an iteration t such that the \mathbf{c} -term becomes the leading component. Consequently, the associated escape point in the matrix space is:

$$\hat{X} \xrightarrow{\text{Multi-step SOD } (\beta\text{-type})} \left\{ \rho^{1/l} (1 - \eta \lambda_n^l)^{t/l} \right\} \cdot u_n q_r^\top. \quad (30)$$

However, increasing l may cause numerical instability due to the fractional power $1/l$. This approach is thus mainly applicable to simple cases, e.g. basic example in Equation (1), where the required value of l is relatively small.

5.5.2 Dominance of $\tilde{\gamma}^{(t)} \mathbf{c}$

Similar to the deduction in Section 5.5.1, we can derive that when $t \in U_\gamma \cap (0, +\infty)$, $\tilde{\gamma}^{(t)} \mathbf{c}$ dominates both $\tilde{\alpha}^{(t)} \mathbf{a}$ and $\tilde{\beta}^{(t)} \mathbf{b}$. The interval U_γ is defined as

$$U_\gamma := \left(\frac{1}{\log(1 - \eta \lambda_n^l)} \max \left\{ \log \left[1 + 2^{l-1} \frac{\|\hat{X}\|_F^l}{\rho} \frac{(-\lambda_n)^l}{\sigma_r^l} \frac{1}{\|E\hat{X}\|_F^l} \right], - \log \left[1 - 2^{l-1} \frac{(-\lambda_n)^l}{\sigma_r^l} \frac{1}{\|E\hat{X}\|_F^l} \right] \right\}, +\infty \right). \quad (U_\gamma)$$

Remark 5.6. Since $\sup U_\beta < \inf U_\gamma$ and $U_\beta \cap U_\gamma = \emptyset$, as established by Equations (U _{β}) and (U _{γ}), the terms $\tilde{\beta}^{(t)} \mathbf{b}$ and $\tilde{\gamma}^{(t)} \mathbf{c}$ cannot simultaneously serve as leading components. Consequently, when $\tilde{\gamma}^{(t)} \mathbf{c}$ dominates, the corresponding escape point in the matrix space is given by:

$$\hat{X} \xrightarrow{\text{Multi-step SOD } (\gamma\text{-type})} \left\{ -\frac{1}{2} (2\eta\rho)^{\frac{1}{l}} \left[\sum_{\tau=0}^{t-1} (1 - \eta \lambda_n^l)^\tau \right]^{1/l} \sigma_r \right\} \cdot E\hat{X}. \quad (31)$$

Note that when $\tilde{\gamma}^{(t)} \mathbf{c}$ becomes the leading term, it is not necessary for l to exceed a specific lower bound. Instead, it only needs to satisfy the condition stated in [21, Thm. 5.4]. Hence, this scenario is particularly more practical.

5.6 Formal Theorem and Limitations of the Multi-Step SOD Escape

Building on the analyses from Sections 5.1, 5.2, 5.3, 5.4, and 5.5, we can reformulate the informal version of Thm. 3.2 into its formal counterpart, Thm. 5.7. It is important to note that the multi-step SOD escape mechanism is established

by using oracle from tensor over-parameterization (proposed in [21, Thm. 5.4]). Therefore, Thm. 5.7 naturally inherits certain conditions on the distance between $\hat{X}\hat{X}^\top$ and M^* , which must be satisfied as follows:

$$2 \frac{(1 + \delta_p)}{1 - \delta_p} \sigma_r^2 \text{Tr}(M^*) \geq \|\hat{X}\hat{X}^\top - M^*\|_F^2 \geq \frac{1 + \delta_p}{1 - \delta_p} \sigma_r^2 \text{Tr}(M^*), \quad (32)$$

Additionally, the lifting order l must satisfy the condition:

$$l > \left\{ 1 - \log_2 \left[\frac{2(1 + \delta_p)\sigma_r^2 \text{Tr}(M^*)}{(1 - \delta_p)\|\hat{X}\hat{X}^\top - M^*\|_F^2} \right] \right\}^{-1}. \quad (33)$$

This highlights the key limitation: the multi-step SOD escape is only applicable when \hat{X} satisfies Equation 32. A second limitation arises from the potential numerical instability introduced by the power of $1/l$, especially when l is large.

Theorem 5.7 (Multi-step SOD Escape, formal). *Given a local minimum \hat{X} of the objective function (P1), which satisfies the condition in Equation 32, we aim to find a valid point \check{X} that escapes the attraction basin of \hat{X} , i.e., $h(\check{X}) < h(\hat{X})$. Let the lifting order l satisfy the condition in Equation 33, and let the two step-sizes $\eta, \rho \in (0, 1)$ satisfy*

$$0 < \rho < \sqrt{\Delta^{(t+1)} / (C \cdot G^{(t+1)})}, \quad 0 < \eta < \min\{\hat{\eta}, 2/L\}.$$

Then, the following holds:

- If l is sufficiently large such that $\rho > \rho_{\min}$ (where ρ_{\min} is defined in Equation 28), and the number of simulation steps $t \in U_\beta$ (as defined in U_β) is relatively small, then the point \check{X}

$$\check{X} = \left\{ \rho^{1/l} (1 - \eta \lambda_n^l)^{t/l} \right\} \cdot u_n q_r^\top \quad (\beta\text{-type})$$

is a valid SOD escape point. However, this point may exhibit numerical instability due to expensive requirement of l .

- If l is not so large, a larger number of simulation steps $t \in U_\gamma$ (as defined in U_γ) may be required. In this case, the point \check{X}

$$\check{X} = \left\{ -\frac{1}{2} (2\eta\rho)^{\frac{1}{l}} \left[\sum_{\tau=0}^{t-1} (1 - \eta \lambda_n^l)^\tau \right]^{1/l} \sigma_r \right\} \cdot E \hat{X} \quad (\gamma\text{-type})$$

remains a valid SOD escape point and exhibits greater numerical stability due to smaller l .

Proof. The proof proceeds step by step, building upon the results established in Prop. 5.1, Prop. 5.2, Prop. 5.3 and Prop. 5.4. \square

6 Numerical Experiments

Our experiments concentrate on the core multi-step SOD escape mechanism. We present two numerical case studies

- **perturbed matrix completion (PMC):** This experiment uses a challenging PMC problem introduced in [61] with many "deep" local minima,
- **real-world case:** In this study, the sensing matrices are obtained from a real system. Spurious local minima are encountered during the simulation,

and the **success rate studies** with larger problem size by running more trials. Although these experiments focus on medium- to large-scale settings, they demonstrate that our SOD escape mechanism can deterministically and verifiably escape spurious local minima in real-world matrix sensing tasks.

6.1 Two Case Studies

We consider the PMC case (see Appendix C.1) following the experimental protocol in [21]. By setting $n = 3$ and $\epsilon = 0.3$, $z = \pm(1, 0, 1)$ serve as ground-truth factorizations, whereas $\hat{x} = \pm(1, 0, -1)$ are two primary spurious

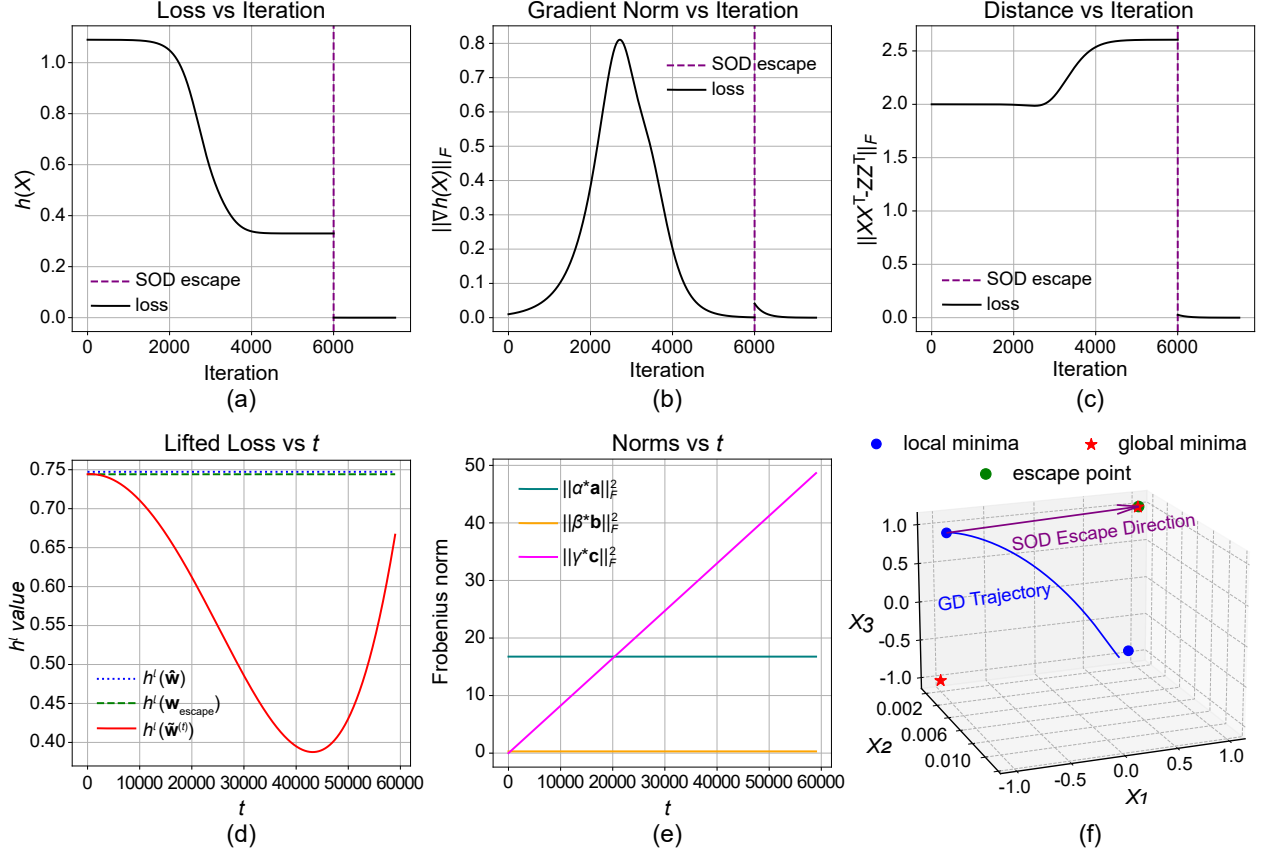


Figure 8: Experimental results of the PMC case. (a) Matrix objective function value vs. iteration. (b) Frobenius norm of the gradient vs. iteration. (c) Distance to ground truth vs. iteration. (d) Tensor objective function value vs. the number of TPGD steps. (e) Frobenius norms of the three tensors within subspace S vs. the number of TPGD steps. (f) Three-dimensional representation of the trajectory of the optimization path.

solutions. We adopt small initialization [62] for GD: draw \tilde{x} from the standard normal distribution and set $x_0 = \zeta \tilde{x}$ with $\zeta = 0.01$. We fix the random seed so that GD converges to the neighborhood of one spurious solution. We run GD for 6000 iterations prior to activating the multi-step SOD escape mechanism, and for an additional 1000 iterations afterward; the step size is 0.001 throughout.

As shown in Figure 8(f), under this setting GD converges to the vicinity of the spurious solution $(-1, 0, 1)$ rather than to either ground truth. Consistently, the curves in the first-row panels (a)–(c) also support this observation, prior to the application of SOD escape mechanism. After applying the multi-step SOD, all three curves ultimately approach zero, indicating convergence to the neighborhood of $(1, 0, 1)$. The second-row panels (d) and (e) detail the internal procedure of the multi-step SOD escape mechanism ($l = 11$). We ensure that after a finite number of simulated steps t , the tensor objective decreases, i.e., $h^l(\tilde{w}^{(t)}) < h^l(\hat{w})$ (as shown in panel (d)), where \hat{w} denotes the lift of the matrix-space spurious point. Panel (e) shows that, at iteration 59000 when the multi-step SOD escape mechanism is triggered, the c -term in Equation (23) dominates the other two and becomes the leading component; projecting this term back to the matrix space yields the desired closed-form escape point \tilde{x} .

We consider another real-world MS case (see Appendix C.2) aimed at recovering a rank-1 low-rank matrix. The ground-truth factor $z = [1, 0, 0]^\top$. In this numerical example, we randomly select the initialization and fix the random seed so that GD with step size 0.1 converges to the local minimum \hat{x} . Figure 9(f) visualizes the 3D GD trajectory: prior to invoking the multi-step SOD escape mechanism, 100 GD steps drive the iterate to the local minimum; the mechanism then computes an escaped point \tilde{x} , from which another 100 GD steps with step size 0.1 reach the ground truth $M^* = zz^\top$. The first-row panels (a)–(c) corroborate this behavior.

As in the previous experiments, panels (d) and (e) depict the multi-step SOD escape procedure, which simulates TPGD in the lifted tensor space. With lifting order $l = 5$ and $k = 150,000$ simulated steps, we simultaneously achieve

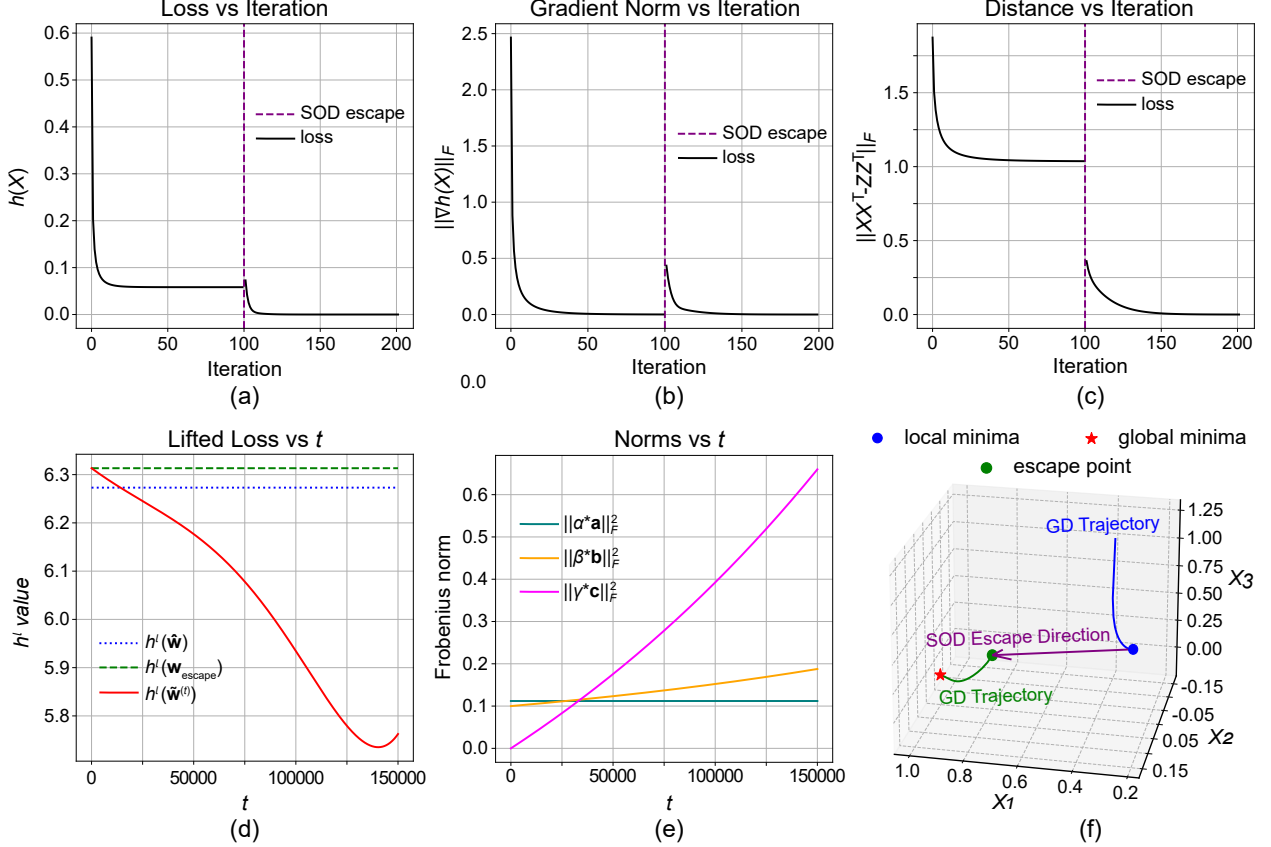


Figure 9: Experimental results of the real-world case. (a) Matrix objective function value vs. iteration. (b) Frobenius norm of the gradient vs. iteration. (c) Distance to ground truth vs. iteration. (d) Tensor objective function value vs. the number of TPGD steps. (e) Frobenius norms of the three tensors within subspace S vs. the number of TPGD steps. (f) Three-dimensional representation of the trajectory of the optimization path.

$h^l(\tilde{\mathbf{w}}^{(t)}) < h^l(\hat{\mathbf{w}})$ and observe that the c -term dominates a -term and b -term, becoming the leading component. We then collapse $\tilde{\gamma}^{(t)}c$ back to the matrix space to obtain the closed-form escape point \tilde{x} . As seen in panel (f), after applying the multi-step SOD escape mechanism, GD starting from \tilde{x} travels a non-negligible distance and converges to the ground truth. This example further validates the effectiveness of the multi-step SOD escape mechanism.

6.2 Success Rate Comparison

In this study, we continue to use the PMC problem as our MS task. We evaluate the effects of increasing the problem size, characterized by the dimension $n \times n$ of the ground-truth matrix M^* , as well as the impact of the perturbation magnitude ϵ , on the convergence success rate. A trial is considered successful if the final solution satisfies $\|XX^\top - M^*\|_F < 0.02$, and the success rate is defined as the proportion of successful trials out of 50. The reason we use success rate instead of average reconstruction error is that failed trials will have very large errors, skewing the statistics by a large margin, distracting readers from the true message. We test five different matrix sizes: $n = 40, 50, 60, 70, 80$. For each size, we run 50 independent trials. The perturbation levels considered are $\epsilon = 0.15$ and $\epsilon = 0.10$. According to [61], smaller ϵ generally results in a larger RIP constant δ_p , which in turn leads to a more complex optimization landscape [63]. We evaluate the performance of two methods: vanilla GD and GD enhanced with our proposed multi-step SOD escape mechanism. As shown in Figure 10, the SOD escape mechanism significantly increases the success rate of GD by effectively escaping many local minima. However, as the problem size increases or ϵ decreases, the optimization landscape becomes more intricate, leading to a general decrease in success rates for both methods. Despite this decline, our method maintains a clear advantage over approaches that optimize entirely in the tensor space: optimization in tensor space becomes computationally infeasible for medium- to large-scale instances (e.g. $n > 10$), as the variable $\mathbf{w} = \text{vec}(X)^{\otimes l}$ grows in size to $(nr)^l$ with $X \in \mathbb{R}^{n \times r}$.

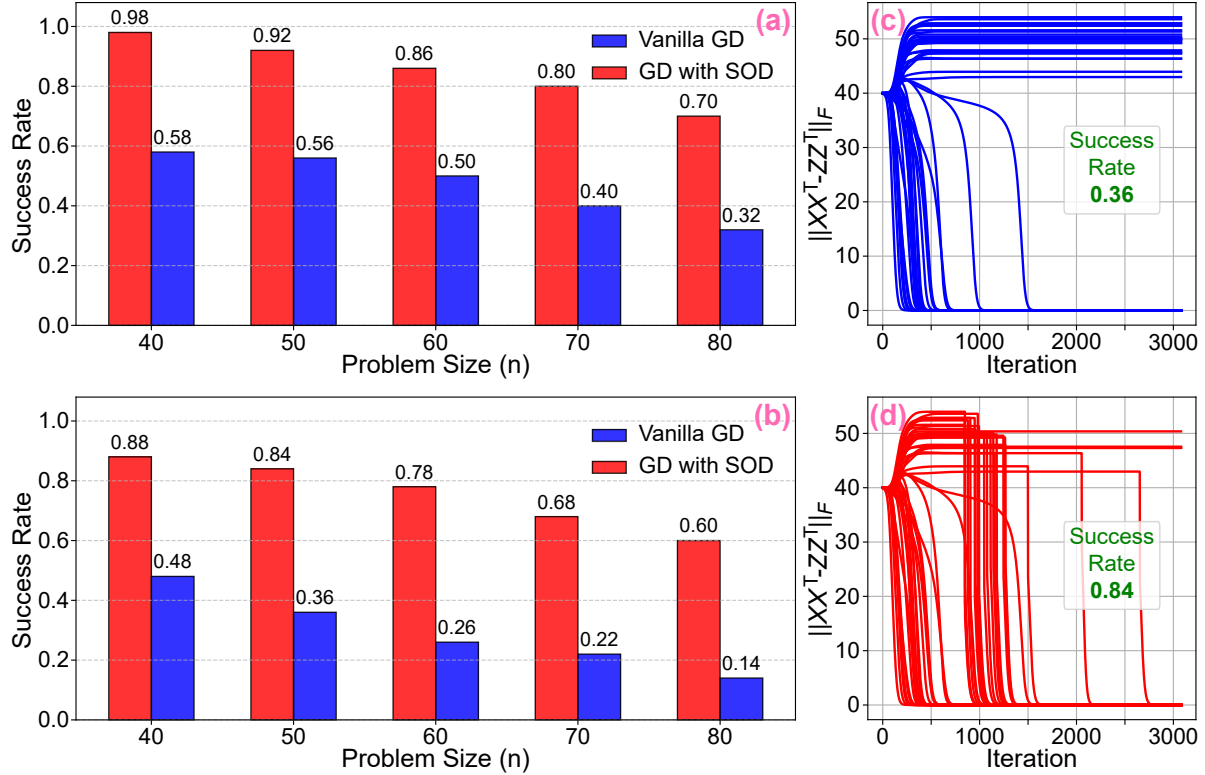


Figure 10: Success rate comparison of vanilla GD and GD with SOD escape. Panels (a) and (b) show the success rates under different problem sizes n , with perturbation parameter $\epsilon = 0.15$ in (a) and $\epsilon = 0.10$ in (b). Panels (c) and (d) present the trajectories of $\|XX^T - ZZ^T\|_F$ over 50 trials across iterations, where (c) corresponds to vanilla GD and (d) corresponds to GD with SOD escape.

7 Conclusions

We proposed Simulated Oracle Direction (SOD) Escape, a deterministic framework for escaping spurious local minima in nonconvex matrix sensing via simulated tensor lifting—capturing the escape geometry of over-parameterized tensor spaces while operating entirely in the original matrix domain and avoiding explicit lifting costs. We provided two complementary analyses: a single-step mechanism that introduces the Escape Feasibility Score (EFS) to certify when a deterministic descent direction exists, and a multi-step mechanism that simulates truncated projected gradient descent (TPGD) within a structured subspace to produce closed-form escape points with explicit parameter dependence and provable objective decrease. Numerical experiments corroborate the theory, showing that SOD reliably escapes local minima and subsequently converges to the global solution across diverse instances. Overall, SOD offers a practical route to deterministic nonconvex optimization by converting over-parameterization insights into computable escape rules; future work may extend this simulated-lifting principle to broader nonconvex models and improve robustness to numerical precision at high lifting orders.

Acknowledgments

We are sincerely grateful to Lu Huang, a PhD candidate at Peking University, for her excellent work in creating the figures and visual content for this paper. We also acknowledge co-author Junze He for assisting in the development of the project website and the use of GPT-4o for its assistance in language polishing.

References

[1] Marina Danilova, Pavel Dvurechensky, Alexander Gasnikov, Eduard Gorbunov, Sergey Guminov, Dmitry Kamzolov, and Innokenti Shibaev. Recent theoretical advances in non-convex optimization. In *High-Dimensional Optimization and Probability: With a View Towards Data Science*, pages 79–163. Springer, 2022.

- [2] Prateek Jain, Purushottam Kar, et al. Non-convex optimization for machine learning. *Foundations and Trends® in Machine Learning*, 10(3-4):142–363, 2017.
- [3] Vivek S Borkar and Vivek S Borkar. *Stochastic approximation: a dynamical systems viewpoint*, volume 100. Springer, 2008.
- [4] Donald J Brown. Equilibrium analysis with non-convex technologies. *Handbook of mathematical economics*, 4:1963–1995, 1991.
- [5] Yuri Nesterov, Henry Wolkowicz, and Yinyu Ye. Semidefinite programming relaxations of nonconvex quadratic optimization. In *Handbook of semidefinite programming: Theory, algorithms, and applications*, pages 361–419. Springer, 2000.
- [6] Masakazu Kojima and Levent Tunçel. Discretization and localization in successive convex relaxation methods for nonconvex quadratic optimization. *Mathematical Programming*, 89(1):79–111, 2000.
- [7] Baturalp Yalcin, Ziye Ma, Javad Lavaei, and Somayeh Sojoudi. Semidefinite programming versus burer-monteiro factorization for matrix sensing. In *Proceedings of the AAAI Conference on Artificial Intelligence*, 2023.
- [8] Christopher De Sa, Christopher Re, and Kunle Olukotun. Global convergence of stochastic gradient descent for some non-convex matrix problems. In *International conference on machine learning*, pages 2332–2341. PMLR, 2015.
- [9] Adam D Bull. Convergence rates of efficient global optimization algorithms. *Journal of Machine Learning Research*, 12(10), 2011.
- [10] Ya-xiang Yuan. Recent advances in trust region algorithms. *Mathematical Programming*, 151(1):249–281, 2015.
- [11] Yann N Dauphin, Razvan Pascanu, Caglar Gulcehre, Kyunghyun Cho, Surya Ganguli, and Yoshua Bengio. Identifying and attacking the saddle point problem in high-dimensional non-convex optimization. *Advances in neural information processing systems*, 27, 2014.
- [12] Simon Du and Jason Lee. On the power of over-parametrization in neural networks with quadratic activation. In *International conference on machine learning*, pages 1329–1338. PMLR, 2018.
- [13] Simon Du, Jason Lee, Haochuan Li, Liwei Wang, and Xiyu Zhai. Gradient descent finds global minima of deep neural networks. In *International conference on machine learning*, pages 1675–1685. PMLR, 2019.
- [14] Zeyuan Allen-Zhu, Yuanzhi Li, and Zhao Song. A convergence theory for deep learning via over-parameterization. In *International conference on machine learning*, pages 242–252. PMLR, 2019.
- [15] Jared Kaplan, Sam McCandlish, Tom Henighan, Tom B Brown, Benjamin Chess, Rewon Child, Scott Gray, Alec Radford, Jeffrey Wu, and Dario Amodei. Scaling laws for neural language models. *arXiv preprint arXiv:2001.08361*, 2020.
- [16] Roozbeh Yousefzadeh. Deep learning generalization, extrapolation, and over-parameterization. *arXiv preprint arXiv:2203.10366*, 2022.
- [17] Fang Liu, Simiao Liu, Yinghao Zhu, Xiaoli Lian, and Li Zhang. Securereviewer: Enhancing large language models for secure code review through secure-aware fine-tuning. *arXiv preprint arXiv:2510.26457*, 2025.
- [18] Shiwei Liu, Lu Yin, Decebal Constantin Mocanu, and Mykola Pechenizkiy. Do we actually need dense over-parameterization? in-time over-parameterization in sparse training. In *International Conference on Machine Learning*, pages 6989–7000. PMLR, 2021.
- [19] Ji Xu, Daniel J Hsu, and Arian Maleki. Benefits of over-parameterization with em. *Advances in Neural Information Processing Systems*, 31, 2018.
- [20] Arsalan Sharifnassab, Saber Salehkaleybar, and S Jamaloddin Golestani. Bounds on over-parameterization for guaranteed existence of descent paths in shallow relu networks. In *International conference on learning representations*, 2020.
- [21] Ziye Ma, Igor Molybog, Javad Lavaei, and Somayeh Sojoudi. Over-parametrization via lifting for low-rank matrix sensing: Conversion of spurious solutions to strict saddle points. In *International Conference on Machine Learning*. PMLR, 2023.
- [22] Ziye Ma, Javad Lavaei, and Somayeh Sojoudi. Algorithmic regularization in tensor optimization: Towards a lifted approach in matrix sensing. *Advances in Neural Information Processing Systems*, 36, 2024.
- [23] Mark A Davenport, Marco F Duarte, Yonina C Eldar, and Gitta Kutyniok. Introduction to compressed sensing., 2012.
- [24] Emmanuel J Candes, Yonina C Eldar, Thomas Strohmer, and Vladislav Voroninski. Phase retrieval via matrix completion. *SIAM review*, 57(2):225–251, 2015.

- [25] Yi-Kai Liu. Universal low-rank matrix recovery from pauli measurements. *Advances in Neural Information Processing Systems*, 24, 2011.
- [26] Anuj Rajani, Paritosh Mittal, Aishwarya Jain, and Angshul Majumdar. A blind compressed sensing formulation for collaborative filtering. In *2014 IEEE International Symposium on Signal Processing and Information Technology (ISSPIT)*, pages 000438–000443. IEEE, 2014.
- [27] Ming Jin, Igor Molybog, Reza Mohammadi-Ghazi, and Javad Lavaei. Towards robust and scalable power system state estimation. In *2019 IEEE 58th Conference on Decision and Control (CDC)*, pages 3245–3252. IEEE, 2019.
- [28] Yudong Wei, Liang Zhang, Bingcong Li, and Niao He. On the benefits of weight normalization for overparameterized matrix sensing. *arXiv preprint arXiv:2510.01175*, 2025.
- [29] Andreas M Tillmann and Marc E Pfetsch. The computational complexity of the restricted isometry property, the nullspace property, and related concepts in compressed sensing. *IEEE Transactions on Information Theory*, 60(2):1248–1259, 2013.
- [30] Igor Molybog, Ramtin Madani, and Javad Lavaei. Conic optimization for quadratic regression under sparse noise. *The Journal of Machine Learning Research*, 21(1):7994–8029, 2020.
- [31] Yuanzhi Li, Tengyu Ma, and Hongyang Zhang. Algorithmic regularization in over-parameterized matrix sensing and neural networks with quadratic activations. In *Conference On Learning Theory*, pages 2–47. PMLR, 2018.
- [32] Richard Y. Zhang, Cédric Josz, Somayeh Sojoudi, and Javad Lavaei. How much restricted isometry is needed in nonconvex matrix recovery? In *Advances in Neural Information Processing Systems*, volume 31, 2018.
- [33] Emmanuel J Candès and Terence Tao. The power of convex relaxation: Near-optimal matrix completion. *IEEE Transactions on Information Theory*, 56(5):2053–2080, 2010.
- [34] Benjamin Recht, Maryam Fazel, and Pablo A Parrilo. Guaranteed minimum-rank solutions of linear matrix equations via nuclear norm minimization. *SIAM Review*, 52(3):471–501, 2010.
- [35] Bubacarr Bah and Jared Tanner. Improved bounds on restricted isometry constants for gaussian matrices. *SIAM Journal on Matrix Analysis and Applications*, 31(5):2882–2898, 2010.
- [36] Ziye Ma, Ying Chen, Javad Lavaei, and Somayeh Sojoudi. Absence of spurious solutions far from ground truth: A low-rank analysis with high-order losses. In *International Conference on Artificial Intelligence and Statistics*, volume 238. PMLR, 2024.
- [37] Stephen P Boyd and Lieven Vandenberghe. *Convex optimization*. Cambridge university press, 2004.
- [38] Sébastien Bubeck. Convex optimization: Algorithms and complexity. *Foundations and trends in Machine Learning*, 8(3-4):231–357, 2015.
- [39] Prateek Jain, Purushottam Kar, et al. Non-convex optimization for machine learning. *Foundations and Trends® in Machine Learning*, 10(3-4):142–363, 2017.
- [40] Yuejie Chi, Yue M Lu, and Yuxin Chen. Nonconvex optimization meets low-rank matrix factorization: An overview. *IEEE Transactions on Signal Processing*, 67(20):5239–5269, 2019.
- [41] Qinqing Zheng and Ryota Tomioka. Interpolating convex and non-convex tensor decompositions via the subspace norm. *Advances in Neural Information Processing Systems*, 28, 2015.
- [42] Léon Bottou, Frank E Curtis, and Jorge Nocedal. Optimization methods for large-scale machine learning. *SIAM Review*, 60(2):223–311, 2018.
- [43] Max Welling and Yee W Teh. Bayesian learning via stochastic gradient langevin dynamics. In *Proceedings of the 28th international conference on machine learning (ICML-11)*, pages 681–688, 2011.
- [44] Alexander G Nikolaev and Sheldon H Jacobson. Simulated annealing. In *Handbook of metaheuristics*, pages 1–39. Springer, 2010.
- [45] Chi Jin, Rong Ge, Praneeth Netrapalli, Sham M Kakade, and Michael I Jordan. How to escape saddle points efficiently. In *International conference on machine learning*, pages 1724–1732. PMLR, 2017.
- [46] Chi Jin, Praneeth Netrapalli, Rong Ge, Sham M Kakade, and Michael I Jordan. On nonconvex optimization for machine learning: Gradients, stochasticity, and saddle points. *Journal of the ACM (JACM)*, 68(2):1–29, 2021.
- [47] Diederik P Kingma and Jimmy Ba. Adam: A method for stochastic optimization. *arXiv preprint arXiv:1412.6980*, 2014.
- [48] Ilya Loshchilov and Frank Hutter. Decoupled weight decay regularization. *arXiv preprint arXiv:1711.05101*, 2017.

- [49] Jonathan Barzilai and Jonathan M Borwein. Two-point step size gradient methods. *IMA journal of numerical analysis*, 8(1):141–148, 1988.
- [50] Yurii Nesterov. A method for solving the convex programming problem with convergence rate $o(1/k^2)$. In *Dokl akad nauk Sssr*, volume 269, page 543, 1983.
- [51] Tong Zhao, Jiacheng Li, Yuanchang Zhou, Guangming Tan, and Weile Jia. Exploring landscapes for better minima along valleys. *arXiv preprint arXiv:2510.27153*, 2025.
- [52] Dong C Liu and Jorge Nocedal. On the limited memory bfgs method for large scale optimization. *Mathematical programming*, 45(1):503–528, 1989.
- [53] Luca Oneto, Sandro Ridella, and Davide Anguita. Do we really need a new theory to understand over-parameterization? *Neurocomputing*, 543:126227, 2023.
- [54] Yin Liu, Jianwen Cai, and Didong Li. Understanding overparametrization in survival models through interpolation. *arXiv e-prints*, pages arXiv–2512, 2025.
- [55] Richard Y Zhang. Improved global guarantees for the nonconvex burer–monteiro factorization via rank overparameterization. *Mathematical Programming*, pages 1–30, 2024.
- [56] Jianhao Ma and Salar Fattah. Global convergence of sub-gradient method for robust matrix recovery: Small initialization, noisy measurements, and over-parameterization. *Journal of Machine Learning Research*, 24(96):1–84, 2023.
- [57] Nuoya Xiong, Lijun Ding, and Simon Shaolei Du. How over-parameterization slows down gradient descent in matrix sensing: The curses of symmetry and initialization. In *The Twelfth International Conference on Learning Representations*, 2024.
- [58] Ziye Ma and Somayeh Sojoudi. Noisy low-rank matrix optimization: Geometry of local minima and convergence rate. In *International Conference on Artificial Intelligence and Statistics*, pages 3125–3150. PMLR, 2023.
- [59] Leon Isserlis. On a formula for the product-moment coefficient of any order of a normal frequency distribution in any number of variables. *Biometrika*, 12(1/2):134–139, 1918.
- [60] Raymond EAC Paley and Antoni Zygmund. A note on analytic functions in the unit circle. In *Mathematical Proceedings of the Cambridge Philosophical Society*, volume 28, pages 266–272. Cambridge University Press, 1932.
- [61] Baturalp Yalçın, Haixiang Zhang, Javad Lavaei, and Somayeh Sojoudi. Factorization approach for low-complexity matrix completion problems: Exponential number of spurious solutions and failure of gradient methods. In *International Conference on Artificial Intelligence and Statistics*, pages 319–341. PMLR, 2022.
- [62] Dominik Stöger and Mahdi Soltanolkotabi. Small random initialization is akin to spectral learning: Optimization and generalization guarantees for overparameterized low-rank matrix reconstruction. *Advances in Neural Information Processing Systems*, 34:23831–23843, 2021.
- [63] Richard Y Zhang, Somayeh Sojoudi, and Javad Lavaei. Sharp restricted isometry bounds for the inexistence of spurious local minima in nonconvex matrix recovery. *Journal of Machine Learning Research*, 20(114):1–34, 2019.
- [64] Pierre Comon, Gene Golub, Lek-Heng Lim, and Bernard Mourrain. Symmetric tensors and symmetric tensor rank. *SIAM Journal on Matrix Analysis and Applications*, 30(3):1254–1279, 2008.
- [65] Tamara G Kolda. Numerical optimization for symmetric tensor decomposition. *Mathematical Programming*, 151(1):225–248, 2015.
- [66] Kaare Brandt Petersen, Michael Syskind Pedersen, et al. The matrix cookbook. *Technical University of Denmark*, 7(15):510, 2008.
- [67] Liqun Qi, Shenglong Hu, Xinzheng Zhang, and Yannan Chen. Tensor norm, cubic power and gelfand limit. *arXiv preprint arXiv:1909.10942*, 2019.
- [68] Lek-Heng Lim and Pierre Comon. Blind multilinear identification. *IEEE Transactions on Information Theory*, 60(2):1260–1280, 2013.
- [69] Han Chen, Garvesh Raskutti, and Ming Yuan. Non-convex projected gradient descent for generalized low-rank tensor regression. *Journal of Machine Learning Research*, 20(5):1–37, 2019.
- [70] Lu Huang, Dangliang Liu, Qijia Wei, Changdong He, Jun Zhang, and Suwei Dong. α -o-glycosylation at tyrosine 10 promotes the astrocyte clearance of amyloid- β peptide 1–42. *ChemBioChem*, 27(1):e202500459, 2026.

A More Details of Preliminary Knowledge

A.1 Tensor Algebra Basics

Definition A.1 (Tensor). *As a generalization of how vectors parametrize finite-dimensional vector spaces, tensors are parametrized using arrays formed from the Cartesian product of such spaces, as discussed in [64]. Specifically, an l -way array is defined as:*

$$\mathbf{s} = \{s_{i_1 i_2 \dots i_l} \mid 1 \leq i_k \leq n_k, 1 \leq k \leq l\} \in \mathbb{R}^{n_1 \times \dots \times n_l}. \quad (34)$$

In this paper, we treat tensors and arrays as synonymous, since there exists a natural isomorphism between them. Furthermore, if $n_1 = \dots = n_l = n$, we refer to the tensor (or array) as an l -order, n -dimensional tensor. For notational convenience, we use $\mathbb{R}^{n \circ l}$, where $n \circ l := n \times \dots \times n$, repeated l times.

Definition A.2 (Symmetric Tensor). *Analogous to the definition of symmetric matrices, an order- l tensor \mathbf{s} with equal dimensions (i.e., $n_1 = \dots = n_l$; also referred to as a hyper-cubic tensor) is said to be symmetric if its entries remain invariant under any permutation of indices:*

$$s_{i_{\sigma(1)} \dots i_{\sigma(l)}} = s_{i_1 \dots i_l}, \quad \forall \sigma \in \mathcal{G}_l, i_1, \dots, i_l \in \{1, \dots, n\}, \quad (35)$$

where \mathcal{G}_l denotes the symmetric group of all permutations on the set $\{1, \dots, l\}$. The space of symmetric tensors is denoted by $\mathcal{S}^l(\mathbb{R}^n)$.

Definition A.3 (Rank of Tensor). *The rank of a cubic tensor $\mathbf{s} \in \mathbb{R}^{n \circ l}$ is defined as*

$$\text{rank}(\mathbf{s}) = \min \left\{ r \mid \mathbf{s} = \sum_{i=1}^r a_i \otimes b_i \otimes \dots \otimes c_i \right\}, \quad (36)$$

for some vectors $a_i, b_i, \dots, c_i \in \mathbb{R}^n$. Furthermore, as noted in [65], if \mathbf{s} is a symmetric tensor, it can be decomposed as

$$\mathbf{s} = \sum_{i=1}^r \varsigma_i a_i \otimes \dots \otimes a_i := \sum_{i=1}^r \varsigma_i a_i^{\otimes l}, \quad (37)$$

where the rank is defined as the number of nonzero ς_i , analogous to the rank of symmetric matrices. A central concept in this work is that of rank-1 tensors. A tensor \mathbf{s} is rank-1 if and only if

$$\mathbf{s} = a^{\otimes l}, \quad (38)$$

for some vector $a \in \mathbb{R}^n$.

Definition A.4 (Tensor Multiplication). *The outer product of two tensors, denoted by \otimes , is an operation that combines two tensors to produce a higher-order tensor. Specifically, the outer product of tensors \mathbf{s} and \mathbf{t} , of orders p and q respectively, yields a tensor of order $p + q$, denoted as $\mathbf{o} = \mathbf{s} \otimes \mathbf{t}$, where*

$$o_{i_1 \dots i_p j_1 \dots j_q} = s_{i_1 \dots i_p} t_{j_1 \dots j_q}. \quad (39)$$

When both tensors have the same dimension, the outer product is defined as

$$\otimes : \mathbb{R}^{n \circ p} \times \mathbb{R}^{n \circ q} \rightarrow \mathbb{R}^{n \circ (p+q)}. \quad (40)$$

For notational convenience, repeated outer products of a vector a are written as

$$\underbrace{a \otimes \dots \otimes a}_{l \text{ times}} := a^{\otimes l}. \quad (41)$$

We also define the inner product between tensors. The mode- l inner product between two tensors, assuming they share the same size in the l -th mode, is denoted by $\langle \mathbf{s}, \mathbf{t} \rangle_l$. Without loss of generality, assuming $l = 1$, the mode-1 inner product is defined as

$$[\langle \mathbf{s}, \mathbf{t} \rangle_1]_{i_2 \dots i_p j_2 \dots j_q} = \sum_{\iota=1}^{n_1} s_{\iota i_2 \dots i_p} t_{\iota j_2 \dots j_q}. \quad (42)$$

In $\langle \cdot, \cdot \rangle_l$, the summation is performed over the l -th mode of both tensors, where the total number of elements is n_l . This definition can be naturally extended to multi-mode inner products by summing over several modes, denoted as $\langle \mathbf{s}, \mathbf{t} \rangle_{l_1, \dots, l_m}$. Such inner products are also referred to as tensor contractions, where the contraction is performed over modes l_1, \dots, l_m .

Lemma A.5 (Tensor Outer Product Identity). *Let P, Q, U, V be arbitrary matrices of compatible dimensions. Then the following identity holds:*

$$\langle P \otimes Q, U \otimes V \rangle_{2,4} = PU \otimes QV. \quad (43)$$

A commonly used special case is:

$$\langle P^{\otimes l}, Q^{\otimes l} \rangle = \langle P, Q \rangle^l = \text{Tr}(P^\top Q)^l. \quad (44)$$

Proof. See Section 10.2 of [66] for a detailed derivation. This identity corresponds to the tensor outer product formulation, where the tensor outer product is equivalent to the unreshaped version of the Kronecker product. \square

Definition A.6 (Tensor Norm). *We adopt norm definitions consistent with those proposed in [67]. For a cubic tensor $s \in \mathbb{R}^{n \times n \times l}$, the nuclear norm $\|\cdot\|_*$ and the spectral norm $\|\cdot\|_S$ are defined as follows:*

$$\|s\|_* = \inf \left\{ \sum_{j=1}^{s_m} |\zeta_j| : s = \sum_{j=1}^{s_m} \zeta_j s_j^{\otimes l}, \|s_j\|_2 = 1, s_j \in \mathbb{R}^n \right\}, \quad (45)$$

$$\|s\|_S = \sup \{ |\langle s, a^{\otimes l} \rangle| : \|a\|_2 = 1, a \in \mathbb{R}^n \}. \quad (46)$$

Lemma A.7 (Dual Relationship Between Tensor Norms). *The spectral norm $\|\cdot\|_S$ is the dual norm of the nuclear norm $\|\cdot\|_*$. That is, for any tensor s , the following identity holds:*

$$\|s\|_S = \sup_{\|\mathbf{t}\|_* \leq 1} |\langle s, \mathbf{t} \rangle|, \quad (47)$$

where \mathbf{t} is a tensor of the same dimensions as s . In particular, the subspace spectral norm of s over a subspace R is defined as

$$\|s\|_{S \otimes R} = \sup_{\mathbf{t} \in R, \|\mathbf{t}\|_* \leq 1} |\langle s, \mathbf{t} \rangle|. \quad (48)$$

Proof. See [68, Lem. 21]. \square

A.2 Matrix Sensing Basics

Lemma A.8 (Gradient of the Tensor Objective Function). *If $\mathbf{w} \in \mathbb{R}^{n \times r \times l}$, then the gradient of $h^l(\mathbf{w})$ is given by:*

$$\nabla h^l(\mathbf{w}) = \left\langle \langle \mathbf{A}_r^{\otimes l}, \mathbf{w} \rangle_{[3l-1]}, \langle \mathbf{A}^{\otimes l}, \tilde{\mathcal{M}}(\mathbf{w}) - \tilde{\mathcal{M}}(\text{vec}(Z)^{\otimes l}) \rangle_{[3l-1, 3l]} \right\rangle_{[2l-1]}, \quad (49)$$

where \mathbf{A}_r is defined as $I_r \otimes_{2,3} \mathbf{A} \in \mathbb{R}^{m \times nr \times nr}$, and $\otimes_{2,3}$ denotes the Kronecker product applied only to the last two dimensions of \mathbf{A} . The operator $\tilde{\mathcal{M}}$ is defined in Equation 19. The subscript $[3l-1, 3l]$ denotes tensor contraction along modes $2, 3, 5, 6, \dots, 3l-1, 3l$; the interpretation of other subscripts follows similarly.

Proof. See the proof of [21, Lem. 5.2]. \square

Lemma A.9. *For an arbitrary matrix $M \in \mathbb{R}^{n \times n}$, we have*

$$\|\mathcal{A}^* \mathcal{A}(M)\|_2^2 \leq m \Xi^2 (1 + \delta_p) \|M\|_F^2, \quad (50)$$

where $\Xi^2 := \max\{\|A_1\|_2^2, \dots, \|A_m\|_2^2\}$.

Proof. By the definition of $\mathcal{A}^* \mathcal{A}$, we have

$$\|\mathcal{A}^* \mathcal{A}(M)\|_2^2 = \left\| \sum_{i=1}^m \langle A_i, M \rangle A_i \right\|_2^2 \leq \left(\sum_{i=1}^m |\langle A_i, M \rangle|^2 \right) \left(\sum_{i=1}^m \|A_i\|_2^2 \right) \leq m \Xi^2 \sum_{i=1}^m \langle A_i, M \rangle^2.$$

By the RIP property,

$$m \Xi^2 \sum_{i=1}^m \langle A_i, M \rangle^2 = m \Xi^2 \|\mathcal{A}(M)\|_2^2 \leq m \Xi^2 (1 + \delta_p) \|M\|_F^2.$$

This concludes the proof. \square

B More Details of Theoretical Results

B.1 Sub-terms and Remaining Terms of TPGD

Lemma B.1. Table 3 summarizes all possible sub-terms that appear in $\nabla h^l(\tilde{\mathbf{w}}^{(t)})$. Table 4 presents the remaining terms from the truncated approximation of the $(t+1)$ -th PGD iterate $\mathbf{v}^{(t)}$. Apart from the 15 remaining terms which are $O((\rho + \eta)\rho\eta)$, we retain only the sub-terms H_1^1 and H_2^1 when η and ρ are sufficiently small.

Table 3: Expressions of the 18 Sub-terms in Tensor Gradient

Term	Expression
0	$\langle\langle \mathbf{A}_r^{\otimes l}, \mathbf{a} \rangle\rangle_{[3l-1]}, \langle\langle \mathbf{A}^{\otimes l}, \tilde{\mathcal{M}}(\tilde{\mathbf{w}}) - \tilde{\mathcal{M}}(\text{vec}(Z)^{\otimes l}) \rangle\rangle_{[3l-1, 3l]} \rangle_{[2l-1]}$
H_1^1	$\langle\langle \mathbf{A}_r^{\otimes l}, \tilde{\beta}^{(t)} \mathbf{b} \rangle\rangle_{[3l-1]}, \langle\langle \mathbf{A}^{\otimes l}, \tilde{\mathcal{M}}(\tilde{\mathbf{w}}) - \tilde{\mathcal{M}}(\text{vec}(Z)^{\otimes l}) \rangle\rangle_{[3l-1, 3l]} \rangle_{[2l-1]}$
H_1^2	$\langle\langle \mathbf{A}_r^{\otimes l}, \tilde{\gamma}^{(t)} \mathbf{c} \rangle\rangle_{[3l-1]}, \langle\langle \mathbf{A}^{\otimes l}, \tilde{\mathcal{M}}(\tilde{\mathbf{w}}) - \tilde{\mathcal{M}}(\text{vec}(Z)^{\otimes l}) \rangle\rangle_{[3l-1, 3l]} \rangle_{[2l-1]}$
H_2^1	$\langle\langle \mathbf{A}_r^{\otimes l}, \mathbf{a} \rangle\rangle_{[3l-1]}, \langle\langle \mathbf{A}^{\otimes l}, \tilde{\beta}^{(t)} \sigma_r^l (v_r u_n^\top)^{\otimes l} + \tilde{\beta}^{(t)} \sigma_r^l (u_n v_r^\top)^{\otimes l} \rangle\rangle_{[3l-1, 3l]} \rangle_{[2l-1]}$
H_2^2	$\langle\langle \mathbf{A}_r^{\otimes l}, \mathbf{a} \rangle\rangle_{[3l-1]}, \langle\langle \mathbf{A}^{\otimes l}, (\tilde{\beta}^{(t)})^2 (u_n u_n^\top)^{\otimes l} \rangle\rangle_{[3l-1, 3l]} \rangle_{[2l-1]}$
H_2^3	$\langle\langle \mathbf{A}_r^{\otimes l}, \tilde{\beta}^{(t)} \mathbf{b} \rangle\rangle_{[3l-1]}, \langle\langle \mathbf{A}^{\otimes l}, \tilde{\beta}^{(t)} \sigma_r^l (v_r u_n^\top)^{\otimes l} + \tilde{\beta}^{(t)} \sigma_r^l (u_n v_r^\top)^{\otimes l} \rangle\rangle_{[3l-1, 3l]} \rangle_{[2l-1]}$
H_2^4	$\langle\langle \mathbf{A}_r^{\otimes l}, \tilde{\beta}^{(t)} \mathbf{b} \rangle\rangle_{[3l-1]}, \langle\langle \mathbf{A}^{\otimes l}, (\tilde{\beta}^{(t)})^2 (u_n u_n^\top)^{\otimes l} \rangle\rangle_{[3l-1, 3l]} \rangle_{[2l-1]}$
H_2^5	$\langle\langle \mathbf{A}_r^{\otimes l}, \tilde{\gamma}^{(t)} \mathbf{c} \rangle\rangle_{[3l-1]}, \langle\langle \mathbf{A}^{\otimes l}, (\tilde{\beta}^{(t)})^2 (u_n u_n^\top)^{\otimes l} + \tilde{\beta}^{(t)} \sigma_r^l (u_n v_r^\top)^{\otimes l} \rangle\rangle_{[3l-1, 3l]} \rangle_{[2l-1]}$
H_2^6	$\langle\langle \mathbf{A}_r^{\otimes l}, \tilde{\gamma}^{(t)} \mathbf{c} \rangle\rangle_{[3l-1]}, \langle\langle \mathbf{A}^{\otimes l}, (\tilde{\beta}^{(t)})^2 (u_n u_n^\top)^{\otimes l} \rangle\rangle_{[3l-1, 3l]} \rangle_{[2l-1]}$
H_3^1	$\langle\langle \mathbf{A}_r^{\otimes l}, \mathbf{a} \rangle\rangle_{[3l-1]}, \langle\langle \mathbf{A}^{\otimes l}, \tilde{\gamma}^{(t)} (\hat{X} \hat{X}^\top E)^{\otimes l} + \tilde{\gamma}^{(t)} (E \hat{X} \hat{X}^\top)^{\otimes l} \rangle\rangle_{[3l-1, 3l]} \rangle_{[2l-1]}$
H_3^2	$\langle\langle \mathbf{A}_r^{\otimes l}, \mathbf{a} \rangle\rangle_{[3l-1]}, \langle\langle \mathbf{A}^{\otimes l}, (\tilde{\gamma}^{(t)})^2 (E \hat{X} \hat{X}^\top E)^{\otimes l} \rangle\rangle_{[3l-1, 3l]} \rangle_{[2l-1]}$
H_3^3	$\langle\langle \mathbf{A}_r^{\otimes l}, \tilde{\beta}^{(t)} \mathbf{b} \rangle\rangle_{[3l-1]}, \langle\langle \mathbf{A}^{\otimes l}, \tilde{\gamma}^{(t)} (\hat{X} \hat{X}^\top E)^{\otimes l} + \tilde{\gamma}^{(t)} (E \hat{X} \hat{X}^\top)^{\otimes l} \rangle\rangle_{[3l-1, 3l]} \rangle_{[2l-1]}$
H_3^4	$\langle\langle \mathbf{A}_r^{\otimes l}, \tilde{\beta}^{(t)} \mathbf{b} \rangle\rangle_{[3l-1]}, \langle\langle \mathbf{A}^{\otimes l}, (\tilde{\gamma}^{(t)})^2 (E \hat{X} \hat{X}^\top E)^{\otimes l} \rangle\rangle_{[3l-1, 3l]} \rangle_{[2l-1]}$
H_3^5	$\langle\langle \mathbf{A}_r^{\otimes l}, \tilde{\gamma}^{(t)} \mathbf{c} \rangle\rangle_{[3l-1]}, \langle\langle \mathbf{A}^{\otimes l}, \tilde{\gamma}^{(t)} (\hat{X} \hat{X}^\top E)^{\otimes l} + \tilde{\gamma}^{(t)} (E \hat{X} \hat{X}^\top)^{\otimes l} \rangle\rangle_{[3l-1, 3l]} \rangle_{[2l-1]}$
H_3^6	$\langle\langle \mathbf{A}_r^{\otimes l}, \tilde{\gamma}^{(t)} \mathbf{c} \rangle\rangle_{[3l-1]}, \langle\langle \mathbf{A}^{\otimes l}, (\tilde{\gamma}^{(t)})^2 (E \hat{X} \hat{X}^\top E)^{\otimes l} \rangle\rangle_{[3l-1, 3l]} \rangle_{[2l-1]}$
H_4^1	$\langle\langle \mathbf{A}_r^{\otimes l}, \mathbf{a} \rangle\rangle_{[3l-1]}, \langle\langle \mathbf{A}^{\otimes l}, (\tilde{\beta}^{(t)} \tilde{\gamma}^{(t)}) \sigma_r^l (u_n v_r^\top E)^{\otimes l} + (\tilde{\gamma}^{(t)} \tilde{\beta}^{(t)}) \sigma_r^l (E v_r u_n^\top)^{\otimes l} \rangle\rangle_{[3l-1, 3l]} \rangle_{[2l-1]}$
H_4^2	$\langle\langle \mathbf{A}_r^{\otimes l}, \tilde{\beta}^{(t)} \mathbf{b} \rangle\rangle_{[3l-1]}, \langle\langle \mathbf{A}^{\otimes l}, (\tilde{\beta}^{(t)} \tilde{\gamma}^{(t)}) \sigma_r^l (u_n v_r^\top E)^{\otimes l} + (\tilde{\gamma}^{(t)} \tilde{\beta}^{(t)}) \sigma_r^l (E v_r u_n^\top)^{\otimes l} \rangle\rangle_{[3l-1, 3l]} \rangle_{[2l-1]}$
H_4^3	$\langle\langle \mathbf{A}_r^{\otimes l}, \tilde{\gamma}^{(t)} \mathbf{c} \rangle\rangle_{[3l-1]}, \langle\langle \mathbf{A}^{\otimes l}, (\tilde{\beta}^{(t)} \tilde{\gamma}^{(t)}) \sigma_r^l (u_n v_r^\top E)^{\otimes l} + (\tilde{\gamma}^{(t)} \tilde{\beta}^{(t)}) \sigma_r^l (E v_r u_n^\top)^{\otimes l} \rangle\rangle_{[3l-1, 3l]} \rangle_{[2l-1]}$

Table 4: Expressions and Asymptotic Orders of the Remaining Terms in $\mathbf{v}^{(t)}$

Term	Expression	Order
$-\eta H_1^2$	$\frac{\eta^2 \rho}{2^{l-1}} [\sum_{\tau=0}^{t-1} (1 - \eta \lambda_n^\tau)^\tau] \sigma_r^l \text{vec}(\nabla f(\hat{X} \hat{X}^\top E \hat{X})^{\otimes l})$	$O(\rho \eta^2)$
$-\eta H_2^2$	$-\eta \rho^2 (1 - \eta \lambda_n^\tau)^{2t} \text{vec}(\mathcal{A}^* \mathcal{A}(u_n u_n^\top) \hat{X})^{\otimes l}$	$O(\rho^2 \eta)$
$-\eta H_3^2$	$-\eta \rho^2 (1 - \eta \lambda_n^\tau)^{2t} \sigma_r^l \frac{1}{2^{l-1}} \text{vec}(E u_n q_r^\top)^{\otimes l}$	$O(\rho^2 \eta)$
$-\eta H_4^2$	$-\eta \rho^3 (1 - \eta \lambda_n^\tau)^{3t} \text{vec}(\mathcal{A}^* \mathcal{A}(u_n u_n^\top) u_n q_r^\top)^{\otimes l}$	$O(\rho^3 \eta)$
$-\eta H_5^2$	$\frac{\eta^2 \rho^2}{2^{2l-2}} [\sum_{\tau=0}^{t-1} (1 - \eta \lambda_n^\tau)^{\tau+t}] \sigma_r^{2l} \text{vec}(\mathcal{A}^* \mathcal{A}(v_r u_n^\top + u_n v_r^\top) E \hat{X})^{\otimes l}$	$O(\rho^2 \eta^2)$
$-\eta H_6^2$	$\frac{\rho^3 \eta^2}{2^{l-1}} [\sum_{\tau=0}^{t-1} (1 - \eta \lambda_n^\tau)^{\tau+2t}] \sigma_r^l \text{vec}(\mathcal{A}^* \mathcal{A}(u_n u_n^\top) E \hat{X})^{\otimes l}$	$O(\rho^3 \eta^2)$
$-\eta H_3^1$	$\frac{\rho \eta^2}{2^{2l-2}} [\sum_{\tau=0}^{t-1} (1 - \eta \lambda_n^\tau)^\tau] \sigma_r^l \text{vec}(\mathcal{A}^* \mathcal{A}(\hat{X} \hat{X}^\top E + E \hat{X} \hat{X}^\top) \hat{X})^{\otimes l}$	$O(\rho \eta^2)$
$-\eta H_3^2$	$-\frac{\rho^2 \eta^3}{2^{2l-2}} [\sum_{\tau=0}^{t-1} (1 - \eta \lambda_n^\tau)^\tau]^2 \sigma_r^{2l} \text{vec}(\mathcal{A}^* \mathcal{A}(E \hat{X} \hat{X}^\top E) \hat{X})^{\otimes l}$	$O(\rho^2 \eta^3)$
$-\eta H_3^3$	$\frac{\rho^2 \eta^2}{2^{2l-2}} [\sum_{\tau=0}^{t-1} (1 - \eta \lambda_n^\tau)^\tau] \sigma_r^l \text{vec}(\mathcal{A}^* \mathcal{A}(\hat{X} \hat{X}^\top E + E \hat{X} \hat{X}^\top) u_n q_r^\top)^{\otimes l}$	$O(\rho^2 \eta^2)$
$-\eta H_3^4$	$-\frac{\rho^3 \eta^3}{2^{2l-2}} [\sum_{\tau=0}^{t-1} (1 - \eta \lambda_n^\tau)^\tau]^2 (1 - \eta \lambda_n^\tau)^t \sigma_r^{2l} \text{vec}(\mathcal{A}^* \mathcal{A}(E \hat{X} \hat{X}^\top E) u_n q_r^\top)^{\otimes l}$	$O(\rho^3 \eta^3)$
$-\eta H_3^5$	$-\frac{\rho^2 \eta^3}{2^{3l-3}} [\sum_{\tau=0}^{t-1} (1 - \eta \lambda_n^\tau)^\tau]^2 \sigma_r^{2l} \text{vec}(\mathcal{A}^* \mathcal{A}(\hat{X} \hat{X}^\top E + E \hat{X} \hat{X}^\top) E \hat{X})^{\otimes l}$	$O(\rho^2 \eta^3)$
$-\eta H_3^6$	$\frac{\rho^3 \eta^4}{2^{3l-3}} [\sum_{\tau=0}^{t-1} (1 - \eta \lambda_n^\tau)^\tau]^3 \sigma_r^{3l} \text{vec}(\mathcal{A}^* \mathcal{A}(E \hat{X} \hat{X}^\top E) E \hat{X})^{\otimes l}$	$O(\rho^3 \eta^4)$
$-\eta H_4^1$	$\frac{\rho^2 \eta^2}{2^{2l-2}} [\sum_{\tau=0}^{t-1} (1 - \eta \lambda_n^\tau)^\tau+t] \sigma_r^{2l} \text{vec}(\mathcal{A}^* \mathcal{A}(u_n v_r^\top E + E v_r u_n^\top) \hat{X})^{\otimes l}$	$O(\rho^2 \eta^2)$
$-\eta H_4^2$	$\frac{\rho^3 \eta^2}{2^{2l-2}} [\sum_{\tau=0}^{t-1} (1 - \eta \lambda_n^\tau)^\tau+2t] \sigma_r^{2l} \text{vec}(\mathcal{A}^* \mathcal{A}(u_n v_r^\top E + E v_r u_n^\top) u_n q_r^\top)^{\otimes l}$	$O(\rho^3 \eta^2)$
$-\eta H_4^3$	$-\frac{\rho^4 \eta^3}{2^{3l-3}} [\sum_{\tau=0}^{t-1} (1 - \eta \lambda_n^\tau)^\tau]^2 (1 - \eta \lambda_n^\tau)^{2t} \sigma_r^{3l} \text{vec}(\mathcal{A}^* \mathcal{A}(u_n v_r^\top E + E v_r u_n^\top) E \hat{X})^{\otimes l}$	$O(\rho^4 \eta^3)$

Proof. The derivations of these sub-terms follow the same procedure as in Section 5.2, and are therefore omitted here. \square

B.2 Sufficient Decrease Condition of PGD

We introduce the generic projected gradient descent (PGD) algorithm in tensor space [69], as its structure is largely analogous to that of PGD in matrix space. In this work, the PGD algorithm in tensor space updates the solution iteratively as follows:

$$\mathbf{w}^{(t+1)} = \Pi_S(\tilde{\mathbf{w}}^{(t)} - \eta \nabla h^l(\tilde{\mathbf{w}}^{(t)})) := \Pi_S(\mathbf{v}^{(t)}),$$

where $\Pi_S(\cdot)$ is defined in Equation (18) and $\eta > 0$ is the step size.

We assume that the tensor objective function $h^l(\cdot)$ is L -smooth, i.e., its gradient is Lipschitz continuous with constant $L > 0$, then

$$\|\nabla h^l(\mathbf{u}) - \nabla h^l(\mathbf{v})\|_F \leq L\|\mathbf{u} - \mathbf{v}\|_F, \quad \forall \mathbf{u}, \mathbf{v} \in \mathbb{R}^{(nr)\circ l}. \quad (51)$$

By the standard descent lemma for L -smooth functions, we have

$$h^l(\mathbf{w}^{(t+1)}) \leq h^l(\tilde{\mathbf{w}}^{(t)}) + \langle \nabla h^l(\tilde{\mathbf{w}}^{(t)}), \mathbf{w}^{(t+1)} - \tilde{\mathbf{w}}^{(t)} \rangle + \frac{L}{2} \|\mathbf{w}^{(t+1)} - \tilde{\mathbf{w}}^{(t)}\|_F^2.$$

To proceed, we utilize the optimality condition of the projection operator. Specifically, for any $\mathbf{v} \in \mathbb{R}^{(nr)\circ l}$, the projection $\mathbf{w} = \Pi_S(\mathbf{v})$ satisfies the following variational inequality:

$$\langle \mathbf{v} - \mathbf{w}, \mathbf{u} - \mathbf{w} \rangle \leq 0, \quad \forall \mathbf{u} \in S.$$

Applying this condition to $(t+1)$ -th iteration, with $\mathbf{v} = \tilde{\mathbf{w}}^{(t)} - \eta \nabla h^l(\tilde{\mathbf{w}}^{(t)})$, $\mathbf{w} = \mathbf{w}^{(t+1)}$, and $\mathbf{u} = \tilde{\mathbf{w}}^{(t)} \in S$, we obtain

$$\begin{aligned} \langle \tilde{\mathbf{w}}^{(t)} - \eta \nabla h^l(\tilde{\mathbf{w}}^{(t)}), \mathbf{w}^{(t+1)} - \tilde{\mathbf{w}}^{(t)} \rangle &\leq 0 \\ \Rightarrow \langle \nabla h^l(\tilde{\mathbf{w}}^{(t)}), \mathbf{w}^{(t+1)} - \tilde{\mathbf{w}}^{(t)} \rangle &\leq -\frac{1}{\eta} \|\mathbf{w}^{(t+1)} - \tilde{\mathbf{w}}^{(t)}\|_F^2. \end{aligned}$$

Substituting this inequality into the smoothness-based upper bound, we obtain:

$$\begin{aligned} h^l(\mathbf{w}^{(t+1)}) &\leq h^l(\tilde{\mathbf{w}}^{(t)}) - \frac{1}{\eta} \|\mathbf{w}^{(t+1)} - \tilde{\mathbf{w}}^{(t)}\|_F^2 + \frac{L}{2} \|\mathbf{w}^{(t+1)} - \tilde{\mathbf{w}}^{(t)}\|_F^2 \\ &\leq h^l(\tilde{\mathbf{w}}^{(t)}) - \left(\frac{1}{\eta} - \frac{L}{2}\right) \|\mathbf{w}^{(t+1)} - \tilde{\mathbf{w}}^{(t)}\|_F^2 := h^l(\tilde{\mathbf{w}}^{(t)}) - \Delta^{(t+1)}. \end{aligned} \quad (52)$$

Therefore, a sufficient decrease condition in the tensor objective function is guaranteed when the step size η satisfies

$$\Delta^{(t+1)} > 0 \quad \Rightarrow \quad \eta < 2/L, \quad (53)$$

which ensures the objective value strictly decreases at each projection step.

C More Details of Experiments

C.1 Experimental Setup of Numerical Case Study 1

The general Perturbed Matrix Completion (PMC) problem aims to recover a ground-truth low-rank matrix $M^* \in \mathbb{R}^{n \times n}$ with $\text{rank}(M^*) = r$ from noisy observations generated by a perturbed linear operator \mathcal{A}_ϵ . This operator is defined as

$$\mathcal{A}_\epsilon(M_{ij}) = \begin{cases} M_{ij}, & \text{if } (i, j) \in \Omega, \\ \epsilon M_{ij}, & \text{otherwise,} \end{cases} \quad (54)$$

where Ω is the measurement set defined by

$$\Omega = \{(i, i), (i, 2k), (2k, i) \mid \forall i \in [n], k \in [\lfloor n/2 \rfloor]\},$$

and $\epsilon > 0$ is a small perturbation parameter. The RIP constant of the PMC problem is approximately $\delta_p \approx (1-\epsilon)/(1+\epsilon)$ [61]. When ϵ is small, many spurious local minima tend to appear near the ground-truth factor z . Note that: (i) compared with the basic example in Equation (1), the PMC landscape is more intricate and requires a higher-order tensor lift to escape spurious regions; and (ii) in such complex regimes, the \mathbf{a} -term and \mathbf{b} -term alone are insufficient to constitute a matrix-space escape oracle.

C.2 Experimental Setup of Numerical Case Study 2

The sensing matrices in this case are derived from a real-world scenario [70]. The matrices are given as follows:

$$\begin{aligned}
A_1 &= \begin{bmatrix} 0.0783 & 0.2372 & -0.0439 \\ 0.2372 & -0.0397 & 0.1456 \\ -0.0439 & 0.1456 & -0.4724 \end{bmatrix}, \quad A_2 = \begin{bmatrix} 0.0389 & 0.0536 & -0.0059 \\ 0.0536 & 0.4614 & -0.3907 \\ -0.0059 & -0.3907 & 0.2760 \end{bmatrix}, \\
A_3 &= \begin{bmatrix} 0.0293 & -0.1456 & -0.1656 \\ -0.1456 & 0.3257 & 0.2528 \\ -0.1656 & 0.2528 & -0.0078 \end{bmatrix}, \quad A_4 = \begin{bmatrix} 0.0762 & 0.3193 & -0.3338 \\ 0.3193 & -0.3364 & 0.5847 \\ -0.3338 & 0.5847 & 0.1873 \end{bmatrix}, \\
A_5 &= \begin{bmatrix} -0.0889 & 0.7089 & 0.4472 \\ 0.7089 & 0.3788 & 0.0902 \\ 0.4472 & 0.0902 & -0.3193 \end{bmatrix}, \quad A_6 = \begin{bmatrix} 0.4097 & 0.1190 & 0.2078 \\ 0.1190 & 0.2282 & -0.2274 \\ 0.2078 & -0.2274 & 0.4046 \end{bmatrix}. \tag{55}
\end{aligned}$$

Moreover, this problem exhibits a pair of prominent local minima:

$$\hat{x} = \pm [0.2234 \quad 0.0918 \quad 0.5985]^\top.$$

C.3 Hyperparameter Analysis of Multi-step SOD Escape

Table 5: Hyperparameter Analysis of l and t based on Real-world MS Example

$l = 3 \Rightarrow \rho_{\min} = 0.208$							
U	t	$U_\beta = \emptyset$	5000	33500	$U_\gamma = (2006.17, +\infty)$		
		1000			100000	500000	2000000
\hat{X}		\mathbf{x}^1	✓	✓	✓	✓	\mathbf{x}^2
$\ \hat{X}\hat{X}^\top - \check{X}\check{X}^\top\ _F$		\mathbf{x}^1	1.08	114.22	4.08×10^6	9.94×10^{33}	\mathbf{x}^2
$\ \check{X}\check{X}^\top - ZZ^\top\ _F$		\mathbf{x}^1	0.36	113.29	4.08×10^6	9.94×10^{33}	\mathbf{x}^2
$\frac{\ \hat{X}\hat{X}^\top - \check{X}\check{X}^\top\ _F}{\ \hat{X}\hat{X}^\top - ZZ^\top\ _F}$		\mathbf{x}^1	3.03	1.01	1.00	1.00	\mathbf{x}^2
X_{final}		\mathbf{x}^1	+	\mathbf{x}^2	\mathbf{x}^2	\mathbf{x}^2	\mathbf{x}^2
$l = 5 \Rightarrow \rho_{\min} = 0.097$							
U	t	$\mathbb{R}^+ \setminus (U_\beta \cup U_\gamma)$	5000	$U_\beta = (26948.72, 33974.73)$	33500	100000	$U_\gamma = (33974.73, +\infty)$
		1000				500000	2000000
\hat{X}		\mathbf{x}^1	\mathbf{x}^1		✓	✓	✓
$\ \hat{X}\hat{X}^\top - \check{X}\check{X}^\top\ _F$		\mathbf{x}^1	\mathbf{x}^1		0.59	0.80	2.00
$\ \check{X}\check{X}^\top - ZZ^\top\ _F$		\mathbf{x}^1	\mathbf{x}^1		0.66	0.43	1.08
$\frac{\ \hat{X}\hat{X}^\top - \check{X}\check{X}^\top\ _F}{\ \hat{X}\hat{X}^\top - ZZ^\top\ _F}$		\mathbf{x}^1	\mathbf{x}^1		0.89	1.86	1.84
X_{final}		\mathbf{x}^1	\mathbf{x}^1		—	+	+
$l = 7 \Rightarrow \rho_{\min} = 0.043$							
U	t	1000	5000	$U_\beta = (0, 1093342.41)$	33500	100000	$U_\gamma = (1093342.41, +\infty)$
						500000	2000000
\hat{X}		✓	✓		✓	✓	✓
$\ \hat{X}\hat{X}^\top - \check{X}\check{X}^\top\ _F$		0.665	0.665		0.665	0.666	0.669
$\ \check{X}\check{X}^\top - ZZ^\top\ _F$		0.601	0.601		0.600	0.600	0.598
$\frac{\ \hat{X}\hat{X}^\top - \check{X}\check{X}^\top\ _F}{\ \hat{X}\hat{X}^\top - ZZ^\top\ _F}$		1.106	1.106		1.107	1.109	1.119
X_{final}		—	—		—	—	+

* ✓ indicates that the quantity is well-defined and numerically stable. \mathbf{x}^1 indicates that the quantity is undefined or not considered. \mathbf{x}^2 indicates that the quantity is numerically unstable (e.g., results in NaN).

* In X_{final} , "+" denotes convergence to $+Z$ under matrix-space gradient descent after SOD escape, while "—" denotes convergence to $-Z$.

As shown in Equation (23), the closed-form solution of $\tilde{w}^{(t)}$ primarily depends on four hyperparameters:

- The lifting order l used to simulate over-parameterization in the tensor space (note that it is not necessary to actually lift to the tensor space).
- The number of TPGD steps t applied to the objective in Equation (P2) (this is a simulated process rather than an actual TPGD).

- The escape step size ρ in Equation (4), which simulates leaving the strict saddle point $\hat{\mathbf{w}}$ in the tensor space.
- The step size η used in the simulated TPGD process.

According to Equation (25), both ρ and η should be chosen as small as possible. Therefore, in practice, they are typically initialized with values less than 1 (e.g., 0.1). Based on these values, U_β is computed using Equation (25), and U_γ is computed using Equation (26). The corresponding escape points after SOD escape are then obtained using Equations (30) and (31), which are subsequently used as initialization for gradient descent in the matrix space. If it is required that $U_\beta \neq \emptyset$, then ρ must not be too small and must satisfy the condition $\rho > \rho_{\min}$ as defined in Equation (28). This condition becomes easier to satisfy as l increases, because a larger l leads to a smaller ρ_{\min} .

As shown in Table 5, we conduct an ablation study on hyperparameters using the matrix sensing instance described in Appendix C.2. As previously mentioned, we fix both ρ and η to a small constant value of 0.1. We then evaluate the effect of different lifting orders $l \in \{3, 5, 7\}$ and various truncation steps $t \in \{1000, 5000, 33500, 1 \times 10^5, 5 \times 10^5, 2 \times 10^6\}$. The effectiveness of the escape is primarily measured by the ratio

$$\frac{\|\hat{X}\hat{X}^\top - \check{X}\check{X}^\top\|_F}{\|\check{X}\check{X}^\top - ZZ^\top\|_F}, \quad (56)$$

which compares the distance between the escape point and the local minimum to the distance between the escape point and the ground truth. A ratio significantly greater than 1 indicates a successful escape. The variable X_{final} denotes the point to which gradient descent converges after the SOD escape. If it converges to QZ where Q is any orthogonal matrix, the escape is considered successful. Otherwise, it is regarded as a failure.

Combining the results from Table 5, our experimental findings are as follows:

- When $l = 3$, $\rho = 0.1 < \rho_{\min}$; thus, $U_\beta = \emptyset$, meaning no $t \in \mathbb{R}^+$ exists such that \mathbf{b} -term becomes the dominant term. However, a small t , such as 5000, allows \mathbf{c} -term to become the dominant term and successfully escape the local minimum \hat{X} .
- When $l = 5$, $\rho = 0.1 > \rho_{\min}$. In this case, a small $t \in U_\beta$ allows \mathbf{b} -term to become the dominant term and successfully escape. For larger t , the iteration falls into U_γ , where the escape effect is more pronounced, with the ratio exceeding 1.
- When $l = 7$, $\rho = 0.1 > \rho_{\min}$. Here, the range of U_β expands significantly, and within U_β , larger values of t yield more pronounced escape effects. Although U_γ exists, it only appears for very large t .

These results align perfectly with Figure 7. Interestingly, we observe that if \mathbf{b} -term becomes the dominant term and an appropriate t is selected for successful escape, the final X_{final} converges to $-Z$. In contrast, if \mathbf{c} -term becomes the dominant term and an appropriate t is selected for successful escape, the final X_{final} converges to $+Z$.